

**ELECTROCHEMISTRY, SPECTROELECTROCHEMISTRY
AND/OR ELECTROSYNTHESIS OF π -EXTENDED
PORPHYRINS IN NONAQUEOUS MEDIA**

A Dissertation

Presented to

the Faculty of the Department of Chemistry

University of Houston

In Partial Fulfillment

of the Requirements for the Degree

Doctor of Philosophy

By

Yuanyuan Fang

May 2014

**ELECTROCHEMISTRY, SPECTROELECTROCHEMISTRY
AND/OR ELECTROSYNTHESIS OF π -EXTENDED
PORPHYRINS IN NONAQUEOUS MEDIA**

Yuanyuan Fang

APPROVED:

Dr. Karl M. Kadish, Chairman

Dr. Roman S. Czernuszewicz

Dr. Angela Moeller

Dr. Randolph Thummel

Dr. James Briggs

Dean, College of Natural Sciences and Mathematics

Dedication

This dissertation is dedicated to

My parents

Qinghe Fang (房庆和) and Youhua Wu (吴友花)

Acknowledgments

I would like to thank my parents Qinghe Fang and Youhua Wu for their love, support, understanding, and encouragement.

I would like to express my grateful appreciation to Dr. Karl M. Kadish for giving me the opportunity to work with him and for his invaluable scientific guidance and support during my years in his laboratory.

I am thankful to Dr. Zhongping Ou for his support and guidance during my study towards an M.S. degree in China and a Ph.D. degree in Houston. I also thank Dr. Maxwell J. Crossley from The University of Sydney and Dr. Daniel T. Gryko from the Polish Academy of Sciences for their comments and contribution to the projects contained within this dissertation. I also thank them for providing some of the compounds studied in this dissertation.

Financial support provided by the Robert A. Welch Foundation is also gratefully acknowledged.

Finally, I wish to express my deep feelings for Dr. Ping Chen, Dr. Zhen Fu, and all the friends and colleagues I have met during my years at the University of Houston.

**ELECTROCHEMISTRY, SPECTROELECTROCHEMISTRY
AND/OR ELECTROSYNTHESIS OF π -EXTENDED
PORPHYRINS IN NONAQUEOUS MEDIA**

An Abstract of a Dissertation

Presented to

the Faculty of the Department of Chemistry

University of Houston

In Partial Fulfillment

of the Requirements for the Degree

Doctor of Philosophy

By

Yuanyuan Fang

May 2014

Abstract

This dissertation presents the electrochemistry, spectroelectrochemistry, and electrosynthesis of π -extended porphyrins. The electrochemistry and UV-vis spectral properties of neutral and protonated Au(III) quinoxalinoporphyrins containing one to four β,β' -fused quinoxalines were characterized in nonaqueous solvents. Multiple Au(III)/Au(II) centered reductions were observed in acidic media, with the exact number depending on the number of fused quinoxaline groups on the compounds. Electrochemical and thin-layer spectroelectrochemical properties of mono- and bis-porphyrins containing a β,β' -fused tetraazaanthracene (TA) group were also examined in different solvents. Each TA-linked bis-porphyrin exhibits a strong interaction between the two equivalent porphyrin macrocycles, the magnitude of which is dependent upon the specific central metal ion. Finally, *meso*-naphthalene-substituted, and *meso*, β -naphthalene-extended porphyrins with five different central ions were characterized as to their electrochemistry and UV-vis spectroelectrochemistry in CH_2Cl_2 and PhCN containing 0.1 M TBAP. All of the naphthalene-substituted porphyrins could be converted to a naphthalene-fused porphyrin after a two-electron oxidation, independent of the metal oxidation state, metal coordination number, or solvent. The electron abstraction site of the second oxidation was shown to be dependent on the porphyrin central metal ion and the naphthalene oxidation potentials.

Table of Contents

Title	Page
List of Abbreviations.....	xii
List of Figures.....	xiv
List of Tables.....	xxii
List of Schemes.....	xxiv
Chapter One Introduction.....	1
1.1 Porphyrins.....	2
1.2 π -Extended porphyrins.....	4
1.3 Electrochemistry.....	9
1.4 Spectroelectrochemistry.....	11
1.5 Quinoxalinoporphyrin.....	11
1.6 Bis-porphyrins.....	13
1.7 Naphthalene fused porphyrin.....	13
1.8 Outline of dissertation.....	14
1.9 References.....	15
Chapter Two Experimental Methods.....	18
2.1 Electrochemical Methods.....	19
2.1.1 Cyclic voltammetry.....	19
2.1.2 Controlled potential electrolysis.....	24

2.2	Spectroscopic Methods.....	26
2.2.1	UV-visible spectroscopy.....	26
2.3	Titration Techniques.....	28
2.3.1	Spectral titration method for determination of equilibrium constants....	28
2.4	Other Experimental Methods.....	31
2.4.1	Degassing of the solution.....	31
2.4.2	Temperature control.....	31
2.5	Chemicals.....	31
2.5.1	Compounds studied.....	31
2.5.2	Other chemicals.....	32
2.6	References.....	33

Chapter Three Unusual Multi-step Sequential Au^{III}/Au^{II} Processes of Gold(III) Quinoxalinoporphyrins in Acidic Nonaqueous Media.....

3.1	Introduction.....	35
3.2	Results and Discussion.....	39
3.2.1	Electrochemistry of Au ^{III} (PQ)PF ₆	39
3.2.2	Electrochemistry of Au ^{III} (QPQ)PF ₆	49
3.2.3	Spectral similarities between protonated and unprotonated gold porphyrins.....	60
3.3	Conclusions.....	64

3.4	References.....	66
Chapter Four	Gold(III) Porphyrins Containing Two, Three, or Four β,β'-Fused Quinoxalines. Synthesis, Electrochemistry, Effect of Structure, and Acidity on Electroreduction Mechanism.....	68
4.1	Introduction.....	69
4.2	Results and Discussion.....	73
4.2.1	Electrochemistry of $\text{Au}^{\text{III}}(\text{PQ}_2)\text{PF}_6$, $\text{Au}^{\text{III}}(\text{PQ}_3)\text{PF}_6$, and $\text{Au}^{\text{III}}(\text{PQ}_4)\text{PF}_6$...	73
4.2.2	Spectra of neutral and reduced compounds.....	82
4.2.3	Electrochemistry of $\text{Au}^{\text{III}}(\text{PQ}_2)\text{PF}_6$, $\text{Au}^{\text{III}}(\text{PQ}_3)\text{PF}_6$, and $\text{Au}^{\text{III}}(\text{PQ}_4)\text{PF}_6$ in the presence of acid.....	88
4.2.4	Spectroelectrochemistry of $\text{Au}^{\text{III}}(\text{PQ}_2)^+$, $\text{Au}^{\text{III}}(\text{PQ}_3)^+$, and $\text{Au}^{\text{III}}(\text{PQ}_4)^+$ in the presence of acid.....	93
4.3	Conclusions.....	98
4.4	References.....	99
Chapter Five	Electrochemistry of Mono- and Bis-porphyrins Containing a β,β'-fused Tetraazaanthracene Group.....	101
5.1	Introduction.....	102
5.2	Results and Discussion.....	106
5.2.1	Electrochemistry of mono-porphyrins.....	106
5.2.1.1	Free-base porphyrin, (PTA) H_2	106

5.2.1.2	Metalated porphyrins, (PTA)M, where M = Cu(II) or Zn(II)...	115
5.2.2	Electrochemistry of TA-linked bis-porphyrins.....	119
5.2.2.1	Free-base bis-porphyrin, H ₂ (P)-TA-(P)H ₂	119
5.2.2.2	Metalated TA-linked bis-porphyrins.....	125
5.3	Conclusions.....	129
5.4	References.....	130
Chapter Six	Electrochemically Driven Intramolecular Oxidative Aromatic Coupling as a Pathway Towards π-Extended Ni(II) Porphyrins.....	133
6.1	Introduction.....	134
6.2	Results and Discussion.....	138
6.2.1	Reduction of Ni(II) porphyrins.....	141
6.2.2	Oxidation of Ni(II) porphyrins.....	142
6.2.3	Spectral monitoring of reduction in thin-layer cell.....	144
6.2.4	Spectral monitoring of oxidation in thin-layer cell.....	147
6.2.5	Fusion of π ring system and conversion of Open-Ni to Fused-Ni during oxidation.....	151
6.3	Conclusions.....	156
6.4	References.....	157

Chapter Seven	Facile Electrosynthesis of π-Extended Zn(II), In(III), Ir(III), and Free-Base Porphyrins.....	162
7.1	Introduction.....	163
7.2	Results and Discussion.....	168
7.2.1	UV-vis spectra.....	168
7.2.2	Electrochemistry of chemically synthesized porphyrins.....	170
7.2.2.1	Ir(CO)Cl compounds.....	176
7.2.2.2	Electrosynthesis of metalated π -extended porphyrins.....	181
7.2.3	Synthesis of fused-freebase porphyrins by electrochemistry.....	198
7.3	Conclusions.....	198
7.4	References.....	200

List of Abbreviation

Abbreviation	Meaning
A	absorbance
CE	counter electrode
CH ₂ Cl ₂	dichloromethane
CV	cyclic voltammetry
DMF	N, N-dimethylformamide
DMSO	dimethylsulfoxide
$\Delta E_{1/2}$	different in half-wave potential
$E_{1/2}$	half-wave potential
E_p	peak potential (by cyclic voltammetry)
E_{pa}	anodic peak potential (by cyclic voltammetry)
E_{pc}	cathodic peak potential (by cyclic voltammetry)
ϵ	molar absorptivity
ESR	electron spin resonance
FTIR	fourier transform infrared
HOMO	highest occupied molecular orbital
i_{pa}	anodic peak current (by cyclic voltammetry)
i_{pc}	cathodic peak current (by cyclic voltammetry)
LUMO	lowest unoccupied molecular orbital
λ_{max}	wavelength at a specific peak maximum
OEP	2, 3, 7, 8, 12, 13, 17, 18-octaethylporphyrin dianion

py	pyridine
PhCN	benzonitrile
PQ _n	quinoxalinoporphyryns, n is the number of quinoxalines
RE	reference electrode
SCE	saturated calomel electrode
TBAP	tetra- <i>n</i> -butylammonium perchlorate
TMP	trimesityltetraphenylporphyrin dianion
TFA	trifluoroacetic acid
TPP	5,10,15,20-tetraphenylporphyrin dianion
WE	working electrode

List of Figures

Figure	Page
Figure 1-1. Core structure of (a) free-base porphyrin with the utilized numbering system at the <i>meso</i> and β pyrrole positions and (b) examples of two commonly studied synthetic porphyrin macrocycles.....	3
Figure 1-2. Scheme of porphyrin ring extension.....	5
Figure 1-3. Examples of β , β - fused (a) quinoxalinoporphyrins and (b) bis-porphyrins.....	6
Figure 1-4. Examples of (a) <i>meso</i> -substituted naphthalene porphyrin and (b) fused naphthalene porphyrin.....	7
Figure 1-5. Examples of (a) β , <i>meso</i> , β - Anthracene fused porphyrin and (b) β , <i>meso</i> , β - bis-porphyrin.	8
Figure 2-1. Schematic illustration of the electrochemical cell. WE, CE and RE are the working, counter and reference electrodes, respectively.....	20
Figure 2-2. Schematic illustration of cyclic voltammetry excitation signal.....	21
Figure 2-3. Schematic illustration of cyclic voltammogram.....	23
Figure 2-4. Schematic illustration of the electrochemical cell for bulk electrolysis. a) platinum tipped electrode, b) magnetic stirring bar, c) fine frit disk, d) platinum net, and e) glass stopcock. WE, CE, and RE are the working, counter and reference electrodes, respectively.....	25

Figure 2-5.	Schematic illustration of the thin-layer UV-visible spectroelectrochemical cell. a) platinum tipped bridge and b) platinum net. WE, CE and RE are the working, counter and reference electrodes, respectively.....	27
Figure 2-6.	Illustration of UV-vis spectra change during titration.....	30
Figure 3-1.	Cyclic voltammograms of gold porphyrins in CH ₂ Cl ₂ containing 0.1 M TBAP.....	40
Figure 3-2.	UV-visible spectra of gold(III) porphyrins in solutions of CH ₂ Cl ₂ containing 0.1 M TBAP. (a) before electroreduction, (b) after electroreduction in the same solution and (c) after electroreduction in the same solution with 2-5 equiv. TFA.....	42
Figure 3-3.	Cyclic voltammograms of Au(PQ) ⁺ in PhCN with 1.5 equivalent of TFA containing 0.1 M TBAP. Scan rate = 0.1 V/s.....	44
Figure 3-4.	UV-vis spectral changes for Au(PQ) ⁺ in CH ₂ Cl ₂ containing 0.1 M TBAP and ~2 equivalents of TFA during reduction at (a) -0.50, (b) -0.80 and (c) -1.25 V.....	47
Figure 3-5.	UV-vis spectral changes of Au(QPQ) ⁺ in CH ₂ Cl ₂ , 0.1 M TBAP during the first and second reductions under application of the indicated potentials.	51
Figure 3-6.	Cyclic voltammograms of Au(QPQ) ⁺ in CH ₂ Cl ₂ containing 0.1 M TBAP and added TFA. Scan rate = 0.1 V/s.....	53

Figure 3-7.	Cyclic voltammograms showing Au(III) reductions of Au(QPQ) ⁺ in CH ₂ Cl ₂ containing 0.1 M TBAP (a) before and (b) after 2.5 equivalents of TFA have been added to solution.	55
Figure 3-8.	UV-vis spectral changes of Au(QPQ)PF ₆ in CH ₂ Cl ₂ containing 0.1 M TBAP and ~3 equivalents of TFA during reduction at (a) -0.30, (b) -0.60 and (c) -0.80 V.....	59
Figure 4-1.	Cyclic voltammograms of Au(III) quinoxalinoporphyrins which undergo (a) 2-3 reductions and (b) 4-5 reductions in CH ₂ Cl ₂ containing 0.1 M TBAP.....	75
Figure 4-2.	Plots of redox potentials of Au ^{III} (PQ _n) ⁺ in CH ₂ Cl ₂ vs the number of quinoxaline groups, where ● represents of P, PQ, and QPQ and ○ represents PQ ₂ , PQ ₃ , and PQ ₄	78
Figure 4-3.	UV-visible spectra of (a) Au ^{III} (P) ⁺ , Au ^{III} (PQ) ⁺ Au ^{III} (QPQ) ⁺ and (b)Au ^{III} (PQ ₂) ⁺ , Au ^{III} (PQ ₃) ⁺ , and Au ^{III} (PQ ₄) ⁺ in CH ₂ Cl ₂ , 0.1 M TBAP.....	83
Figure 4-4.	Plots of energy for the Soret and two visible bands of Au ^{III} (PQ _n) ⁺ vs the number of Q groups on the macrocycle for P, PQ, and QPQ (black solid points) and PQ ₂ , PQ ₃ , and PQ ₄ (red open points).....	84
Figure 4-5.	Thin-layer UV-visible spectral changes of Au ^{III} (PQ ₂)PF ₆ , Au ^{III} (PQ ₃)PF ₆ , and Au ^{III} (PQ ₄)PF ₆ in CH ₂ Cl ₂ containing 0.1 M TBAP during the reductions at indicated potential.	86

Figure 4-6.	Comparisons of the UV-visible spectra of $\text{Au}^{\text{II}}(\text{PQ}_n)$, $\text{Zn}^{\text{II}}(\text{PQ}_n)$, and $\text{Pd}^{\text{II}}(\text{PQ}_n)$ ($n = 3$ and 4) in CH_2Cl_2 containing 0.1 M TBAP	87
Figure 4-7.	Cyclic voltammograms of (a) $\text{Au}^{\text{III}}(\text{PQ}_2)^+$, (b) $\text{Au}^{\text{III}}(\text{PQ}_3)^+$, and (c) $\text{Au}^{\text{III}}(\text{PQ}_4)^+$ in CH_2Cl_2 containing 0.1 M TBAP in the absence and presence of $2.5, 3.5$ or 4.5 eq added TFA.....	90
Figure 4-8.	Thin-layer UV-visible spectral changes of $\text{Au}(\text{PQ}_2)^+$ during reductions at (a) -0.30 (b) -0.55 , (c) -0.90 , and (d) -1.35 V in CH_2Cl_2 containing 0.1 M TBAP and 2.5 eq added TFA.....	95
Figure 4-9.	Thin-layer UV-visible spectral changes of $\text{Au}(\text{PQ}_3)^+$ during reductions at (a) -0.25 (b) -0.40 , (c) -0.60 , and (d) -0.80 V in CH_2Cl_2 containing 0.1 M TBAP and 3.5 eq added TFA.....	96
Figure 4-10.	UV-visible spectra of $\text{Au}^{\text{III}}(\text{PQ}_4)^+$ and its stepwise reduction products in CH_2Cl_2 containing 0.1 M TBAP and 4.5 equivalents added TFA.....	97
Figure 5-1.	Cyclic voltammograms of $\text{H}_2(\text{P})$, $\text{H}_2(\text{PQ})$ and $\text{H}_2(\text{PTA})$ in PhCN containing 0.1 M TBAP . Scan rate = 0.1 V/s . The reductions labelled with an asterisk are associated with a ‘side reaction’ involving a protonated form of the reduced porphyrin.	107
Figure 5-2.	Cyclic voltammograms of $\text{H}_2(\text{P})$, $\text{H}_2(\text{PQ})$ and $\text{H}_2(\text{PTA})$ in pyridine containing 0.1 M TBAP	109

Figure 5-3.	UV-visible spectral changes obtained during the first two controlled potential reductions of (a) H ₂ (PTA) and (b) H ₂ (PQ) at the indicated potential in PhCN, 0.1 M TBAP.....	113
Figure 5-4.	Cyclic voltammograms of (a) Cu(PTA) and (b) Zn(PTA) in PhCN containing 0.1 M TBAP. Scan rate = 0.1 V/s. The reduction labeled with an asterisk is associated with a ‘side reaction’ involving a protonated form of the reduced porphyrin.	116
Figure 5-5.	UV-visible spectral changes obtained during controlled potential reductions of (a) (PTA)Zn and (b) (PTA)Cu at the indicated potential in PhCN, 0.1 M TBAP.....	118
Figure 5-6.	Cyclic voltammograms showing porphyrin ring-centered reductions of (a) H ₂ (P), (b) H ₂ (PTA), and (c) H ₂ (P)-TA-(P) H ₂ in pyridine containing 0.1 M TBAP.....	120
Figure 5-7.	UV-visible spectral changes of H ₂ (P)-TA-(P)H ₂ during reductions in PhCN containing 0.1 M TBAP.....	124
Figure 5-8.	Cyclic voltammograms showing reductions of M(P) and M(P)-TA-(P)M in PhCN containing 0.1 M TBAP.....	126
Figure 5-9.	UV-visible spectral changes during the controlled potential reductions of (a) Cu(P)-TA-(P)Cu and (b) Pd(P)-TA-(P)Pd in PhCN, 0.1 M TBAP.....	128

Figure 6-1.	Cyclic voltammograms of 1-4 in (a) CH ₂ Cl ₂ and (b) PhCN containing 0.1 M TBAP. Scan rate = 0.1 V/s.....	140
Figure 6-2.	UV-visible spectral changes of (a) Fused-Ni 4 and (b) Open-Ni 3 during the controlled potential reduction at in PhCN containing 0.1 M TBAP.....	146
Figure 6-3.	UV-visible spectral changes of Fused-Ni 4 during the controlled potential oxidations at (a) 0.90 V, (b) 1.20 V, and (c) 1.75 V in PhCN containing 0.1 M TBAP.....	148
Figure 6-4.	(a) Thin-layer cyclic voltammograms of Open-Ni 3 in PhCN containing 0.1 M TBAP at a scan rate of 20 mV/s and (b) stepwise UV-visible spectral changes of Open-Ni 3 during the indicated applied potential under the same solution conditions.....	153
Figure 7-1.	Cyclic voltammograms of the chemically synthesized π -extended porphyrins in CH ₂ Cl ₂ , 0.1 M TBAP. The $\Delta E_{1/2}$ between the various redox progresses is also given in the figure.....	171
Figure 7-2.	Cyclic voltammograms illustrating the reduction and oxidation of porphyrins with TMP and fused macrocycles in PhCN, 0.1 M TBAP. The $\Delta E_{1/2}$ between the two reversible redox progresses (the HOMO-LUMO gap) is also given in the figure.....	174
Figure 7-3.	UV-visible spectral changes obtained during the first reduction of (a) TMP-Ir(CO)Cl, (b) Open-Ir(CO)Cl, and (c) Fused-Ir(CO)Cl in PhCN, 0.1 M TBAP.....	178

Figure 7-4.	Cyclic voltammograms of Ir(CO)Cl centered orphyrins with TMP and Fused macrocycles in PhCN, 0.1 M TBAP.....	180
Figure 7-5.	Cyclic voltammograms showing electrochemically induced generation of the fused Zn(II) complex from the porphyrin dication of the related open macrocycle (a) after initial positive scans from 0.0 to 1.50 V and (b) after an initial negative scan from 1.50 to 0.0 V in PhCN, 0.1 M TBAP, scan rate = 0.1 V/s. For comparison, a cyclic voltammograms of the chemically generated Zn(II) porphyrin with the fused π -extended system is shown in part c.....	183
Figure 7-6.	UV-visible spectrum of Open-InCl and Fused-InCl in PhCN, 0.1 M TBAP (a) before electrochemistry, (b) after a two electron oxidation, and (c) after a two electron rereduction of the doubly oxidized species.....	187
Figure 7-7.	UV-visible spectral changes (a) during oxidation of Open-Ir(CO)Cl in a thin-layer cell at an applied potential of 1.60 V, (b) after rereduction of the above compound at $E_{app} = 0.00$ V to electrogenerate the neutral fused compounds in PhCN, 0.1 M TBAP, and (c) UV-vis spectra of the chemically synthesized Fused-Ir(CO)Cl under the same solution condition.....	190
Figure 7-8.	Cyclic voltammogram of (a) naphthalene and TMP-H ₂ , (b) Open-H ₂ and (c) Fused-H ₂ in CH ₂ Cl ₂ , 0.1 M TBAP.....	194

Figure 7-9. UV-visible spectrum of (a) Open-H₂ during oxidation and rereduction in CH₂Cl₂, 0.1 M TBAP and (b) Fused-H₂ before (—) and (-----) after addition of TFA in CH₂Cl₂..... 196

List of Tables

Table		Page
Table 3-1.	UV-visible spectral data and reduction potentials (V vs SCE) of Au(III) porphyrins in CH ₂ Cl ₂ containing 0.1 M TBAP and added TFA.....	61
Table 3-2.	UV-visible spectral data and reduction potentials (V vs SCE) of Au(II) porphyrins in CH ₂ Cl ₂ containing 0.1 M TBAP and added TFA.....	62
Table 4-1.	Half-wave potentials (V vs SCE) of Au ^{III} (PQ _n) PF ₆ (n = 0-4) in CH ₂ Cl ₂ , Pyridine, and THF, 0.1 M TBAP.....	76
Table 4-2.	Reduction potentials (V vs SCE) of Au ^{III} (PQ _n) ⁺ , Au ^{III} (PQ _n H _n) ⁺ , and Au ^{II} (PQ _n H _n) in CH ₂ Cl ₂ , 0.1 M TBAP with added TFA.....	92
Table 5-1.	Half-wave potentials (V vs SCE) of mono-porphyrins M(PTA), M(PQ) and M(P), where M = H ₂ , Cu, or Zn in different solvents containing 0.1 M TBAP.....	111
Table 5-2.	Half-wave potentials (V vs SCE) of bis-porphyrins M(P)-TA-(P)M in different solvents containing 0.1 M TBAP.....	121
Table 6-1.	Half-wave or peak potentials (V vs SCE) and proposed site of electron transfer for redox reactions of investigated porphyrins in CH ₂ Cl ₂ and PhCN containing 0.1 M TBAP. Scan rate =0.1 V/s.....	139
Table 7-1.	UV-vis spectral data of neutral investigated porphyrins in CH ₂ Cl ₂ , 0.1 M TBAP.....	169

Table 7-2. Half-wave or peak potentials (V vs SCE) in PhCN, containing 0.1

M TBAP..... 173

List of Schemes

Scheme	Page
Scheme 3-1. Proposed reduction/oxidation mechanism of Au(PQ)^+ in nonaqueous media containing TFA. The compounds in bold undergo the $\text{Au}^{\text{III}}/\text{Au}^{\text{II}}$ process. The listed potentials were measured in PhCN, 0.1 M TBAP.....	48
Scheme 3-2. Proposed reduction/oxidation mechanism of Au(QPQ)^+ in nonaqueous media containing TFA. The listed potentials were measured in CH_2Cl_2 . The compounds in bold undergo the $\text{Au}^{\text{III}}/\text{Au}^{\text{II}}$ process.....	56
Scheme 3-3. Soret band maximum of investigated compounds.....	63
Scheme 4-1. Published mechanism for the reduction of $\text{Au}^{\text{III}}(\text{PQ})^+$ in nonaqueous media containing TFA.....	72
Scheme 4-2. Proposed mechanism for first three reductions of $\text{Au}^{\text{III}}(\text{PQ}_2)^+$, $\text{Au}^{\text{III}}(\text{PQ}_3)^+$, and $\text{Au}^{\text{III}}(\text{PQ}_4)^+$ in CH_2Cl_2	81
Scheme 4-3. Proposed reduction/oxidation mechanism of $\text{Au(PQ}_2)^+$, $\text{Au(PQ}_3)^+$ and $\text{Au}^{\text{III}}(\text{PQ}_4)^+$ in CH_2Cl_2 containing 2.5, 3.5, or 4.5 equivalents TFA.....	89
Scheme 6-1. Proposed mechanism for the reversible conversion between compound Open-Ni 3 and Fused-Ni 4	155
Scheme 7-1. Electrosynthesis mechanism for conversion of Open porphyrin to the Fused porphyrin.....	186

Scheme 7-2. Electrosynthesis mechanism for conversion of Open-H₂ porphyrin to [Fused-H₄]²⁺ porphyrin..... 197

Chapter One

Introduction

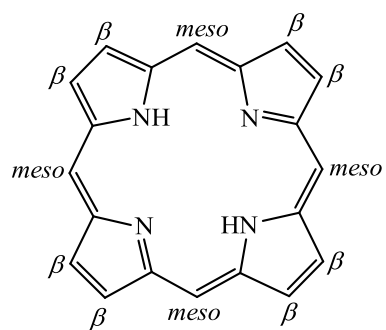
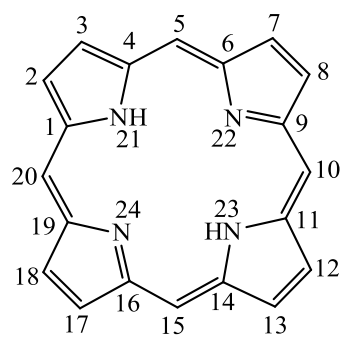
1.1 Porphyrins

Porphyrins and structurally related porphyrinoids occur widely in nature and play important roles in applications ranging from materials to biological processes.¹ Metalloporphyrins participate in a wide range of biological processes, including oxygen transport, electron transfer, energy conversion, and biological oxidation.^{2,3}

Porphyrins are aromatic macrocyclic compounds which consist of four pyrrole rings connected via carbon methane bridges (Figure 1-1). The peripheral positions of a porphyrin macrocycle may be substituted by electron-donating or electron-withdrawing groups to form different porphyrin derivatives. There are two kinds of substitution positions on a porphyrin ring. One is at the four methine bridges of the macrocycle which are defined as the *meso* position (labeled as 5, 10, 15, and 20 in Figure 1-1a) and the other is at the eight β -pyrrole positions of the macrocycle (labeled as 2, 3, 7, 8, 12, 13, 17, and 18 in Figure 1-1a).

The porphyrin macrocycle contains 22 π electrons, but only 18 of them are involved in the delocalization. As they obey Huckel's rule ($(4n+2) \pi$ electrons where $n \geq 2$), porphyrins have a highly conjugated π -ring system and aromatic properties.⁴⁻⁶ All twelve peripheral positions of the porphyrin macrocycle can be substituted by the same or different groups to form different porphyrin derivatives. Two examples of the most commonly studied synthetic porphyrins are given in Figure 1-1b. There are tetraphenylporphyrin (TPP) H_2 and octaethylporphyrin (OEP) H_2 .

(a) Porphyrin



(b) *meso*/ β -Substituted Porphyrin

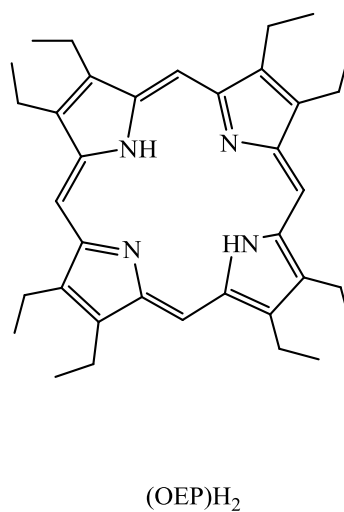
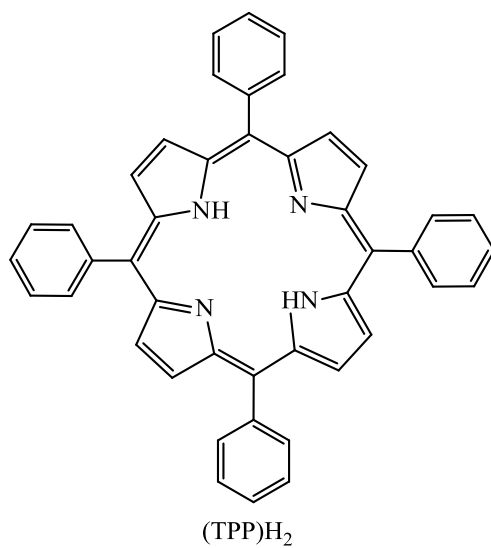


Figure 1-1. Core structure of (a) free-base porphyrin with the utilized numbering system at the *meso* and β pyrrole positions and (b) examples of two commonly studied synthetic porphyrin macrocycles.

1.2 π -Extended porphyrins

The fusion of aromatic rings to a porphyrin core has received much attention in recent years.⁷⁻¹⁹ The unusual optical and electronic properties of these π -expanded porphyrins make them interesting for a variety of applications, including photodynamic therapy,²⁰ two-photon absorption,²¹ nonlinear optics,^{15,22,23} and photovoltaics.^{13,24,25}

A variety of π -extended porphyrins have been synthesized by fusing benzene,²⁶⁻³⁰ naphthalene,^{14,16,24} pyrene,⁸ azulene,¹⁰ and anthracene^{7,11} across the *meso*- and/or β -positions of the porphyrin macrocycle in several different ways (see Figure 1-2). Examples of β , β -fused quinoxalinoporphyrins having 1-4 fused quinoxaline groups are shown in Figure 1-3a, while Figure 1-3b illustrates a bis-porphyrin with a fused tetraazaanthracene bridge. These six types of macrocycles with different metal ions are characterized in Chapters Three, Four, and Five of this dissertation.

Conjugated ring system can be fused to porphyrins at adjacent *meso*, β -positions to give a π extended porphyrin. An example of a fused naphthalene porphyrin is given in Figure 1-4 along with a *meso*-substituted naphthalene porphyrin. These two types of macrocycles are examined in Chapters Six and Seven. A third example of a fused porphyrins is one with fusion of a ring system at the β , *meso*, and β -positions,³¹ but this type of compound is not characterized in this dissertation.

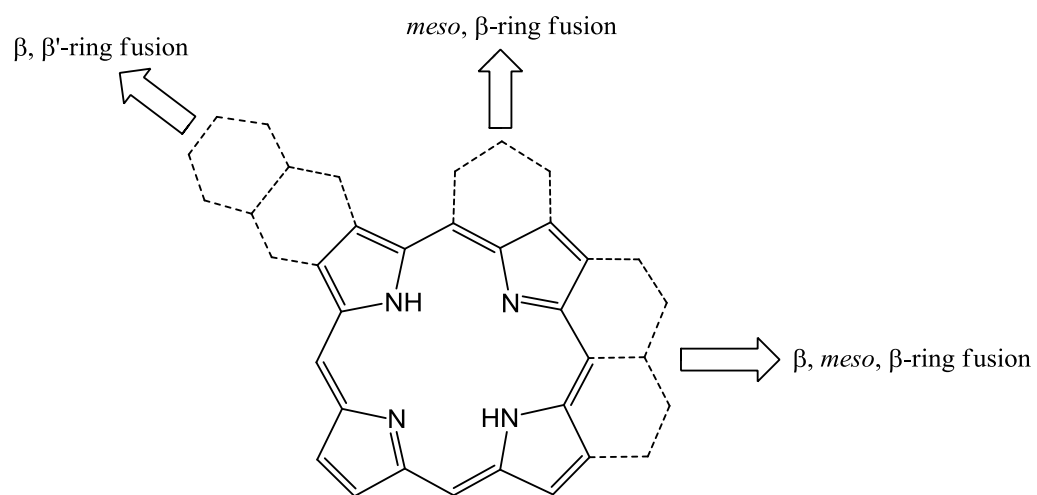
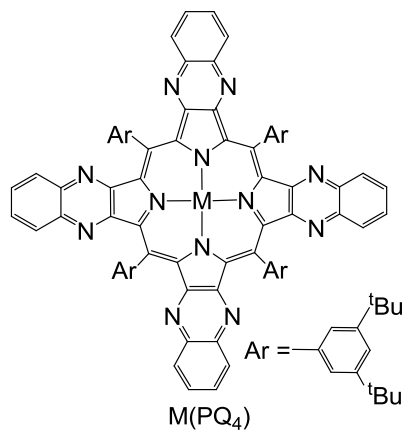
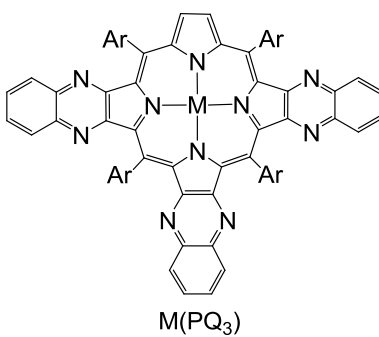
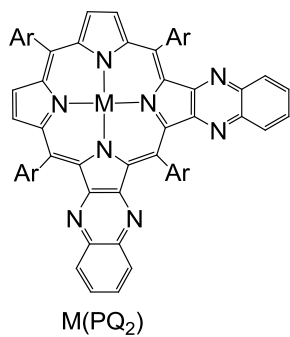
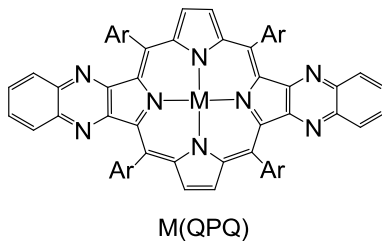
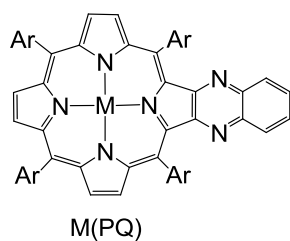


Figure 1-2. Scheme of porphyrin ring extension.

(a) Quinoxalinoporphyrin



(b) Bis-porphyrin

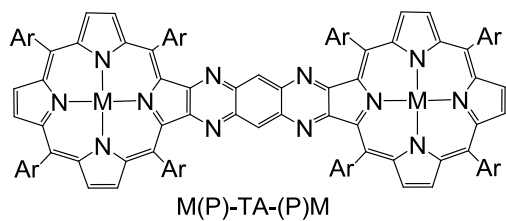


Figure 1-3. Examples of β , β - fused (a) quinoxalinoporphyryns and (b) bis-porphyrins.

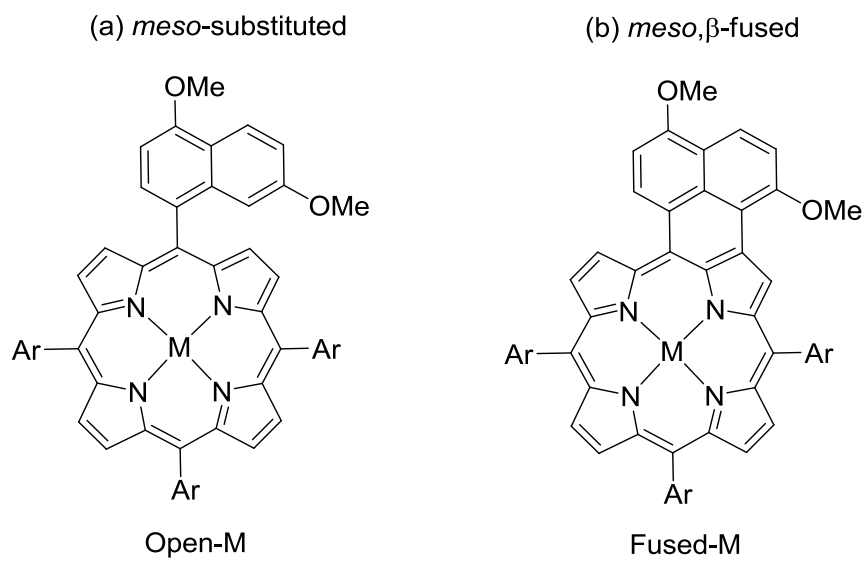


Figure 1-4. Examples of (a) *meso*-substituted naphthalene porphyrin and (b) fused naphthalene porphyrin

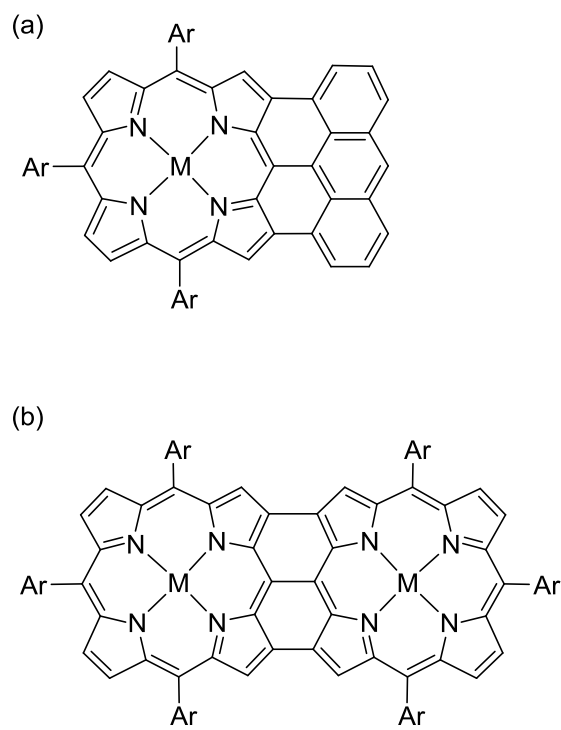


Figure 1-5. Examples of (a) β , *meso*, β - anthracene fused porphyrin and (b) β , *meso*, β -bis-porphyrin.³¹

1.3 Electrochemistry

The electrochemistry of metalloporphyrins can be described according to the nature of the central metal ion or the nature of porphyrin macrocycle, since the majority of metalloporphyrin electrochemistry involves electron addition or electron abstraction at the central metal ion or the conjugated π -ring system of the macrocycle.

Virtually all known metalloporphyrins are electroactive and virtually all exhibit three or more electron transfer reactions in nonaqueous media, with the exact number of processes depending on the potential range of the utilized electrochemical solvent, the type of macrocycle, the type of central metal ion, and/or the type of axially coordinated ligand(s). The metalloporphyrin electrooxidation or electroreduction will, in the vast majority of cases, involve either the central metal ion or the conjugated π -ring system of the macrocycle. However, some electrode reactions might also involve a coordinated axial ligand or an electroactive group which is linked to the porphyrin macrocycle.

Most metalloporphyrins with electroinactive central metal ions (such as Zn^{II} and Cu^{II}) are known to undergo two oxidations and two reductions in nonaqueous media, all of which occur at the conjugated π -ring system of the porphyrin macrocycle as shown in Equations 1-1 to 1-4. Electrode reactions involving the porphyrin π -ring system will most often be reversible on the time scale of the voltammetric measurement, but each electrogenerated metalloporphyrin will have a different degree of stability in its cationic or anionic form, depending on the specific macrocycle which may or may not undergo a variety of chemical reactions after oxidation or reduction, leading in some cases to an irreversibility of the overall electron transfer process.



The redox reactions may also occur at the central metal ions, the most common example being for complexes of Fe, Co, Mn, Cr, and Au. The oxidation state of the central metal ion will most often vary between +4 and +2, although higher and lower oxidation states are possible. Electrooxidation or reduction can in some cases yield a change in the oxidation state of the central metal ion with the values of the redox potentials depending on the specific central metal ion, the size of porphyrin π system, the substituents on the macrocycle, and the selected solvent-supporting electrolyte.

Irreversible electron transfer processes are sometimes observed on the electrochemical timescale. Irreversible electron transfers can be observed for several different reasons, examples being: (1) when the product of the electron transfer reacts with the solvent or a component in the solution, (2) when radical coupling occurs, (3) when there is intermolecular electron transfer between the central metal ion and the porphyrin macrocycle, (4) when the generated anion reacts with protons in solvent, (5) when the dication reacts with nucleophiles in the solvent and (6) when intermolecular coupling reaction occurs between two electrooxidation or electron reduction units on the porphyrin. Some examples for these irreversible reactions will be described in this dissertation.

1.4 Spectroelectrochemistry

Spectroelectrochemistry is a useful technique which combines electrochemistry with in situ spectroscopic measurements such as UV-visible, FTIR, or ESR. Studies of the spectral changes have often been used to distinguish metal-centered reactions from ring-centered ones in metalloporphyrins. Generally, metal-centered reactions (oxidation or reduction) of a porphyrin will lead to red or blue shifts in the most intense UV-visible band located between 400 to 500 nm (the Soret band), but with little loss of molar absorptivity of this band. In contrast, when the electron transferred site is the porphyrin conjugated π -ring system, there is often a significant decrease in intensity of the Soret band along with the appearance of new weak, broad visible or near-IR bands located between 600-900 nm. These types of spectra changes indicated formation of a porphyrin π anion or cation radical.³²⁻³⁴

1.5 Quinoxalinoporphyrin

Quinoxalinoporphyrins, whose structures are shown in Figure 1-3, are porphyrins having quinoxaline groups fused on one or more adjacent β , β -positions. The extent of coupling or communication between the porphyrin and the fused aromatic system is an important property that will control the use that can be made of these compounds in molecular electronics, either of the “single” quinoxalinoporphyrin or in more extended oligoporphyrin systems that have aromatic bridging units.³⁵

For the compounds examined in this dissertation, the starting porphyrins without the quinoxaline group is represented as M(P), and the simplest fused complex is represented as M(PQ), (see Figure 1-3a). Bis-quinoxalinoporphyrins are presented by two types of compounds, “linear” M(QPQ) and “corner” M(PQ₂). Compounds with

three fused quinoxaline groups are represented as (PQ₃)M, and those with four quinoxaline groups are represented as (PQ₄)M.

In a previous studies from our laboratories,³⁶⁻³⁹ it was demonstrated that fusion of one or more quinoxaline groups to the β,β' -pyrrolic units of (P)M has only a minimal effect on the oxidation potentials.^{37,39-43} In contrast, the reductions are positively shifted in potential by 90-190 mV per each fused quinoxaline group, with the exact magnitude of the shift depending upon the solvent, type, and oxidation state of the central metal ion and number of fused quinoxaline groups on the porphyrin macrocycle, which may vary from one to four, as shown in Figure 1-3a. The site of electron transfer in free-base quinoxalinoporphyrins and quinoxalinoporphyrins containing non-redox active transition metal ions involves primarily the conjugated π -ring system of the porphyrin macrocycle. But some electron density is located on the quinoxaline part of the molecule after reduction,⁴⁰⁻⁴² especially in solutions containing added protons or scandium(III) ions, both of which will bind or ion pair with the quinoxaline nitrogen atoms.

Understanding the most important factors which affect the site of electron transfer in quinoxalinoporphyrins is of vital interest to tune and direct the chemical reactivity of larger arrays containing the quinoxalinoporphyrin unit.⁴⁴ This is especially true in the case of redox active transition metal derivatives; where the porphyrin central metal ion can be stepwise cycled between its M^I, M^{II}, and M^{III} oxidation states or even between the M^{IV} and M^V forms of the compound with changes in the applied potential or changes in the type and number of bound axial ligands.^{43,45,46}

As will be shown in this dissertation, protonation of the quinoxaline nitrogen atoms can also have a significant effect on the electrochemical behavior of

quinoxainoporphyrins.^{39,47} Because the fused quinoxaline groups can directly interact with the porphyrin π -ring system⁴⁸⁻⁵⁰ one might reasonably predict that the largest effect of protonation would be observed for ring-centered reductions and the smallest for metal-centered redox processes. The protonation of the quinoxaline nitrogens will also affect the site of electron transfer and the reduction mechanism of quinoxalinoporphyrins with redox active central metal ions.

1.6 Bis-porphyrins

Tetraazaanthracene (TA) can be used as a bridge to fuse two porphyrin macrocycles, linking them in a linear fashion. One example is the TA-linked bis-porphyrin is shown in Figure 1-3b. The tetraazaanthracene (TA) bridging unit confines the appended M(P) macrocycles in a rigid coplanar arrangement.

Bis-porphyrins show a rich electrochemistry in nonaqueous media, with electron transfer reactions occurring in some cases at the conjugated π -ring system of the two macrocycles and in others at the central metal ions. Each TA-linked bis-porphyrin exhibits a strong interaction between the two electroactive macrocycles, the magnitude of which is dependent upon the specific metal ion.³⁶

1.7 Naphthalene-fused porphyrin

The structure of a naphthalene-fused porphyrinoid is shown in Figure 1-4. The fused naphthalene group leads to a broadened absorption spectrum for the compounds along with an increased intensity of the porphyrin Q bands which are located at 500 to 900 nm. Porphyrins are relatively rich in electrons, and introducing additional aromatic rings bearing electron-donating substituents causes a further increase in electron density.

As will be shown in this dissertation, metalloporphyrins bearing one electron-rich naphthalene moiety can be converted to a fused naphthalene porphyrin with a two electron oxidation. The overall process initially involves two stepwise one-electron oxidations, the first at the porphyrin π ring system and the second at the electron-rich naphthalene moiety, followed by an intramolecular oxidative aromatic coupling to give the electrooxidized π -extended porphyrin.

1.8 Outline of dissertation

A brief description of each chapter is given below. There are seven chapters, in which more than 30 complexes are characterized by electrochemistry and spectroelectrochemistry in nonaqueous media. Chapter One gives an introduction to π -extended porphyrins and Chapter Two describes experimental methods used in this dissertation. Chapters Three and Four examine the electrochemical and spectroelectrochemical properties of gold(III) quinoxalinoporphyrins in neutral and nonaqueous media. Chapter Five focuses on the characterization of bisporphyrins while Chapters Six and Seven report the electrochemistry and spectroscopic properties of chemically synthesized naphthalene substituted and naphthalene fused porphyrins. The electrosynthesis of fused naphthalene porphyrins is also described in Chapters Six and Seven.

1.9 References

- (1) Kadish, K. M.; Smith, K. M.; Guillard, R. *Handbook of Porphyrin Science*; World Scientific: Singapore, 2012; Vol. 15.
- (2) Kadish, K. M.; Smith, K. M.; Guillard, R. *The Porphyrin Handbook*; Academic: New York, 2000; Vol. 4.
- (3) Kalish, H.; Lee, H. M.; Olmstead, M. M.; Latos-Grazynski, L.-I.; Rath, S. P.; Balch, A. L. *J. Am. Chem. Soc.* **2003**, *125*, 4674.
- (4) Webb, L. E.; Fleischer, E. B. *J. Am. Chem. Soc.* **1965**, *87*, 667.
- (5) Brueckner, C.; Barta, C. A.; Brinas, R. P.; Bauer, J. A. K. *Inorg. Chem.* **2003**, *42*, 1673.
- (6) Bonnett, R. In *The Porphyrins*; Dolphin, D., Ed.; Academic: New York, 2000; Vol. 1.
- (7) Davis, N. K. S.; Thompson, A. L.; Anderson, H. L. *Org. Lett.* **2010**, *12*, 2124.
- (8) Yamane, O.; Sugiura, K.-i.; Miyasaka, H.; Nakamura, K.; Fujimoto, T.; Nakamura, K.; Kaneda, T.; Sakata, Y.; Yamashita, M. *Chem. Lett.* **2004**, *33*, 40.
- (9) Tokuji, S.; Takahashi, Y.; Shinmori, H.; Shinokubo, H.; Osuka, A. *Chem. Commun.* **2009**, 1028.
- (10) Kurotobi, K.; Kim, K. S.; Noh, S. B.; Kim, D.; Osuka, A. *Angew. Chem., Int. Ed.* **2006**, *45*, 3944.
- (11) Davis, N. K. S.; Pawlicki, M.; Anderson, H. L. *Org. Lett.* **2008**, *10*, 3945.
- (12) Jimenez, A. J.; Jeandon, C.; Gisselbrecht, J.-P.; Ruppert, R. *Eur. J. Org. Chem.* **2009**, 5725.
- (13) Hayashi, S.; Tanaka, M.; Hayashi, H.; Eu, S.; Umeyama, T.; Matano, Y.; Araki, Y.; Imahori, H. *J. Phys. Chem. C* **2008**, *112*, 15576.
- (14) Gill, H. S.; Harmjanz, M.; Santamaria, J.; Finger, I.; Scott, M. J. *Angew. Chem., Int. Ed.* **2004**, *43*, 485.
- (15) Aratani, N.; Kim, D.; Osuka, A. *Chem. - Asian J.* **2009**, *4*, 1172.
- (16) Cammidge, A. N.; Scaife, P. J.; Berber, G.; Hughes, D. L. *Org. Lett.* **2005**, *7*, 3413.

- (17) Sooambar, C.; Troiani, V.; Bruno, C.; Marcaccio, M.; Paolucci, F.; Listorti, A.; Belbakra, A.; Armaroli, N.; Magistrato, A.; De Zorzi, R.; Geremia, S.; Bonifazi, D. *Org. Biomol. Chem.* **2009**, *7*, 2402.
- (18) Lash, T. D.; Werner, T. M.; Thompson, M. L.; Manley, J. M. *J. Org. Chem.* **2001**, *66*, 3152.
- (19) Richeter, S.; Jeandon, C.; Kyritsakas, N.; Ruppert, R.; Callot, H. J. *J. Org. Chem.* **2003**, *68*, 9200.
- (20) Bonnett, R. *Chem. Soc. Rev.* **1995**, *24*, 19.
- (21) Pawlicki, M.; Collins, H. A.; Denning, R. G.; Anderson, H. L. *Angew. Chem., Int. Ed.* **2009**, *48*, 3244.
- (22) Calvete, M.; Yang, G. Y.; Hanack, M. *Synth. Met.* **2004**, *141*, 231..
- (23) Senge, M. O.; Fazekas, M.; Notaras, E. G. A.; Blau, W. J.; Zawadzka, M.; Locos, O. B.; Mhuirheartaigh, E. M. N. *Adv. Mater. (Weinheim, Ger.)* **2007**, *19*, 2737.
- (24) Tanaka, M.; Hayashi, S.; Eu, S.; Umeyama, T.; Matano, Y.; Imahori, H. *Chem. Commun.* **2007**, 2069.
- (25) Mai, C.-L.; Huang, W.-K.; Lu, H.-P.; Lee, C.-W.; Chiu, C.-L.; Liang, Y.-R.; Diao, E. W.-G.; Yeh, C.-Y. *Chem. Commun.* **2010**, *46*, 809.
- (26) Richeter, S.; Jeandon, C.; Gisselbrecht, J.-P.; Ruppert, R.; Callot, H. J. *J. Am. Chem. Soc.* **2002**, *124*, 6168.
- (27) Shen, D.-M.; Liu, C.; Chen, Q.-Y. *Chem. Commun.* **2005**, 4982.
- (28) Hao, E.; Fronczek, F. R.; Vicente, M. G. H. *J. Org. Chem.* **2006**, *71*, 1233.
- (29) Shen, D.-M.; Liu, C.; Chen, Q.-Y. *J. Org. Chem.* **2006**, *71*, 6508.
- (30) Fox, S.; Boyle, R. W. *Tetrahedron* **2006**, *62*, 10039.
- (31) Tsuda, A.; Furuta, H.; Osuka, A. *Angew. Chem., Int. Ed.* **2000**, *39*, 2549.
- (32) Fuhrhop, J. H. *Struct. Bonding (Berlin)* **1974**, *18*, 1.
- (33) Gouterman, M. *J. Mol. Spectrosc.* **1961**, *6*, 138.
- (34) Perrin, M. H.; Gouterman, M.; Perrin, C. L. *J. Chem. Phys.* **1969**, *50*, 4137.
- (35) Reimers, J. R.; Hush, N. S.; Crossley, M. J. *J. Porphyrins Phthalocyanines* **2002**, *6*, 795.

- (36) Ou, Z.; Zhu, W.; Santic, P. J.; Fang, Y.; Crossley, M. J.; Kadish, K. M. *J. Porphyrins Phthalocyanines* **2012**, *16*, 674.
- (37) Zhu, W.; Santic, M.; Ou, Z.; Santic, P. J.; McDonald, J. A.; Brotherhood, P. R.; Crossley, M. J.; Kadish, K. M. *Inorg. Chem.* **2010**, *49*, 1027.
- (38) Kadish, K. M.; E, W.; Santic, P. J.; Ou, Z.; Shao, J.; Ohkubo, K.; Fukuzumi, S.; Govenlock, L. J.; McDonald, J. A.; Try, A. C.; Cai, Z.-L.; Reimers, J. R.; Crossley, M. J. *J. Phys. Chem. B* **2007**, *111*, 8762.
- (39) Ou, Z.; E, W.; Zhu, W.; Thordarson, P.; Santic, P. J.; Crossley, M. J.; Kadish, K. M. *Inorg. Chem.* **2007**, *46*, 10840.
- (40) Fukuzumi, S.; Ohkubo, K.; Zhu, W.; Santic, M.; Khoury, T.; Santic, P. J.; E, W.; Ou, Z.; Crossley, M. J.; Kadish, K. M. *J. Am. Chem. Soc.* **2008**, *130*, 9451.
- (41) Santic, P. J.; E, W.; Ou, Z.; Shao, J.; McDonald, J. A.; Cai, Z.-L.; Kadish, K. M.; Crossley, M. J.; Reimers, J. R. *Phys. Chem. Chem. Phys.* **2008**, *10*, 268.
- (42) Ou, Z.; E, W.; Shao, J.; Burn, P. L.; Sheehan, C. S.; Walton, R.; Kadish, K. M.; Crossley, M. J. *J. Porphyrins Phthalocyanines* **2005**, *9*, 142.
- (43) Ou, Z.; Kadish, K. M.; E, W.; Shao, J.; Santic, P. J.; Ohkubo, K.; Fukuzumi, S.; Crossley, M. J. *Inorg. Chem.* **2004**, *43*, 2078.
- (44) Crossley, M. J.; Santic, P. J.; Walton, R.; Reimers, J. R. *Org. Biomol. Chem.* **2003**, *1*, 2777.
- (45) Kadish, K. M.; Van Caemelbecke, E.; Royal, G. in *The porphyrin Handbook*; Kadish, K. M., Smith, K. M., Guillard, R., Eds.; Academic Press: New York, 2000; Vol. 8, p 1.
- (46) Kadish, K. M. *Prog. Inorg. Chem.* **1986**, *34*, 435.
- (47) Ou, Z.; Zhu, W.; Fang, Y.; Santic, P. J.; Khoury, T.; Crossley, M. J.; Kadish, K. M. *Inorg. Chem.* **2011**, *50*, 12802.
- (48) Ohkubo, K.; Garcia, R.; Santic, P. J.; Khoury, T.; Crossley, M. J.; Kadish, K. M.; Fukuzumi, S. *Chem. - Eur. J.* **2009**, *15*, 10493.
- (49) Crossley, M. J.; Prashar, J. K. *Tetrahedron Lett.* **1997**, *38*, 6751.
- (50) Khoury, T.; Crossley, M. J. *New J. Chem.* **2009**, *33*, 1076.

Chapter Two

Experimental Methods

2.1 Electrochemical Methods

2.1.1 Cyclic voltammetry

Cyclic voltammetry was carried out using an EG&G Princeton Applied Research (PAR) 173 Potentiostat/Galvanostat. A homemade three-electrode cell (Figure 2-1) was used for cyclic voltammetric measurements and consisted of a platinum button or glassy carbon working electrode, a platinum counter electrode and a homemade saturated calomel reference electrode (SCE). The SCE was separated from the bulk of the solution by a fritted glass bridge of low porosity that contained the solvent/supporting electrolyte mixture.

The potential of the working electrode is measured against a reference electrode, and the resulting applied potential produces an excitation signal as shown in Figure 2-2. In the forward scan of Figure 2-2, the potential first scans negatively, starting from point **A** (a larger potential) and ending at a point **C** (lower potential). The potential extreme at point **C** is called the switching potential, and is the point where the voltage is sufficient enough to have caused an oxidation or reduction of an analyt. As reverse the scan from point **C** to point **E**, the potential scans positively. Figure 2-2 shows a typical reduction occurring from **A** to **C** and an oxidation occurring from **C** to **E**. It is important to note that some analyses undergo oxidation first, in which case the potential would first scan positively. This cycle can be repeated, and the scan rate can be varied. The slope of the excitation signal gives the scan rate used.

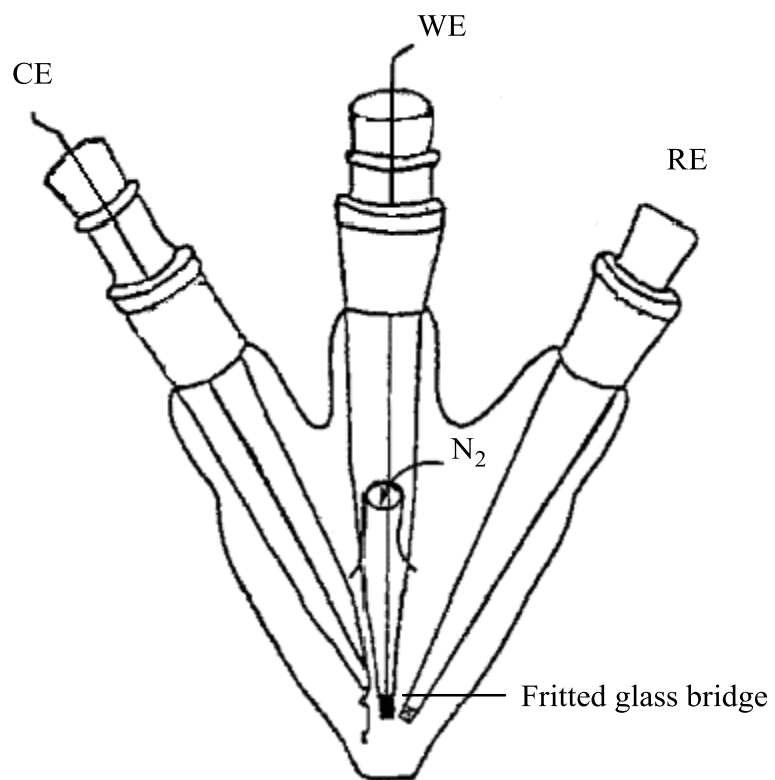


Figure 2-1. Schematic illustration of the electrochemical cell. WE, CE, and RE are the working, counter and reference electrodes, respectively.

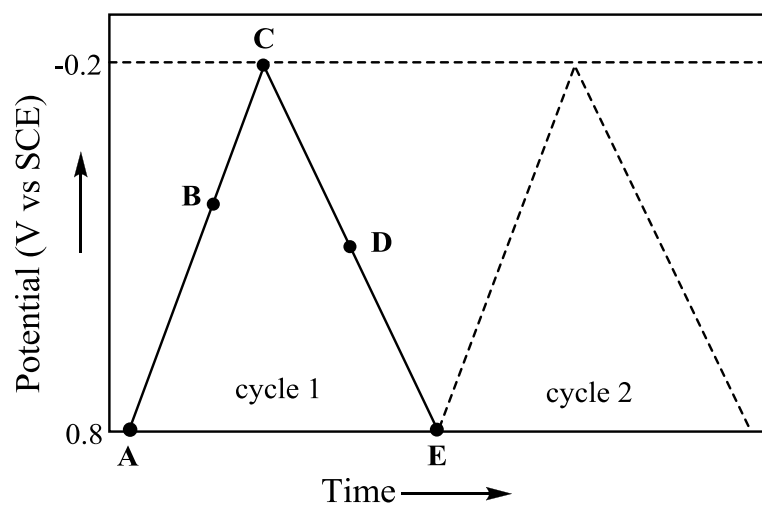
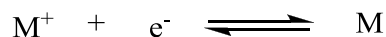


Figure 2-2. Schematic illustration of cyclic voltammetry excitation signal.

A cyclic voltammogram is obtained by measuring the current at the working electrode during the potential scan. Figure 2-3 shows a cyclic voltammogram resulting from a single electron reduction and oxidation as shown below.



In Figure 2-3, the reduction process occurs from point **A** (the initial potential) to **C** (the switching potential). In this region the potential is scanned from positive to negative for reduction. The resulting current is called cathodic current (i_{pc}). The corresponding peak potential occurs at point **B** as cathodic peak potential (E_{pc}). The cathodic peak potential is reached when all of the substrate on electrode surface has been reduced. After point **C** (the switching potential) has been reached, the potential scans positively from point **C** to **E**. This results in anodic current (i_{pa}) and oxidation to occur. The peak potential at point **D** is called the anodic peak potential (E_{pa}), and is reached when all of the substrate at the surface of the electrode has been oxidized.

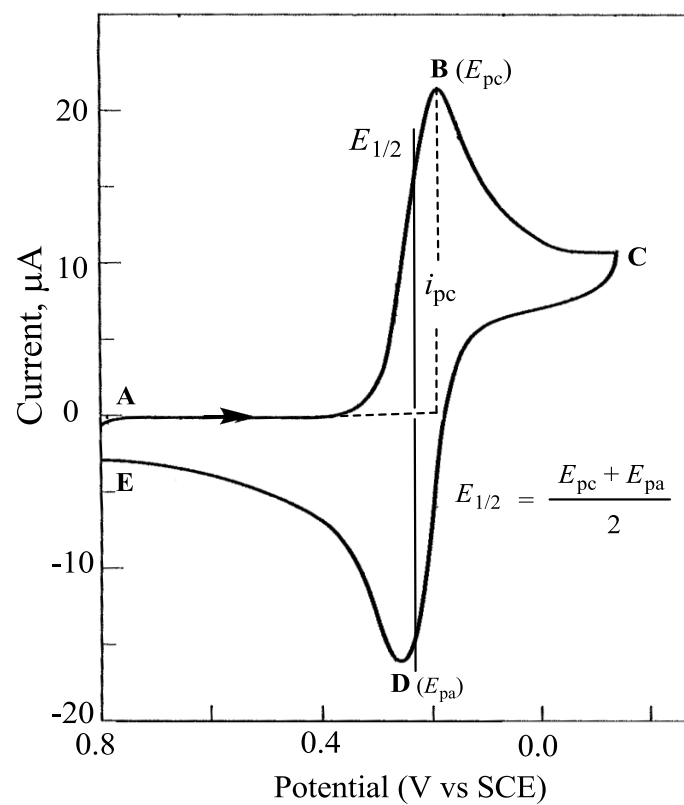


Figure 2-3. Schematic illustration of cyclic voltammogram.

2.1.2 Controlled potential electrolysis

Controlled potential electrolysis was performed with an EG&G PAR 173 Potentiostat/Galvanostat. A homemade "H" type cell (Figure 2-4) with a fritted glass to separate the cathode and anode portions of the cell was used for bulk electrolysis. The working and counter electrodes were made from platinum gauze; the reference electrode was an SCE. The sample and solvent were transferred into the electrolysis cell under nitrogen. The solution was stirred during electrolysis using a Fisher magnetic stirrer. The total quantity of electricity consumed during electrolysis could be obtained from a direct reading of the coulometer or by integration of the current-time (i - t) curve recorded during electrolysis. The number of electrons involved in the electrochemical reaction was calculated according to Faraday's Law.¹

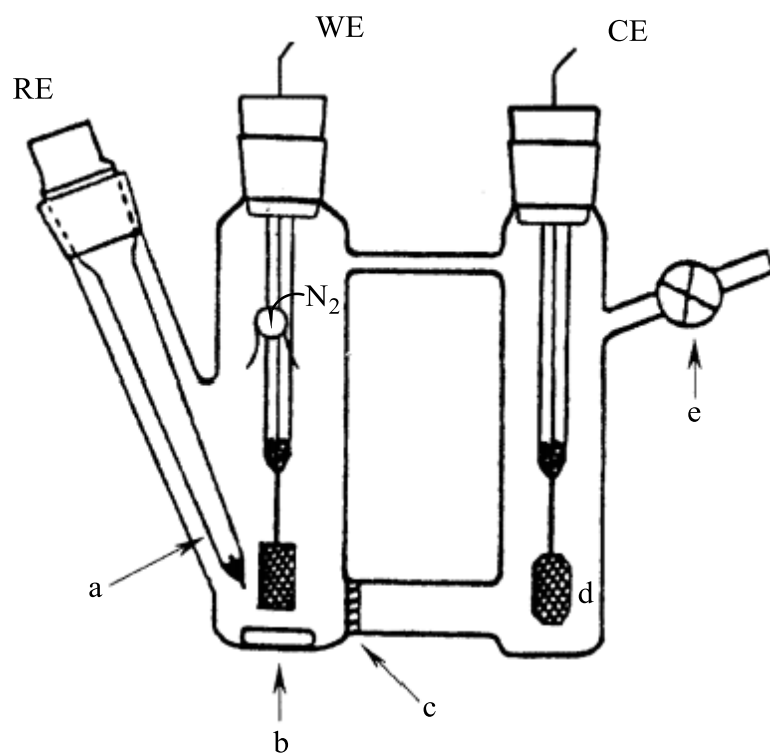


Figure 2-4. Schematic illustration of the electrochemical cell for bulk electrolysis. a) platinum tipped electrode, b) magnetic stirring bar, c) fine frit disk, d) platinum net, and e) glass stopcock. WE, CE, and RE are the working, counter and reference electrodes, respectively.

2.2 Spectroscopic Methods

2.2.1 UV-visible spectroscopy

UV-visible spectroelectrochemical experiments were performed with a home-built thin-layer cell^{2,3} that had a light transparent platinum gauze working electrode (Figure 2-5). Potentials were applied and monitored with an EG&G PAR Model 173 Potentiostat. Time-resolved UV-visible spectra were recorded with a Hewlett-Packard Model 8453 diode array spectrophotometer.

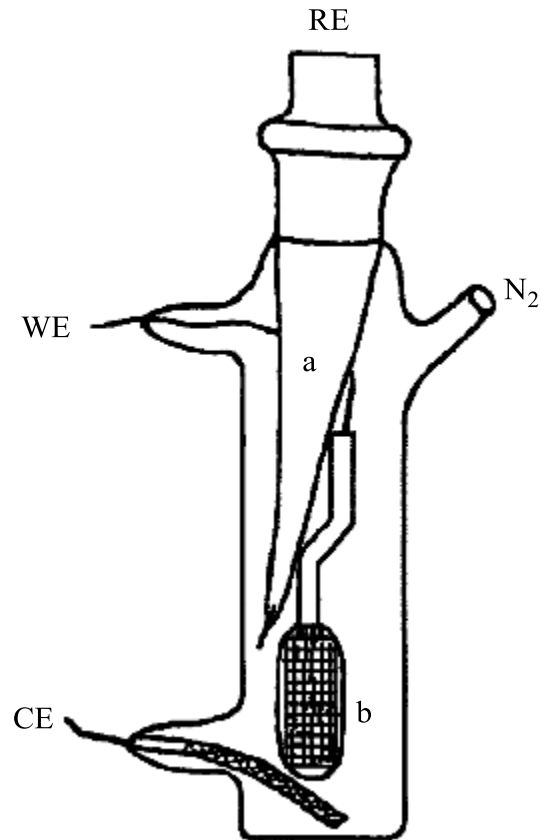


Figure 2-5. Schematic illustration of the thin-layer UV-visible spectroelectrochemical cell. a) platinum tipped bridge and b) platinum net. WE, CE, and RE are the working, counter and reference electrodes, respectively.

2.3 Titration Techniques

Equilibrium constants for the binding of an axial ligand to porphyrin were determined using both spectra and electrochemical titration methods. Stock solutions were prepared for the specific ligand and were quantitatively added to the porphyrin solution. UV-visible absorbance changes or the half-wave potential changes by cyclic voltammetry were recorded as a function of the free ligand concentration in the solution using methods described in the following section to obtain equilibrium constants and the coordination number.

2.3.1 Spectral titration method for determination of equilibrium constants⁴

For the ligand binding reaction: $M + pL = ML_p$, the relationship between the concentration of the species in solution and the equilibrium constant, $\log K$, is given by equation (2-1).

$$\log([ML_p]/[M]) = \log K + p \log [L] \quad (2-1)$$

Where $[M]$ and $[ML_p]$ are the concentration of the unligated and ligated metalloporphyrin species and $[L]$ is the free-ligand concentration in solution. If M and ML_p have different spectra, then we have:

$$A_0 = \epsilon_M b C_M$$

$$A_f = \epsilon_{ML_p} b C_{ML_p}$$

$$A_i = \epsilon_M b [M] + \epsilon_{ML_p} b [ML_p]$$

Where C_M and C_{ML_p} are the total concentration of M or ML_p , ϵ is the molar absorptivity and b is the path length, A_0 and A_f are the initial and final absorbance at a given wavelength (λ_{max}) for the species M and ML_p and A_i is the absorbance at λ_{max} at any point during the titration as shown in Figure 2-6.

According to the mass balance equation: $C_M = C_{ML_p} = [M] + [ML_p]$, we have:

$$\begin{aligned} A_i &= \varepsilon_M b [M] + \varepsilon_{ML_p} b [ML_p] \\ &= \varepsilon_M b (C_M - [ML_p]) + \varepsilon_{ML_p} b [ML_p] \\ &= \varepsilon_M b C_M - \varepsilon_M b [ML_p] + \varepsilon_{ML_p} b [ML_p] \\ &= A_0 + (\varepsilon_{ML_p} b - \varepsilon_M b) [ML_p] \end{aligned}$$

or

$$\begin{aligned} A_i &= \varepsilon_M b [M] + \varepsilon_{ML_p} b [ML_p] \\ &= \varepsilon_M b [M] + \varepsilon_{ML_p} b (C_{ML_p} - [M]) \\ &= \varepsilon_M b [M] + \varepsilon_{ML_p} b C_{ML_p} - \varepsilon_{ML_p} b [M] \end{aligned}$$

$$[M] = (A_f - A_i) / (\varepsilon_{ML_p} b - \varepsilon_M b)$$

Substituting the values of $[M]$ and $[ML_p]$ into equation (2-1) gives a useful result:

$$\log((A_i - A_0)/(A_f - A_i)) = \log K + p \log [L] \quad (2-2)$$

A graph of $\log((A_i - A_0)/(A_f - A_i))$ versus $\log [L]$ should be a straight line whose slope should be equal to the number of ligands (p) axially bound to the metalloporphyrin and the intercept will give the formation constant ($\log K$) as shown in Figure 2-6. The multiple step coordination is defined as $\log \beta_n$ which related to $\log K$ as: $\log \beta_n = \log K_1 \cdot \log K_2 \dots \log K_n$.

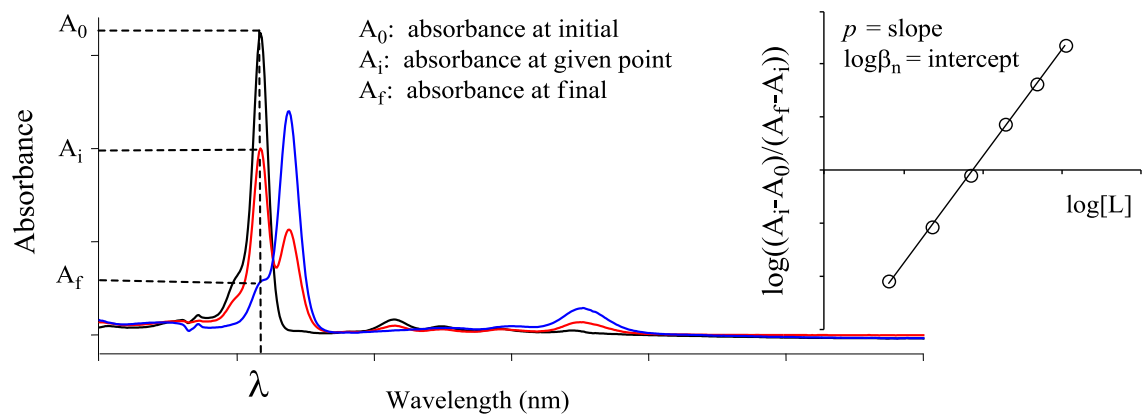


Figure 2-6. Illustration of UV-vis spectra change during titration.

2.4 Other Experimental Methods

2.4.1 Degassing of the solution

High purity nitrogen was used to deoxygenate the solutions for 5-10 minutes before each electrochemical experiment and a positive nitrogen pressure was maintained above the solution throughout the experiment.

2.4.2 Temperature control

All experiments are performed at room temperature (22 ± 1 °C) unless otherwise noted. A dry ice and acetone mixture was used to obtain low temperature that varied from 22 to -75 °C. The exact temperature was monitored using a mercury thermometer and the cell was centered in a slush bath of the dry ice and acetone.

2.5 Chemicals

2.5.1 Compounds studied

All the macrocycles characterized in this dissertation (Chapters Three to Seven) were obtained from our collaborators. The gold(III) quinoxalinoporphyrins ($\text{Au}(\text{PQ}_n)\text{PF}_6$) described in Chapters Three and Four and the bisporphyrins ($\text{M}(\text{P})\text{-TA-(P)M}$) were synthesized by Dr. Maxwell J. Crossley in Sydney, Australia.⁵⁻⁷ The Zn(II), Ni(II), In(III), Ir(III), and 2H trimethyltetraphenylporphyrin (TMP-M), *meso*-naphthalene substituted porphyrin (Open-M) and *meso*, β -naphthalene fused porphyrin (Fused-M) were synthesized by Dr. Daniel T. Gryko⁸ from the Polish Academy Science in Warsaw, Poland. All of the compounds were stored in the dark and in some cases under vacuum condition. The UV-visible spectrum of each compound was measured before carrying out experiments in Houston and our spectral data were compared to that provided by our collaborator or published in the literature. If this was the case, which happened in a few

instances, we identified the reason for the difference or informed our collaborator of the problem so that we could resynthesize the compound if needed. In this way, we could be assured that the examined compound was in the same form as provided by our collaborators who had characterized the same compounds by a number of standard methods prior to sending the samples to Houston.

2.5.2 Other chemicals

Benzonitrile (PhCN) obtained from Fluka Chemika or Sigma-Aldrich Co. was distilled over phosphorous (P_2O_5) under vacuum prior to use. Absolute dichloromethane (CH_2Cl_2) and pyridine were used as received without further purification. High purity N_2 from Trigas was used for deoxygenate the solution before each electrochemical experiment. Tetra-*n*-butylammonium perchlorate (TBAP) were purchased from Sigma-Aldrich Chemical or Fluka Chemika Co., recrystallized from ethyl alcohol, and dried under vacuum at 40 °C for at least 1 week prior to use. Trifluoroacetic acid (TFA) was obtained from Sigma-Aldrich Chemical Co. and used as received.

2.6 References

- (1) Bard, A. J.; Faulkner, L. R. *Electrochemical Methods*, John Wiley & Sons: New York, **1980**, p. 383.
- (2) Lin, X. Q.; Kadish, K. M. *Anal. Chem.* **1985**, *57*, 1498.
- (3) Kadish, K. M.; Mu, X. H.; Lin, X. Q. *Electroanalysis* **1989**, *1*, 35.
- (4) Bronit, D.; Dougee, M. *Biochemistry* **1974**, *13*, 4519.
- (5) Ou, Z.; Zhu, W.; Fang, Y.; Sintic, J. P.; Khoury, T.; Crossley, J. M.; Kadish, K. M. *Inorg. Chem.* **2011**, *50*, 12802.
- (6) Ou, Z.; Khoury, T.; Fang, Y.; Zhu, W.; Sintic, J. P.; Crossley, J. M.; Kadish, K. M. *Inorg. Chem.* **2013**, *52*, 2474
- (7) Ou, Z.; Zhu, W.; Sintic, J. P.; Fang, Y.; Crossley, J. M.; Kadish, K. M. *J. Porphyrins Phthalocyanines* **2012**, *16*, 674.
- (8) Chen, P.; Fang, Y.; Kadish, K. M.; Lewtak, J. P.; Koszelewski, D.; Janiga, A.; Gryko, D. T. *Inorg. Chem.* **2013**, *52*, 9532

Chapter Three

Unusual Multi-step Sequential Au^{III}/Au^{II} Processes of Gold(III)

Quinoxalinoporphyrins in Acidic Nonaqueous Media

3.1 Introduction

The electron transfer reductions of quinoxalinoporphyrins can involve the central metal ion, the porphyrin macrocycle or the fused quinoxaline group(s), all of which are redox active.¹⁻⁷ The site of electron transfer, whether at the metal, at the macrocycle or at the quinoxaline (Q) part of the molecule, are important factors to know and control since the electron transfer reactivity of these metalloporphyrins are directly related to their possible applications in photovoltaics^{8,9} and molecular electronics.¹⁰⁻²³ Among the quinoxalinoporphyrins previously examined are the gold(III) derivatives which have been shown to undergo three or more one-electron reductions in nonaqueous media.^{2-4,6,7} The first reduction is in almost all cases a metal-centered $\text{Au}^{\text{III}}/\text{Au}^{\text{II}}$ process and leads to formation of an Au(II) porphyrin which can be further reduced at more negative potentials to give stepwise an Au(II) porphyrin π -anion radical and dianion under the given solution conditions. Further reductions beyond that of the Au(II) porphyrin dianion are also possible. These are located at the fused quinoxaline group and occur at potentials close to -2.0 V in the absence of electron-withdrawing substituents on the macrocycle.^{3,13}

The measured half-wave potentials for reduction of quinoxalinoporphyrins will depend upon the number of fused quinoxaline groups as well as upon the specific electron-donating or electron-withdrawing substituents on the macrocycle or Q group.^{3,4,6,7,24} Shifts of redox potentials may also be seen upon changing the type of axial ligand on the metal center of the quinoxalinoporphyrin²¹ or upon the binding of Sc^{3+} ions to the Q nitrogens of the quinoxalinoporphyrins in nonaqueous media, as was recently demonstrated for Au(III) mono- and bis-quinoxalinoporphyrins where the initial

electroreduction was shifted from the Au(III) center to the quinoxaline part of the molecule.⁵

Protonation of the quinoxaline nitrogen atoms can also have a significant effect on the electrochemical behavior of quinoxalinoporphyrins as was demonstrated for derivatives containing electrochemically inert Sn(IV), Cu(II), and Ni(II) central metal ions.⁷ Because the fused quinoxaline group(s) can directly interact with the porphyrin π -ring system^{5,19,20} one might reasonably predict the largest effect of protonation would be observed for ring-centered reductions and the smallest for metal-centered redox processes, but this has never been investigated in detail for quinoxalinoporphyrins with redox active central metal ions. It is also not known how protonation of the Q nitrogens would affect the site of electron transfer and reduction mechanism of quinoxalinoporphyrins with redox active central metal ions. Both points are addressed in the present study for two gold(III) quinoxalinoporphyrins, represented as Au(PQ)PF₆ and Au(QPQ)PF₆, where P is a dianion of the 5,10,15,20-tetrakis(3,5-di-tert-butylphenyl)porphyrin and Q is the quinoxaline group fused on the β, β' -pyrrolic positions of the porphyrin macrocycle (Chart 3-1). As will be demonstrated, the results are quite surprising in that Au(P)PF₆ undergoes one metal-centered reduction while Au(PQ)PF₆ and Au(QPQ)PF₆ exhibit two and three Au^{III}/Au^{II} processes, respectively. Combined data from electrochemistry and spectroelectrochemistry were utilized to elucidate the fate of the products after each electroreduction in dichloromethane or benzonitrile with and without added trifluoroacetic acid (TFA). The effects of the Q protonation on the site of electron transfer

and spectra of the reduction products are discussed and an overall reduction/oxidation mechanism for Au(PQ)PF_6 and Au(QPQ)PF_6 in acidic nonaqueous media are proposed.

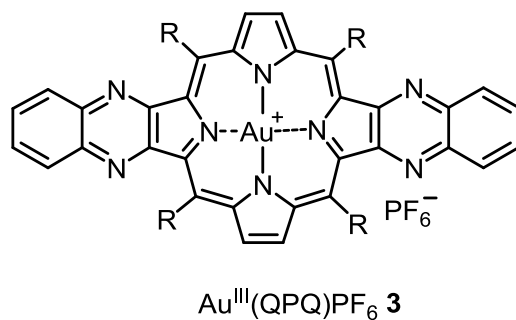
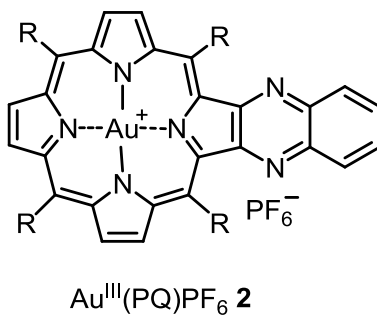
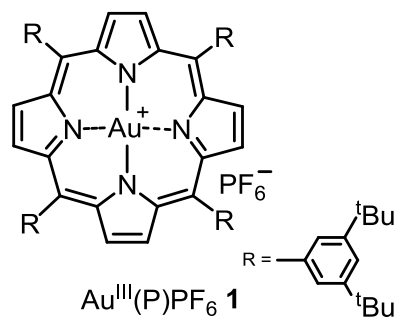


Chart 3-1. Structures of the investigated gold(III) porphyrins

3.2 Results and Discussion

3.2.1 Electrochemistry of Au^{III}(PQ)PF₆

Au(P)PF₆ **1** exhibits two one-electron reductions in CH₂Cl₂ or PhCN containing 0.1 M TBAP^{2,3} while three reversible electron additions are seen for Au(PQ)PF₆ **2** within the negative potential limit of the solvent.³ The bis-quinoxalinoporphyrin, Au(QPQ)PF₆ **3**, also undergoes three one-electron reductions in these two solvents as shown in Figure 3-1 where cyclic voltammograms (CVs) of the three compounds are presented in CH₂Cl₂ containing 0.1 M TBAP. $E_{1/2}$ for the first one-electron reduction of the easiest to reduce QPQ complex (-0.26 V, Figure 3-1c) is positively shifted by 210 mV as compared to the PQ derivative ($E_{1/2} = -0.47$ V, Figure 3-1b) and this $E_{1/2}$ value is positively shifted by 170 mV as compared to the same electrode reactions of the porphyrin in the absence of a fused quinoxaline group, *i.e.* Au(P)PF₆ (-0.64 V, Figure 3-1a). A similar trend in $E_{1/2}$ values with increasing number of Q groups is seen for the second reduction of the three porphyrins and it has also been reported for a number of quinoxalinoporphyrins with redox inactive central metal ions.^{3,7,25}

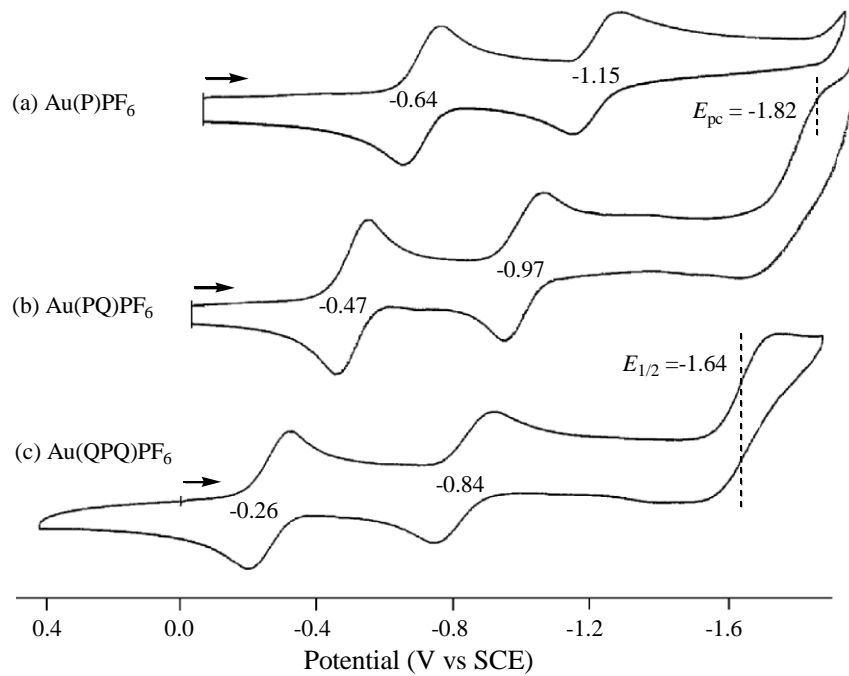


Figure 3-1. Cyclic voltammograms of gold porphyrins in CH_2Cl_2 containing 0.1 M TBAP.

The first reversible one-electron reduction of all three porphyrins (Figure 3-1) is facile and metal-centered as characterized by ESR in the case of Au(P)PF₆ and Au(PQ)PF₆.³ The approximately 800 mV separation between the second and third reductions of Au^{III}(PQ)⁺ and Au^{III}(QPQ)⁺ is much larger than the average 450-500 mV separation reported for ring-centered reductions of mono- and bis-quinoxalinoporphyrins with redox inactive central metal ions,^{4,7,25} but the redox processes in the case of the gold(III) derivatives are also assigned as occurring at the porphyrin π -ring system to give first an Au(II) porphyrin π -anion radical and then the corresponding dianion.

The addition of acid to quinoxalinoporphyrins in nonaqueous media can result in protonation of the quinoxaline nitrogens, either before or after electroreduction and it was therefore necessary to examine UV-visible spectra of the starting compounds in acidic CH₂Cl₂ or PhCN solutions prior to carrying out the electrochemical measurements. The measured spectra of the unreduced compounds are shown in Figure 3-2a where the associated PF₆⁻ counterion is not included in the formula. Au^{III}(P)⁺ in CH₂Cl₂ is characterized by a sharp Soret band at 415 nm and a single Q band at 523 nm. The Soret bands of Au^{III}(PQ)⁺ and Au^{III}(QPQ)⁺ are also sharp and located at 435 and 450 nm, respectively, in neat CH₂Cl₂. Identical UV-visible spectra are obtained for each porphyrin in CH₂Cl₂ after addition of up to 100 equivalents TFA to solution, thus ruling out protonation of the neutral compounds under these experimental conditions.

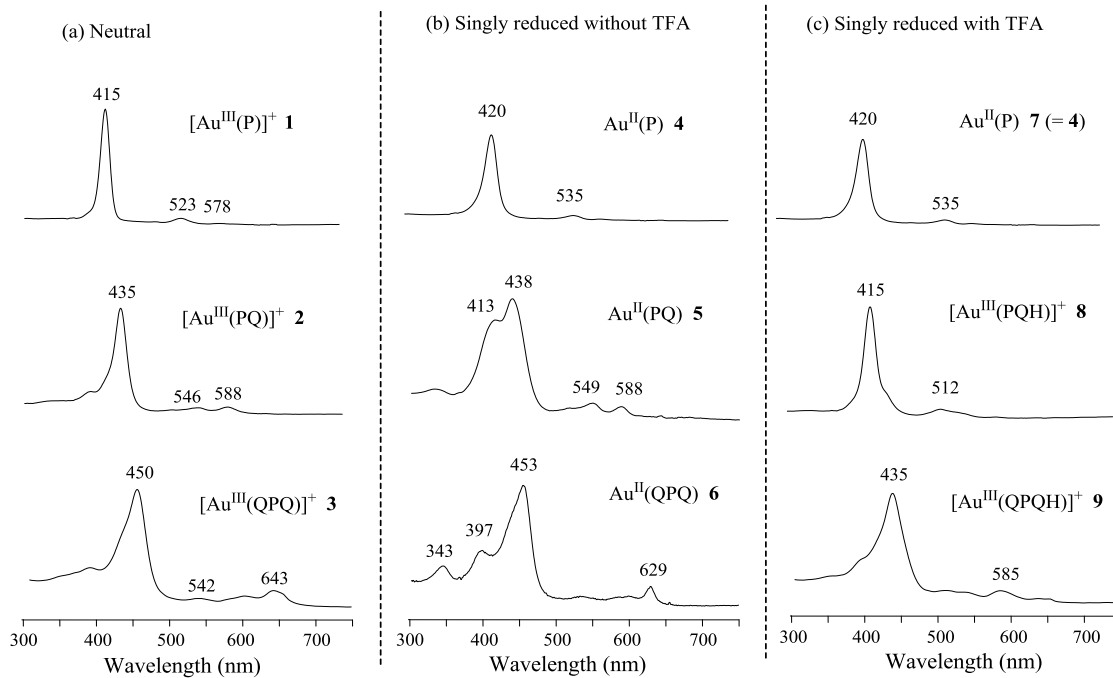


Figure 3-2. UV-visible spectra of gold(III) porphyrins in solutions of CH_2Cl_2 containing 0.1 M TBAP. (a) before electroreduction, (b) after electroreduction in the same solution and (c) after electroreduction in the same solution with 2-5 equiv. TFA.

The electrochemistry of Au(P)^+ in PhCN or CH_2Cl_2 (Figure 3-1a) is also invariant after adding TFA to solution, and this contrasts with what is seen for Au(PQ)^+ and Au(QPQ)^+ , where significant differences are observed in the cyclic voltammograms upon addition of 1-3 eq acid to solution. This is illustrated in Figure 3-3 for Au(PQ)^+ in PhCN containing 0.1 M TBAP and 1.5 equivalents TFA. Under these solution conditions, the first metal-centered reduction at $E_{\text{pc}} = -0.36$ V is no longer reversible and the shape of the current-voltage curve is consistent with the occurrence of a fast chemical reaction following a reversible one-electron transfer.²⁶ The second, third, and fourth reductions which follow the initial metal-centered reduction of $\text{Au}^{\text{III}}(\text{PQ})^+$ occur at $E_{1/2} = -0.60, -1.11$ and -1.83 V. The $\Delta E_{1/2}$ between the second and third reductions in PhCN is 510 mV (Figure 3-3) and an identical $\Delta E_{1/2}$ is seen for the first two reductions of $\text{Au}^{\text{III}}(\text{P})^+$ in CH_2Cl_2 (Figure 3-1a). $\text{Au}^{\text{III}}(\text{PQ})^+$ also exhibits an irreversible oxidation in acidic media at $E_{\text{pa}} = 0.34$ V which is coupled to the first reduction (Figure 3-3). This oxidation is never seen for $\text{Au}^{\text{III}}(\text{P})^+$, it is not seen for $\text{Au}^{\text{III}}(\text{PQ})^+$ in acid solutions upon initial scans in a positive direction from 0.0 V (Figure 3-3, top) and it is also not observed prior to adding TFA to the solution.

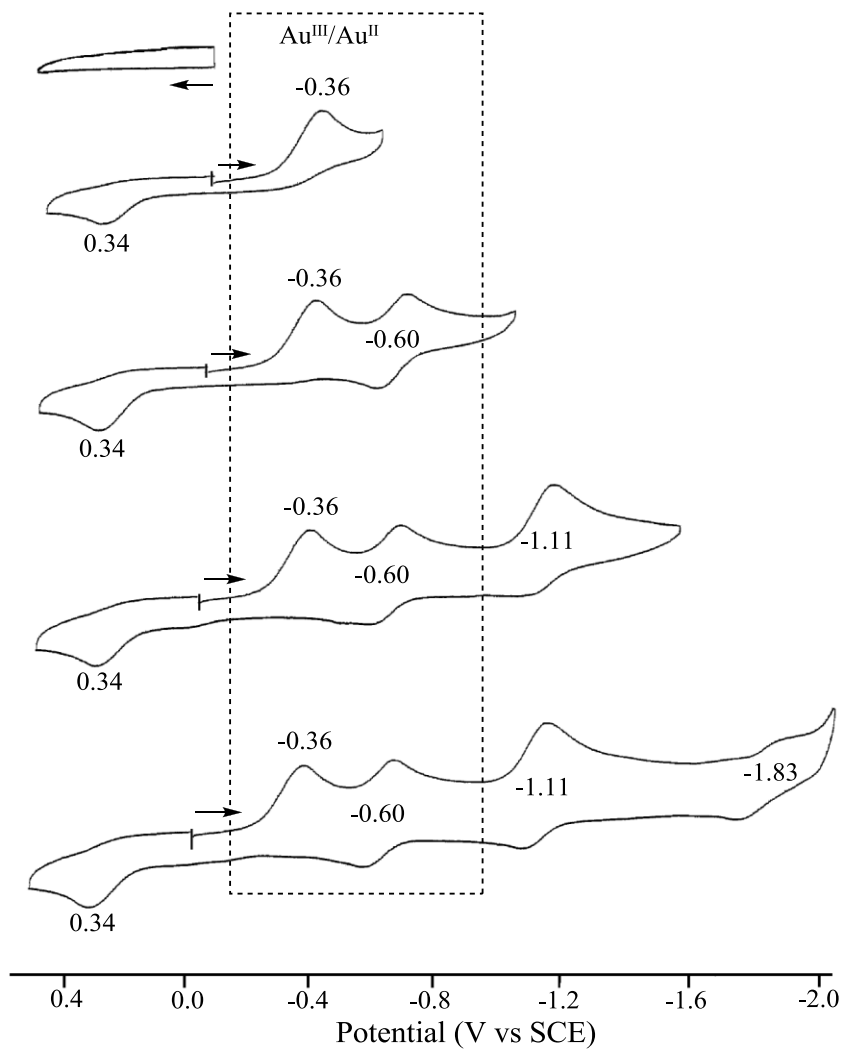


Figure 3-3. Cyclic voltammograms of Au(PQ)^+ in PhCN with 1.5 equivalent of TFA containing 0.1 M TBAP. Scan rate = 0.1 V/s.

We earlier reported that the first ring-centered one-electron reduction of $M^{II}(PQ)$ derivatives in PhCN containing added TFA is irreversible, resulting in formation of $M^{II}(PQH)^7$ which is then reduced to its π -anion radical and dianion forms at half-wave potentials, which are 220-230 mV negative of $E_{1/2}$ values for reduction of the same quinoxalinoporphyrins in their unprotonated form. The overall shape of current-voltage curve in Figure 3-3 for reduction of $Au^{III}(PQ)PF_6$ in PhCN containing 1.5 equivalents TFA is similar to that reported for the reduction of Ni(II), Cu(II), and Sn(IV) quinoxalinoporphyrins in that an irreversible first reduction is followed by a second and third reversible one-electron addition at more negative potentials. However, a major difference between the electrochemistry of $Au^{III}(PQ)^+$ and previously characterized $M^{II}(PQ)$ compounds, is that the irreversible first reduction of the gold(III) quinoxalinoporphyrin at $E_{pc} = -0.36$ V is followed by three and not two one-electron transfers, as occurs for the previously characterized protonated quinoxalinoporphyrins with redox inactive central metal ions. The reason for the “extra” process after the first irreversible reduction of $Au^{III}(PQ)^+$ becomes quite clear upon analyzing UV-visible spectra obtained during electroreduction in a thin-layer cell, which indicates that the final product of the first reduction is the protonated quinoxalinoporphyrin containing an Au(III) central metal ion, i.e. $Au^{III}(PQH)^+$.

The relevant spectral data obtained during the three reductions of $Au^{III}(PQ)^+$ are shown in Figure 3-4. The product of the one-electron reduction at a controlled potential of -0.50 V is characterized by a spectrum with a Soret band at 415 nm and single Q band at 512 nm (Figure 3-4a). The UV-visible spectrum of unreduced $Au^{III}(P)^+$ also has a well-

defined Soret band at 415 nm (**1** in Figure 3-2a) and both spectra are assigned as containing an Au(III) central metal ion. Further evidence in support of this oxidation state assignment for the singly reduced PQ compound is given by the spectroelectrochemical data in Figure 3-4b, where the product of the second controlled potential reduction at -0.80 V has well-defined bands at 420 and 525 nm, and is almost identical to the UV-visible spectrum of electrogenerated Au^{II}(P) under the same solution conditions (see **7** in Figure 3-2b). The last two reductions of Au^{III}(PQH)⁺ in Figure 3-3, at $E_{1/2} = -1.11$ and -1.83 V, are assigned to occur at the porphyrin π -ring system and the decreased intensity Soret band in the final spectrum after reduction at -1.25 V in the thin-layer cell (Figure 3-4c) suggests this assignment.

In summary, the overall reduction of Au^{III}(PQ)⁺ in acidic nonaqueous media is proposed to occur as shown in Scheme 3-1 and involves *two* Au^{III}/Au^{II} processes being exhibited by Au^{III}(PQ)⁺, one at $E_{pc} = -0.36$ V ($E_{1/2} = -0.39$ V in the absence of acid) and the other at $E_{1/2} = -0.60$ V. There is also a new irreversible oxidation peak at $E_{pa} = 0.34$ V in solutions of Au^{III}(PQ)⁺ with TFA. This process involves an electrochemical “EC” mechanism, *i.e.* an electrochemical conversion of Au^{III}(PQH)⁺ to Au^{III}(PQH)²⁺ (E) followed by loss of the proton on Q (C) and reformation of the original Au^{III}(PQ)⁺ species at the electrode surface.

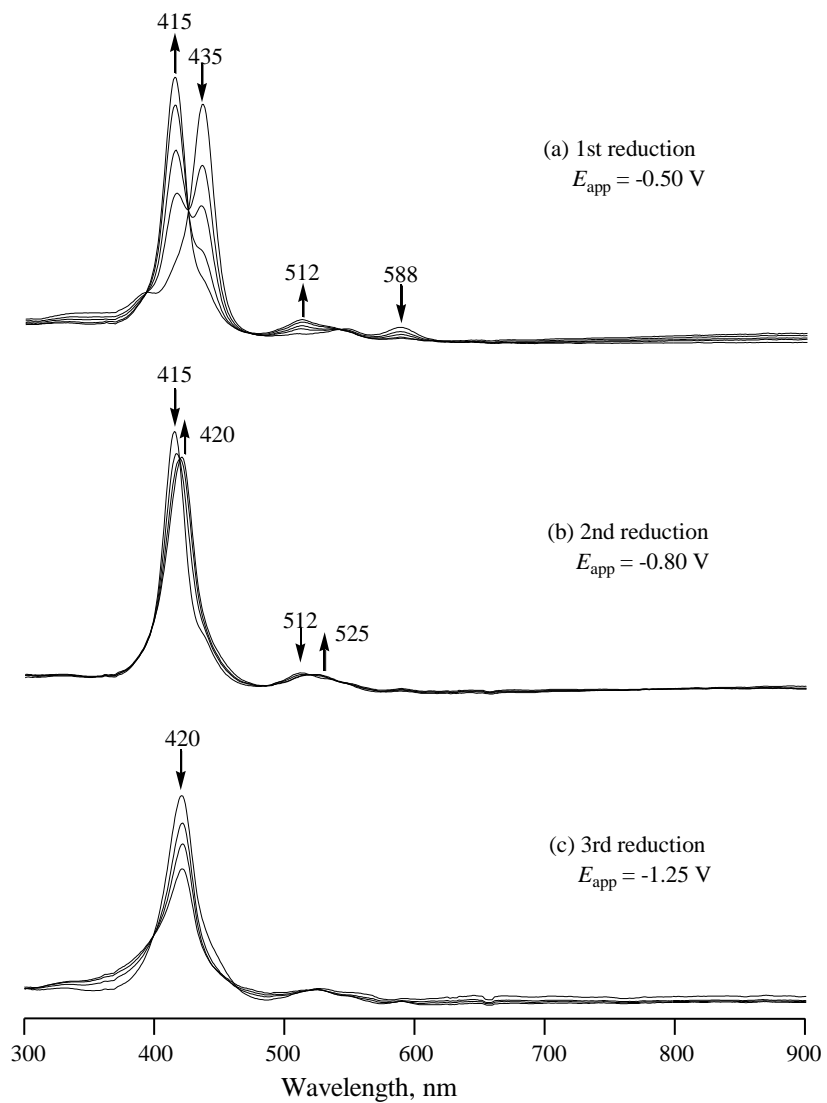
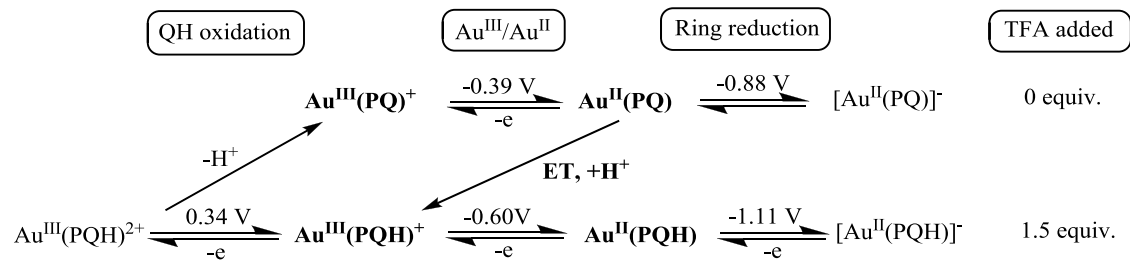


Figure 3-4. UV-vis spectral changes for Au(PQ)⁺ in CH₂Cl₂ containing 0.1 M TBAP and ~2 equivalents of TFA during reduction at (a) -0.50, (b) -0.80 and (c) -1.25 V.

Scheme 3-1. Proposed reduction/oxidation mechanism of $\text{Au}(\text{PQ})^+$ in nonaqueous media containing TFA. The compounds in bold undergo the $\text{Au}^{\text{III}}/\text{Au}^{\text{II}}$ process. The listed potentials were measured in PhCN, 0.1 M TBAP.



3.2.2 Electrochemistry of Au^{III}(QPQ)PF₆

The electrochemistry of Au^{III}(QPQ)⁺ in CH₂Cl₂ containing 0.1 M TBAP is in many respects similar to what is described above for Au^{III}(PQ)⁺ under the same solution conditions. In the absence of acid, three one-electron reductions are observed (see Figure 3-1c), the first of which is located at $E_{1/2} = -0.26$ V and associated with an Au^{III}/Au^{II} process. The second reduction at $E_{1/2} = -0.84$ V is assigned to formation of the Au(II) π -anion radical, and the third at $E_{1/2} = -1.64$ V to formation of the Au(II) porphyrin dianion. In the absence of acid, the first two reductions are reversible on both the electrochemical and spectroelectrochemical time scale, and UV-visible spectra obtained in a thin-layer cell during the first two controlled potential reductions at -0.40 and -1.00 V are given in Figure 3-5. The initial and final spectra of the singly reduced QPQ product in CH₂Cl₂ containing 0.1 M TBAP (without TFA) are also shown in Figure 3-2, where the compounds are numbered as **3** and **6**. As seen in these figures the most intense Soret band shifts from 450 nm for Au^{III}(QPQ)⁺ to 453 nm for Au^{II}(QPQ), while the Q band shifts from 643 to 629 nm upon conversion of Au(III) to Au(II). A small shift in λ_{\max} values for the single Soret band peak with no change in shape of the spectrum is also seen upon conversion of Au^{III}(P)⁺ to Au^{II}(P) (see **1** and **4** in Figure 3-2), and this is consistent with the metal-centered electron transfer process.

Larger differences are seen in the overall spectral features of Au^{II}(QPQ), Au^{II}(P), and Au^{II}(PQ) which differ in symmetry by virtue of the nature and placement of the fused Q groups. As seen in Figure 3-2b, Au^{II}(P) (**4**) exhibits a single Soret band is seen at 420

nm, Au^{II}(PQ) (**5**) exhibits a split Soret band at 413 and 438 nm, and Au^{II}(QPQ) (**6**) shows three well-defined Soret bands located at 343, 397, and 453 nm.

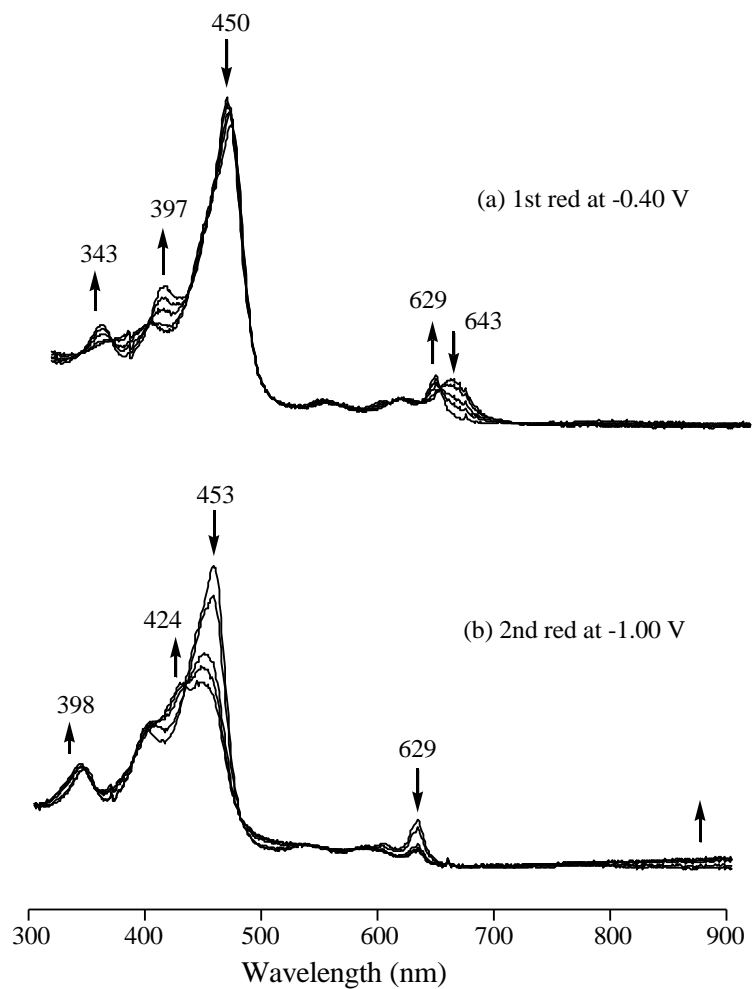


Figure 3-5. UV-vis spectral changes of Au(QPQ)⁺ in CH₂Cl₂, 0.1 M TBAP during the first and second reductions under application of the indicated potentials.

Significant differences are also observed in the electrochemistry of $\text{Au}^{\text{III}}(\text{QPQ})^+$ after the addition of TFA to solution. Two sequential metal-centered reductions (at $E_{\text{pc}} = -0.31$ and $E_{1/2} = -0.48$ V) are seen in a cyclic voltammogram (CV) of the compound when 1.0 equivalent TFA is added to a CH_2Cl_2 solution of $\text{Au}^{\text{III}}(\text{QPQ})^+$ (Figure 3-6). The CV of the bis-quinoxalinoporphyrin in the presence of 1.0 equivalent TFA is similar in shape and number of reduction processes to that for the mono-quinoxalinoporphyrin, $\text{Au}^{\text{III}}(\text{PQ})^+$ in the presence of 1.5 equivalents TFA (Figure 3-3). This is because only one of the two Q groups of $\text{Au}^{\text{III}}(\text{QPQ})^+$ can be protonated upon the first one-electron reduction when the solution contains only one equivalent TFA. The first metal-centered reduction under these solution conditions is irreversible, and like in the case of $\text{Au}^{\text{III}}(\text{PQ})^+$, this is due to an internal electron transfer and a quinoxaline group protonation, giving as a product of the homogenous reaction the mono-protonated Au(III) bis-quinoxalinoporphyrin, $\text{Au}^{\text{III}}(\text{QPQH})^+$. This mono-protonated Au(III) product of the first reduction can be reversibly reduced at $E_{\text{pc}} = -0.48$ V to give the mono-protonated Au(II) product, $\text{Au}^{\text{II}}(\text{QPQH})$ or it can be re-oxidized at $E_{\text{pa}} = 0.38$ V to give $\text{Au}^{\text{III}}(\text{QPQH})^{2+}$ as seen by cyclic voltammograms in Figure 3-6. The oxidation follows an electrochemical *EC* mechanism and is assigned as a reversible electron abstraction followed by a rapid chemical reaction involving dissociation of the single proton on the Q group and reformation of the starting unprotonated porphyrin $\text{Au}^{\text{III}}(\text{QPQ})^+$.

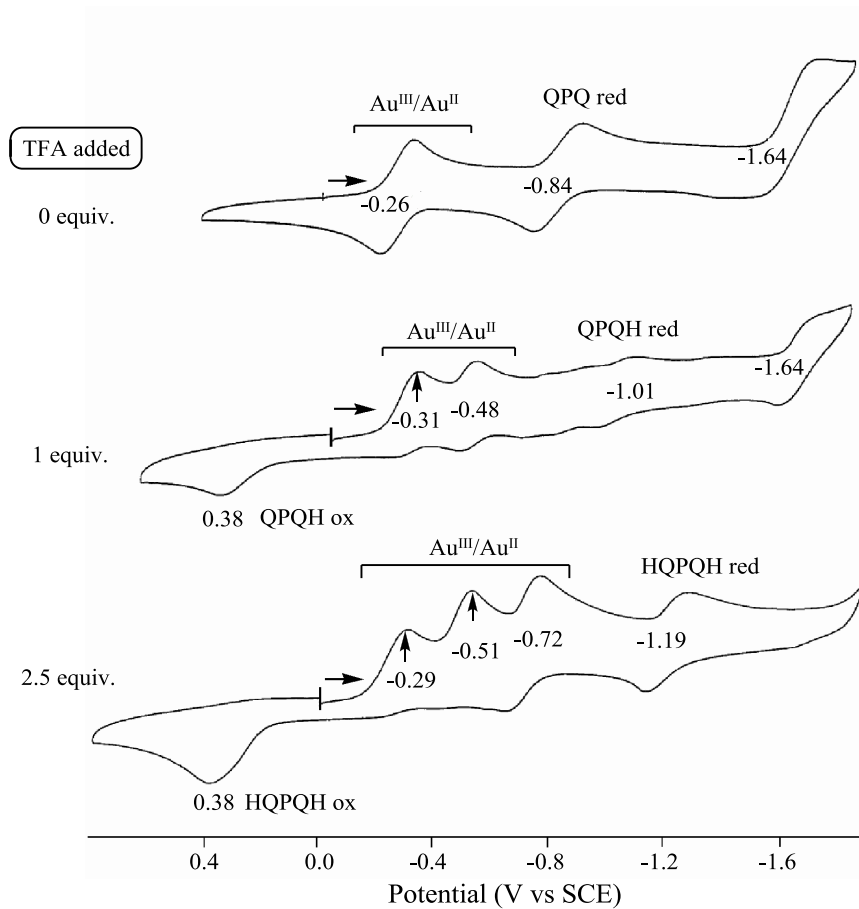


Figure 3-6. Cyclic voltammograms of $\text{Au}(\text{QPQ})^+$ in CH_2Cl_2 containing 0.1 M TBAP and added TFA. Scan rate = 0.1 V/s.

Three well-defined metal-centered reductions can be observed for $\text{Au}^{\text{III}}(\text{QPQ})^+$ when 2.5 equivalents TFA are added to the CH_2Cl_2 solution. These sequential processes are located at $E_{\text{pc}} = -0.29$ and -0.51 and $E_{1/2} = -0.72$ V (see Figure 3-7). All are assigned as involving a $\text{Au}^{\text{III}}/\text{Au}^{\text{II}}$ process to give $\text{Au}^{\text{III}}(\text{QPQH})^+$, $\text{Au}^{\text{III}}(\text{HQPQH})^+$, and $\text{Au}^{\text{II}}(\text{HQPQH})$ as sequential reduction products, with the proposed sequence of steps being given in Scheme 3-2.

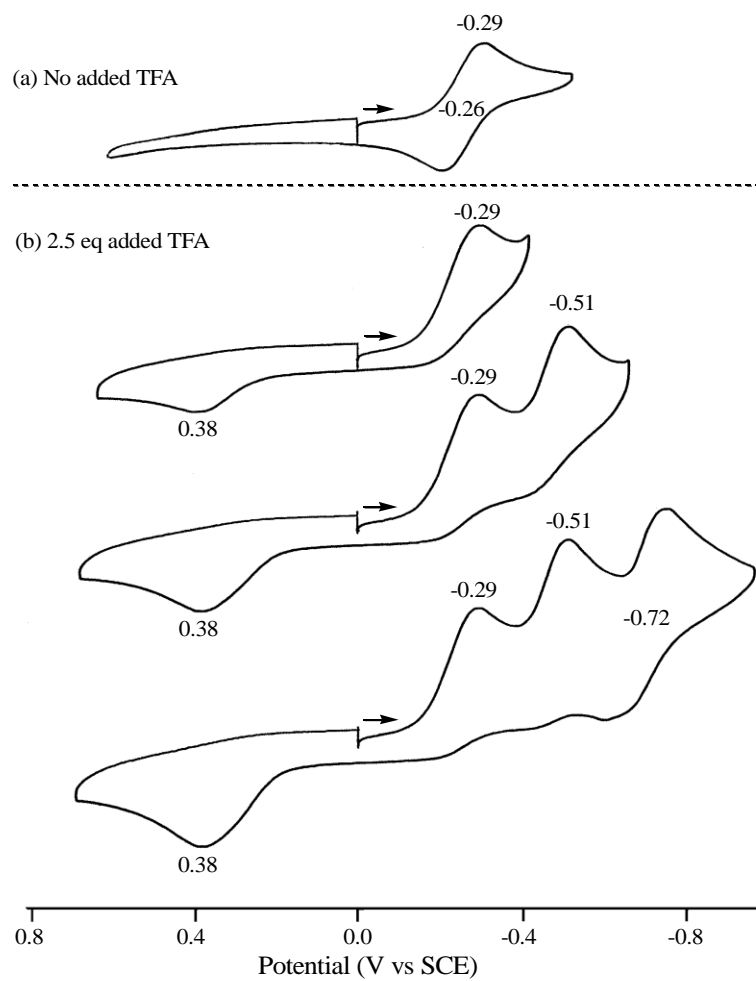
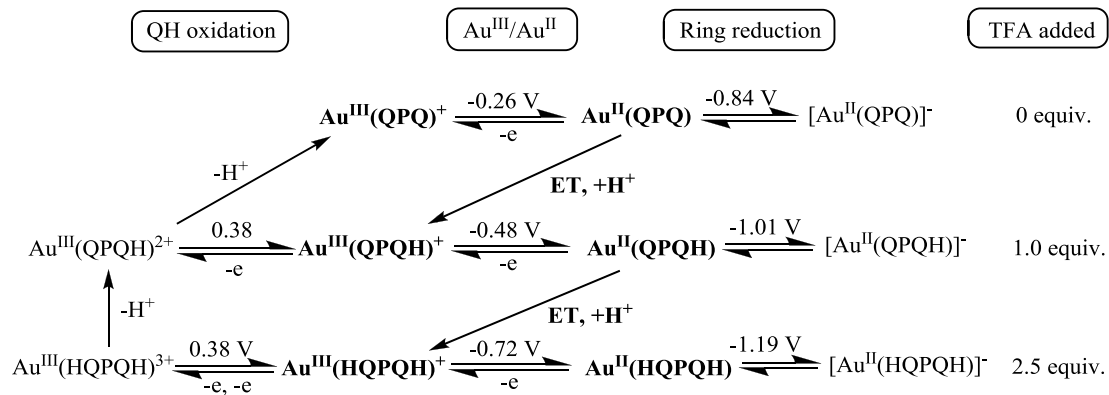


Figure 3-7. Cyclic voltammograms showing Au(III) reductions of Au(QPQ)⁺ in CH₂Cl₂ containing 0.1 M TBAP (a) before and (b) after 2.5 equivalents of TFA have been added to solution.

Scheme 3-2. Proposed reduction/oxidation mechanism of $\text{Au}(\text{QPQ})^+$ in nonaqueous media containing TFA. The listed potentials were measured in CH_2Cl_2 . The compounds in bold undergo the $\text{Au}^{\text{III}}/\text{Au}^{\text{II}}$ process.



The Au(III) mono- and bis-protonated bis-quinoxalinoporphyrins, $\text{Au}^{\text{III}}(\text{QPQH})^+$ and $\text{Au}^{\text{III}}(\text{HQPQH})^+$, generated after the reductions at $E_{\text{pc}} = -0.29$ and -0.51 V in CH_2Cl_2 with 1.0 equivalent added TFA can also be re-oxidized at $E_{\text{pa}} = 0.38$ V to give $\text{Au}^{\text{III}}(\text{QPQH})^{2+}$ and $\text{Au}^{\text{III}}(\text{HQPQH})^{3+}$ prior to loss of one or two protons and reformation of the neutral compound, $\text{Au}^{\text{III}}(\text{PQ})^+$. Both reactions proceed via an *EC* mechanism which resembles that described above for $\text{Au}^{\text{III}}(\text{PQ})^+$, the only difference being in the measured anodic peak potential of the oxidation peak which is 0.34 V in the case of $\text{Au}^{\text{III}}(\text{PQH})^+$ and 0.38 V in the case of $\text{Au}^{\text{III}}(\text{QPQH})^+$ and $\text{Au}^{\text{III}}(\text{HQPQH})^+$.

As seen in Figure 3-7b, the peak current for the irreversible oxidation at $E_{\text{pa}} = 0.38$ V is approximately twice as high when the scan is reversed after the second metal-centered reduction at $E_{\text{pc}} = -0.51$ V. This result is consistent with one Q group being protonated after the first reduction and two Q groups being protonated after addition of the second. This interpretation is also consistent with the fact that the current for the irreversible oxidation of $\text{Au}(\text{QPQ})^+$ in the presence of 2.5 equivalents TFA is also approximately double that when only 1.0 equivalent acid has been added to a solution of $\text{Au}^{\text{III}}(\text{QPQ})^+$ (see Figure 3-6).

Thin-layer UV-visible spectral changes of $\text{Au}^{\text{III}}(\text{QPQ})^+$ obtained during the first three controlled potential reductions in CH_2Cl_2 containing 0.1 M TBAP and ~3 equivalents of TFA, as shown in Figure 3-8, differ from what is observed for the same compound in the absence of TFA (Figure 3-6). Under both solution conditions, the initial bis-quinoxalinoporphyrin has a Soret band at 450 nm, a Q band at 643 nm, and is unprotonated in its neutral form. When one electron is added during controlled potential reduction at -0.30 V in CH_2Cl_2 containing TFA (Figure 3-8a), the final product of the

reaction has a single Soret band at 435 nm along with a Q band at 585 nm. Both the reactant and product are assigned as Au(III) porphyrins, *i.e.* $\text{Au}^{\text{III}}(\text{QPQ})^+$, and $\text{Au}^{\text{III}}(\text{QPQH})^+$ (see also **3** and **9** in Figure 3-2).

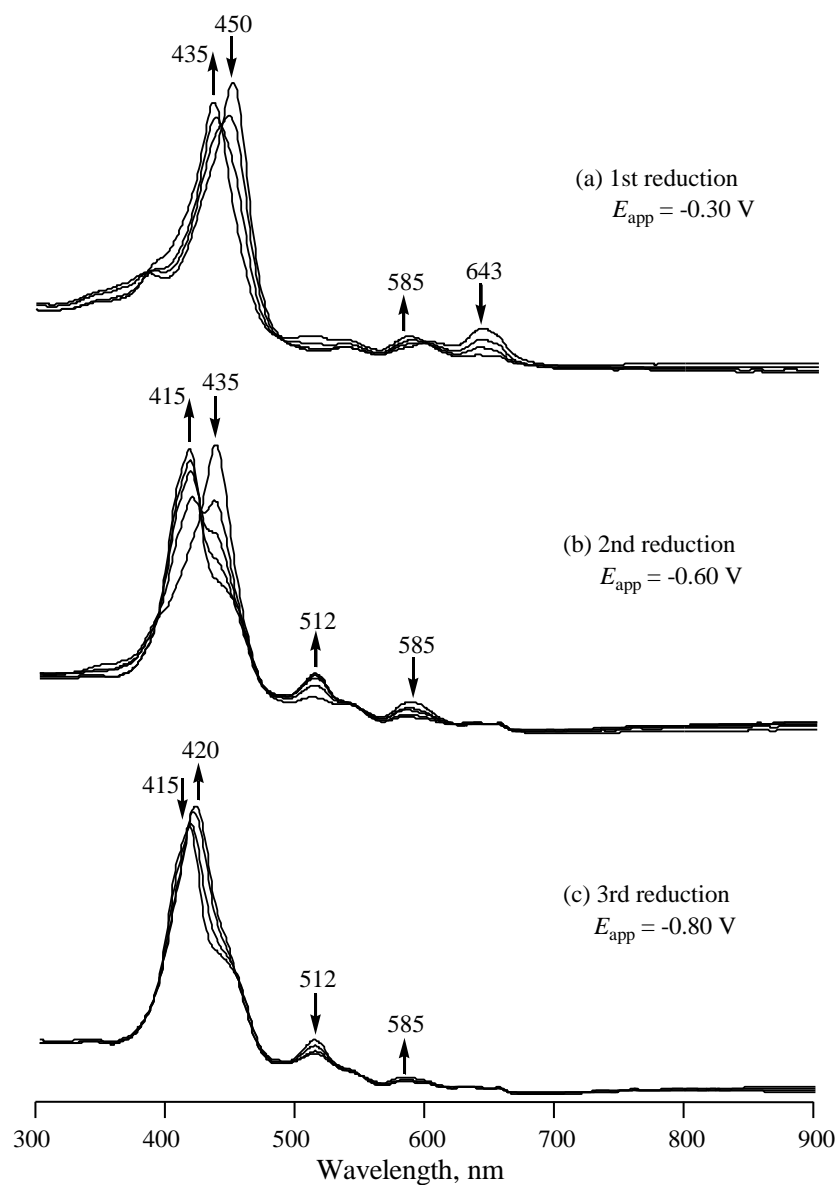


Figure 3-8. UV-vis spectral changes of Au(QPQ)PF₆ in CH₂Cl₂ containing 0.1 M TBAP and ~3 equivalents of TFA during reduction at (a) -0.30, (b) -0.60, and (c) -0.80 V.

Further reduction of $\text{Au}^{\text{III}}(\text{QPQH})^+$ at -0.60 V in the acid containing solution gives a product with a single Soret band at 415 nm and a Q band at 512 nm (Figure 3-8b). This spectrum is consistent with a species containing Au(III) porphyrin and is almost identical to the spectrum of $\text{Au}^{\text{III}}(\text{P})^+$, which has bands at 415 and 523 nm (see **1** in Figure 3-2). The third reduction of $\text{Au}^{\text{III}}(\text{QPQ})^+$ at a controlled potential of -0.80 V is also assigned to an $\text{Au}^{\text{III}}/\text{Au}^{\text{II}}$ process, but in this case no chemical reaction follows the electron transfer. The UV-visible spectrum for the stable product of the third reduction is shown in Figure 3-8c. It is characterized by a Soret band at 420 nm, a Q band at 585 nm, and is clearly diagnostic of an Au(II) porphyrin.

3.2.3 Spectral similarities between protonated and unprotonated gold porphyrins

Altogether six different Au(III) and three different Au(II) porphyrins were spectrally characterized in the presence of added acid. The data for these compounds are summarized in Tables 3-1 and 3-2 and examples of UV-visible spectra for the initial and singly reduced porphyrins are given in Figure 3-2. Three of Au(III) compounds have a Soret band at 415 nm, two have Soret band at 435 nm and one has Soret band at 450 nm. The identical Soret bands for each compound in the three groups of porphyrins suggest a quite similar extent of π -conjugation and charge distribution for each porphyrin in a given group, one comprising $\text{Au}^{\text{III}}(\text{P})^+$, $\text{Au}^{\text{III}}(\text{PQH})^+$, and $\text{Au}^{\text{III}}(\text{HQPQH})^+$ (415 nm), another $\text{Au}^{\text{III}}(\text{PQ})^+$ and $\text{Au}^{\text{III}}(\text{QPQH})^+$ (435 nm), and the third $\text{Au}^{\text{III}}(\text{QPQ})^+$ (450 nm) (see Scheme 3-3).

Table 3-1. UV-vis absorption wavelength (nm) and reduction potentials (V vs SCE) of Au(III) porphyrins in CH₂Cl₂ containing 0.1 M TBAP and added TFA.

Q number	compound	UV-vis spectra		potential
		Soret band	Q band	Au ^{III} /Au ^{II} process
none	Au ^{III} (P) ⁺	415	523	-0.64
Mono-Q	Au ^{III} (PQ) ⁺	435	588	-0.36 ^{a,b}
	Au ^{III} (PQH) ⁺	415	512	-0.60 ^a
Bis-Q	Au ^{III} (QPQ) ⁺	450	643	-0.29 ^b
	Au ^{III} (QPQH) ⁺	435	585	-0.48
	Au ^{III} (HQPQH) ⁺	415	512	-0.72

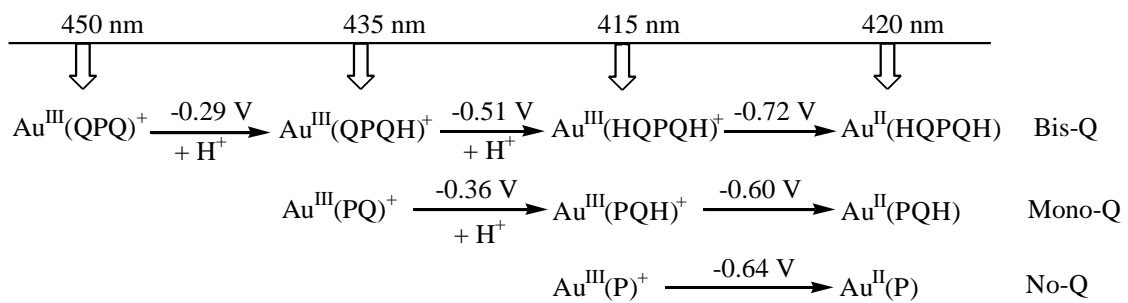
^aMeasured in PhCN, 0.1 M TBAP. ^bPeak potential at scan rate of 0.10 V/s.

Table 3-2. UV-visible spectral data and reduction potentials (V vs SCE) of Au(II) porphyrins in CH₂Cl₂ containing 0.1 M TBAP and added TFA.

compound	UV-vis spectra		potential		ΔE (mV) ^d
	Soret band	Q band	ring reduction		
Au ^{II} (P) ^a	420	535	-1.09	-1.81	720
Au ^{II} (PQH) ^a	420	525	-1.11	-1.83	720
Au ^{II} (HQPQH)	420	515	-1.19	--	--
Au ^{II} (PQ) ^b	413, 438	588	-0.97	-1.82 ^c	850
Au ^{II} (QPQ) ^b	343, 397, 453	629	-0.84	-1.64	800

^aPotential measured in PhCN, 0.1 M TBAP. ^bSpectra and potential measured in solution without added TFA. ^cPeak potential at a scan rate of 0.10 V/s. ^dpotential difference between the two reductions.

Scheme 3-3. Soret band maximum of investigated compounds.



A similar conjugated π -ring system is also suggested for the three Au(II) porphyrins, Au^{II}(P), Au^{II}(PQH), and Au^{II}(HQPQH); in the presence of acid, all of which have a single intense Soret band at 420 nm (Scheme 3-3). These three Au(II) porphyrins also have similar reduction potentials for formation of the π -anion radical, *i.e.* -1.09, -1.11 and -1.19 V (see Table 3-2).

The above results imply that conjugation between the porphyrin π -ring system and the β,β -fused Q group(s), of Au^{III}(PQ)⁺ and Au^{III}(QPQ)⁺ is interrupted upon protonation of the Q group(s) and thus similar spectra and similar reduction potentials are seen for Au^{III}(P)⁺ and the two fully protonated Au(III) quinoxalinoporphyrins. The same can be said for the Au(II) porphyrins, where the same spectral pattern is exhibited for Au^{II}(HQPQH), Au^{II}(PQH), and Au^{III}(P), each of which is characterized by a Soret band at 420 nm. Again, the data suggest that conjugation between the Q group and the porphyrin macrocycle is interrupted upon protonation, and this is consistent with the electrochemical data described in the manuscript.

3.3 Conclusions

In summary, the electrochemical and spectroelectrochemical properties of Au^{III}(P)⁺, Au^{III}(PQ)⁺, and Au^{III}(QPQ)⁺ were examined in CH₂Cl₂ containing 0.1 M TBAP. In the absence of TFA, each porphyrin undergoes one metal-centered reduction to form the corresponding Au(II) porphyrin, and this reaction is followed by two porphyrin ring-centered reductions leading to the formation of Au(II) π -anion radicals and dianions. Surprisingly, the two Au(III) quinoxalinoporphyrins, in the presence of few equivalents of TFA, will undergo unusual multi-step sequential Au^{III}/Au^{II} processes due to an internal

electron transfer and protonation of the fused Q group(s) on the porphyrin macrocycle. Thus, Au(P)PF_6 undergoes one metal-centered reduction, while Au(PQ)PF_6 and Au(QPQ)PF_6 exhibit two and three $\text{Au}^{\text{III}}/\text{Au}^{\text{II}}$ processes, respectively in the presence of acid.

Finally, it is important to point out that the protonation which accompanies the reduction of $\text{Au}^{\text{III}}(\text{PQ})^+$, $\text{Au}^{\text{III}}(\text{QPQ})^+$, and $\text{Au}^{\text{III}}(\text{QPQH})^+$ is reversible and the original compound can be regenerated by oxidation at a positive potential. These electrochemically initiated protonation and deprotonation steps change not only redox potentials of the compounds, but also their UV-visible properties which may have possible application in building of ON-OFF switching devices.

3.4 References

- (1) Kadish, K. M.; Van Caemelbecke, E.; Rotal, G. In *The Porphyrin Handbook*, Kadish, K. M.; Smith, K. M.; Guillard, R., Eds, Academic Press: New York, 2000; Vol. 8, pp 1.
- (2) Kadish, K. M.; E, W.; Ou, Z.; Shao, J.; Santic, P. J. Ohkubo, K.; Fukuzumi, S.; Crossley, M. J. *Chem. Commun.* **2002**, 356.
- (3) Ou, Z.; Kadish, K. M.; E, W.; Shao, J.; Santic, P. J.; Ohkubo, K.; Fukuzumi, S.; Crossley, M. J. *Inorg. Chem.* **2004**, *43*, 2078.
- (4) Zhu, W.; Santic, M.; Ou, Z.; Santic, P. J.; McDonald, J. A.; Brotherhood, P. R.; Crossley, M. J.; Kadish, K. M. *Inorg. Chem.* **2010**, *49*, 1027.
- (5) Ohkubo, K.; Garcia, R.; Santic, P. J.; Khoury, T.; Crossley, M. J.; Kadish, K. M.; Fukuzumi, S. *Chem.-A Eur. J.* **2009**, *15*, 10493.
- (6) Santic, P. J.; E, W.; Ou, Z.; Shao, J.; McDonald, J. A.; Cai, Z.; Kadish, K. M.; Crossley, M. J.; Reimers, J. R. *Phys. Chem. Chem. Phys.* **2008**, *10*, 515.
- (7) Ou, Z.; E, W.; Zhu, W.; Thordarson, P.; Santic, P. J.; Crossley, M. J. and Kadish, K. M. *Inorg. Chem.* **2007**, *46*, 10840.
- (8) Kira, A.; Matsubara, Y.; Iijima, H.; Umeyama, T.; Matano, Y.; Ito, S.; Niemi, M.; Tkachenko, N. V.; Lemmetyinen, H.; Imahori, H. *J. Phys. Chem. C* **2010**, *114*, 11293.
- (9) Walter, M. G.; Rudine, A. B.; Wamser, C. C.; *J. Porphyrins Phthalocyanines* **2010**, *14*, 759.
- (10) Sharma, S.; Nath, M. *New J. Chem.* **2011**, *35*, 1630.
- (11) Eu, S.; Hayashi, S.; Umeyama, T.; Matano, Y.; Araki, Y.; Imahori, H. *J. Phys. Chem. C* **2008**, *112*, 4396.
- (12) Carroll, R. L.; Gorman, C. B. *Angew. Chem. Int. Ed.*, **2002**, *41*, 4378.
- (13) Crossley, M. J.; Santic, P. J.; Walton, R.; Reimers, J. R. *Org. Biomol. Chem.* **2003**, *1*, 2777.
- (14) Ohkubo, K.; Santic, P. J.; Tkachenko, N. V.; Lemmetyinen, H.; E, W.; Ou, Z.; Shao, J.; Kadish, K. M.; Crossley, M. J.; Fukuzumi, S. *Chem. Phys.* **2006**, *326*, 3.

- (15) Crossley, Maxwell J.; Sintic, Paul J.; Hutchison, James A.; Ghiggino, Kenneth P. *Org. Biomol. Chem.* **2005**, *3*, 852.
- (16) Fukuzumi, S.; Hasobe, T.; Ohkubo, K.; Crossley, M. J.; Kamat, P. V.; Imahori, H. *J. Porphyrins Phthalocyanines* **2004**, *8*, 191.
- (17) Fukuzumi, S.; Ohkubo, K.; E, W.; Ou, Z.; Shao, J.; Kadish, K. M.; Hutchison, J. A.; Ghiggino, K. P.; Sintic, P. J.; Crossley, M. J. *J. Am. Chem. Soc.* **2003**, *125*, 14984.
- (18) Yeow, E. K. L.; Sintic, P. J.; Cabral, N. M.; Reek, J. N. H.; Crossley, M. J.; Ghiggino, K. P. *Phys. Chem. Chem. Phys.* **2000**, *2*, 4281.
- (19) Crossley, M. J.; Prashar, J. K. *Tetrahedron Lett.* **1997**, *38*, 6751.
- (20) Khoury, T.; Crossley, M. J. *New J. Chem.* **2009**, *33*, 1076.
- (21) Hutchison, J. A.; Sintic, P. J.; Crossley, M. J.; Nagamura, T.; Ghiggino, K. P. *Phys. Chem. Chem. Phys.* **2009**, *11*, 3478.
- (22) Crossley, M. J.; Sheehan, C. S.; Khoury, T.; Reimers, J. R.; Sintic, P. J. *New J. Chem.* **2008**, *32*, 340.
- (23) Fukuzumi, S.; Ohkubo, K.; Zhu, W.; Sintic, M.; Khoury, T.; Sintic, P. J.; E, W.; Ou, Z.; Crossley, M. J.; Kadish, K. M. *J. Am. Chem. Soc.* **2008**, *130*, 9451.
- (24) Kadish, K. M.; E, W.; Sintic, P. J.; Ou, Z.; Shao, J.; Ohkubo, K.; Fukuzumi, S.; Govenlock, L. J.; McDonald, J. A.; Try, A. C.; Cai, Z.; Reimers, J. R.; Crossley, M. J. *J. Phys. Chem. B* **2007**, *111*, 8762.
- (25) Ou, Z.; E, W.; Shao, J.; Burn, P. L.; Sheehan, C. S.; Walton, R.; Kadish, K. M.; Crossley, M. J. *J. Porphyrins Phthalocyanines* **2005**, *9*, 142.
- (26) Bard, A. J.; Faulkner, L. R. *Electrochemical Methods, Fundamentals and Applications*, Second Ed., John Wiley & Son: 2001.

Chapter Four

Gold(III) Porphyrins Containing Two, Three or Four β,β' -fused Quinoxalines. Synthesis, Electrochemistry and Effect of Structures, and Acidity on Electroreduction Mechanism

4.1 Introduction

The electroreduction of quinoxalinoporphyrins can involve the central metal ion, the conjugated porphyrin macrocycle or the fused quinoxaline group(s), depending upon the specific compound and the experimental conditions.¹⁻⁸ The measured redox potentials will depend in each case upon the site of electron transfer, the type and oxidation state of the central metal ion, the number of fused quinoxaline groups, the specific electron-donating or electron-withdrawing substituents on the macrocycle,^{3,4,6-8} and the type and number of axial ligands.⁹ Protonation of the quinoxaline nitrogen atoms can also have a significant effect on the electrochemical behavior of these compounds as was demonstrated for derivatives containing both electrochemically inert Sn(IV), Cu(II), or Ni(II) central metal ions,⁷ and redox active central metal ions such as Co(II),⁴ Mn(III),¹⁰ Ag(III),¹¹ and Au(III).¹²

A positive linear shift in reduction potentials with increase in the number of fused quinoxaline (Q) groups has been well-documented upon going from simple metalloporphyrins to derivatives of mono- and “linear” bis-quinoxalinoporphyrins, with the magnitude of the shift depending upon the type and oxidation state of the central metal ion and the specific site of electron transfer.^{3-8,11-16} A much smaller shift in macrocycle-centered reduction potentials was reported upon going from the PQ to corner PQ₂ quinoxalinoporphyrins with redox inactive centers,¹³ but it was not known if the same trend would be observed for metal-centered reactions, nor was it known how the addition of three or four Q groups to the gold(III) porphyrins would be reflected in $E_{1/2}$ values for the multiple reductions of these compounds in nonaqueous media. This is investigated in the present study for three newly synthesized gold(III) porphyrins which

are represented as Au(PQ₂)PF₆, Au(PQ₃)PF₆, and Au(PQ₄)PF₆, where P is the dianion of the 5,10,15,20-tetrakis(3,5-di-*tert*-butylphenyl)porphyrin and Q is a quinoxaline group fused to the β,β'-pyrrolic positions of the porphyrin macrocycle (Chart 4-1).

Gold(III) quinoxalinoporphyrins have attracted a great deal of interest, in part because they are easy to reduce and can undergo multiple electron additions.^{2-4,6,7} The first reduction involves an Au^{III}/Au^{II} conversion in all cases, while the second and third one-electron reductions are proposed to be porphyrin ring-centered electron transfers. Further reductions are also possible at the fused quinoxaline group(s), and are often observed at more negative potentials.^{5,17} Gold(III) quinoxalinoporphyrins are also of interest, since the mono- and bis-quinoxaline derivatives were recently shown to undergo multiple Au^{III}/Au^{II} process in acidic solutions of CH₂Cl₂ or PhCN,¹² as shown in Scheme 4-1 for the case of Au(PQ)PF₆.

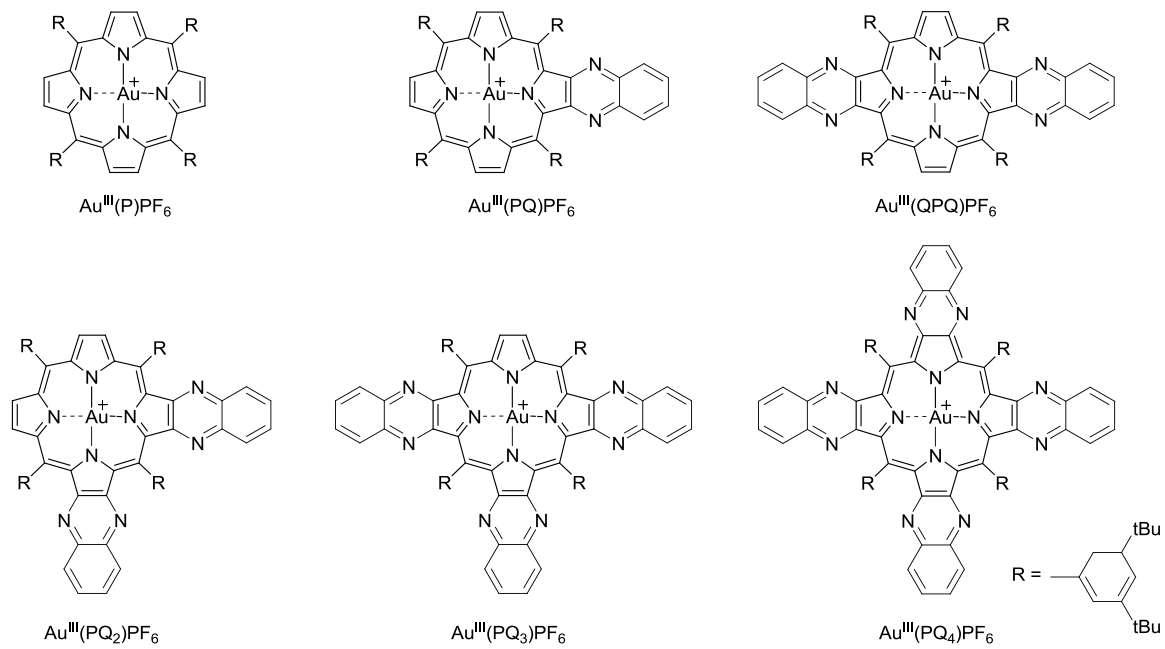
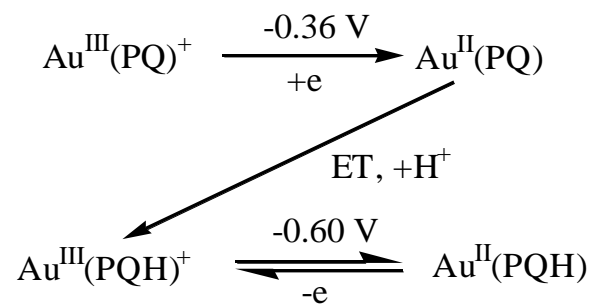


Chart 4-1. Structures of gold(III) quinoxalinoporphyrim.

Scheme 4-1. Published mechanism for the reduction of $\text{Au}^{\text{III}}(\text{PQ})^+$ in nonaqueous media containing TFA.¹²



In order to determine if additional proton induced metal-centered reductions might occur with further increase in the number of Q groups, the three newly synthesized compounds were therefore examined not only as to their electrochemical properties in THF, pyridine and CH₂Cl₂, but also in CH₂Cl₂ containing added acid in the form of trifluoroacetic acid (TFA). The effect of the number of Q groups on the redox potentials and protonation reactions is discussed and an overall reduction/oxidation mechanism is then proposed. For simplification, the examined Au(III) porphyrins are represented in the manuscript as Au(PQ₂)⁺, Au(PQ₃)⁺, and Au(PQ₄)⁺.

4.2 Results and Discussion

4.2.1 Electrochemistry of Au^{III}(PQ₂)PF₆, Au^{III}(PQ₃)PF₆, and Au^{III}(PQ₄)PF₆

The electrochemistry of Au(PQ₂)⁺, Au(PQ₃)⁺, and Au(PQ₄)⁺ was initially carried out in CH₂Cl₂, pyridine and THF containing 0.1 M TBAP as supporting electrolyte. The half-wave potentials are summarized in Table 4-1, which also includes data for previously investigated gold(III) porphyrins having zero, one, or two linear β,β'-fused quinoxaline groups on the macrocycle.^{2,3,12} Cyclic voltammograms of the six Au^{III}(PQ_{*n*})PF₆ complexes analyzed in the present study are illustrated in Figure 4-1 for the reductions in CH₂Cl₂ containing 0.1 M TBAP. As seen in the figure, and also previously reported,¹² Au^{III}(P)⁺, Au^{III}(PQ)⁺, and Au^{III}(QPQ)⁺ undergo two or three one-electron reductions in CH₂Cl₂ (Figure 4-1a), while four or five reductions are observed for Au^{III}(PQ₂)⁺, Au(PQ₃)⁺, and Au^{III}(PQ₄)⁺ under the same solution conditions (Figure 4-1b).

The first one-electron reduction of $\text{Au}^{\text{III}}(\text{PQ}_n)^+$ is metal-centered,^{3,12} and this was verified by ESR in the present study for the product of singly-reduced $\text{Au}^{\text{III}}(\text{PQ}_3)^+$ and $\text{Au}^{\text{III}}(\text{PQ}_4)^+$, which show typical Au(II) signals at $g = 2.06$. The reversible half-wave potentials for the $\text{Au}^{\text{III}}/\text{Au}^{\text{II}}$ process ranges from -0.64 to 0.17 V, depending upon the solvent (CH_2Cl_2 , Py or THF) and number of Q groups (0 to 4) fused to the macrocycle (see Table 4-1). The first oxidation of the six $\text{Au}^{\text{III}}(\text{PQ}_n)^+$ complexes is reversible in CH_2Cl_2 , and involves a one-electron abstraction from the conjugated π -ring system, with $E_{1/2}$ values ranging from 1.59 to 1.24 V (see Table 4-1). The absolute potential difference between the reversible first reduction of the six Au(III) porphyrins at the central metal ion and the reversible first oxidation at the conjugated macrocycle ($\Delta E_{1/2}$) ranges from 2.23 to 1.30 V in CH_2Cl_2 , and is smallest in the case of $\text{Au}(\text{PQ}_3)^+$ (1.53 V) and $\text{Au}(\text{PQ}_4)^+$ (1.30 V). This separation is solvent dependent, as seen by the data in THF, where reversible oxidations are seen only for the PQ_2 , PQ_3 , and PQ_4 derivatives, leading to $\Delta E_{1/2}$ values of 1.61, 1.54, and 1.49, respectively.

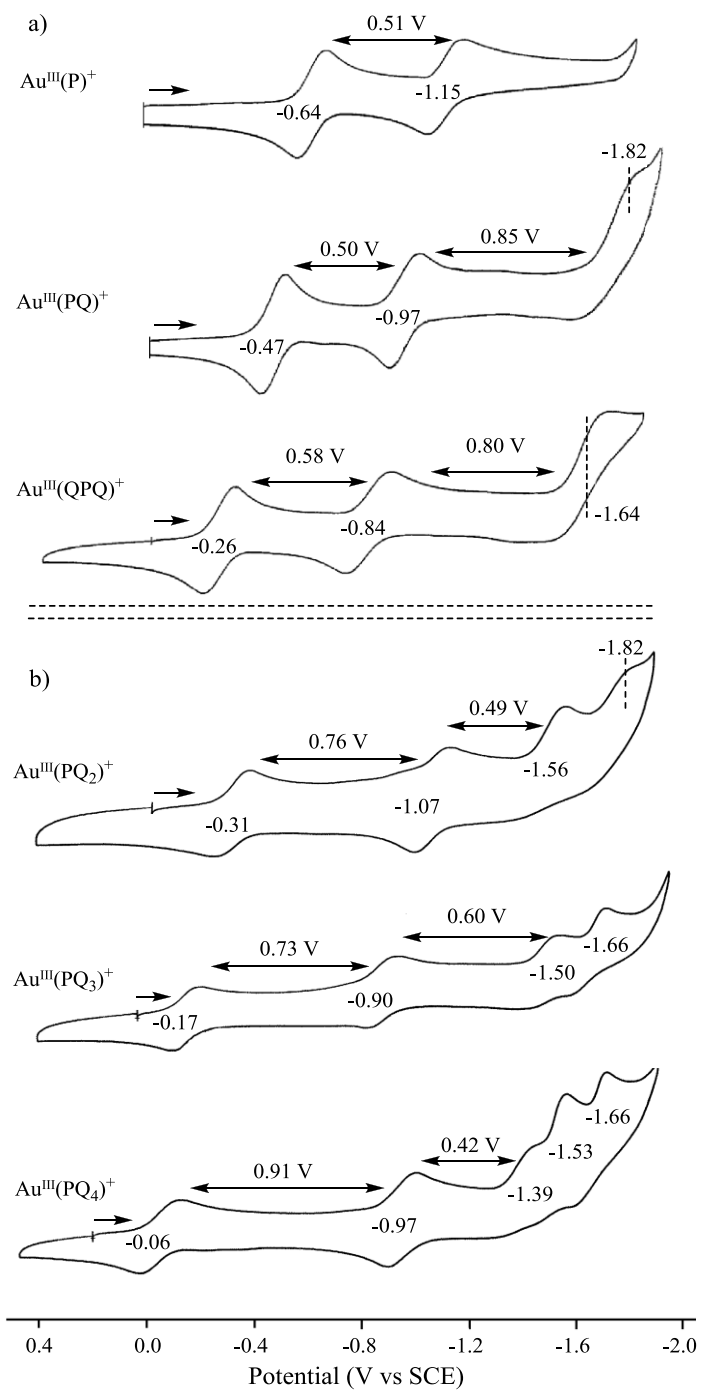


Figure 4-1. Cyclic voltammograms of Au(III) quinoxalinoporphyryns which undergo (a) 2-3 reductions and (b) 4-5 reductions in CH₂Cl₂ containing 0.1 M TBAP.

Table 4-1. Half-wave potentials (V vs SCE) of Au^{III}(PQ_n) PF₆ (*n* = 0-4) in CH₂Cl₂, Pyridine, and THF, 0.1 M TBAP.

solvent	cpd	Ox	Red					potential separation ($\Delta E_{1/2}$, V)			ref
		1st	1st	2nd	3rd	4th	5th	1red- 2red	2red- 3red	1ox- 1red	
CH ₂ Cl ₂	P	1.59	-0.64	-1.15				0.51		2.23	3, 12
	PQ	1.54	-0.47	-0.97	-1.82 ^a			0.50	0.85	2.01	3, 12
	QPQ	1.48	-0.26	-0.84	-1.64 ^a			0.58	0.80	1.74	12
	PQ ₂	1.48	-0.31	-1.05	-1.55 ^a	-1.82 ^a		0.74	0.50	1.79	<i>tw</i>
	PQ ₃	1.36	-0.17	-0.90	-1.50	-1.66		0.73	0.60	1.53	<i>tw</i>
	PQ ₄	1.24	-0.06	-0.97	-1.39	-1.53	-1.66	0.91	0.42	1.30	<i>tw</i>
Py	P		-0.52	-1.08	-1.76			0.56	0.68		2
	PQ		-0.35	-0.87	-1.69			0.52	0.82		3
	QPQ		-0.17	-0.71	-1.56			0.54	0.85		<i>tw</i>
	PQ ₂		-0.24	-0.97	-1.48	-1.85 ^a		0.73	0.51		<i>tw</i>
	PQ ₃		-0.11	-0.82	-1.44	-1.68 ^a	-1.97 ^a	0.71	0.60		<i>tw</i>
	PQ ₄		-0.01	-0.86	-1.32	-1.76 ^b	-1.76 ^b	0.85	0.46		<i>tw</i>
THF ^c	P	1.89 ^a	-0.40	-1.10	-1.77			0.70	0.67	2.29	2
	PQ	1.77 ^a	-0.20	-0.88	-1.65	-2.22 ^a		0.68	0.77	1.97	3
	QPQ	1.60 ^a	-0.02	-0.70	-1.53	-2.04 ^a	-2.22 ^a	0.68	0.83	1.62	<i>tw</i>
	PQ ₂	1.53	-0.07	-0.95	-1.45	-1.97 ^a	-2.26 ^a	0.88	0.50	1.61	<i>tw</i>
	PQ ₃	1.45	0.09	-0.76	-1.37	-1.85 ^a	-2.05 ^a	0.85	0.61	1.54	<i>tw</i>
	PQ ₄	1.32	0.17	-0.80	-1.28	-1.79 ^a	-2.01 ^a	0.97	0.48	1.49	<i>tw</i>

^aIrreversible peak potential at a scan rate of 0.10 V/s. ^bTwo overlapping one-electron reductions. ^cPotentials vs Ag/AgCl.

The second and third reversible reductions of Au(P)^+ , Au(PQ)^+ , and Au(QPQ)^+ have been shown to occur at the conjugated π -ring system to give Au^{II} π -anion radical and dianions under all solution conditions. The potential difference between the $\text{Au}^{\text{III}}/\text{Au}^{\text{II}}$ process and the first ring-centered reduction of the three newly synthesized quinoxalinoporphyrins depends slightly upon solvent, with measured $\Delta E_{1/2}$ values ranging from 0.50 to 0.58 V in CH_2Cl_2 , or pyridine and from 0.68 to 0.70 V in THF. Much larger potential separations are seen between the second and third one-electron reductions of Au(PQ)^+ and Au(QPQ)^+ in the above listed solvents, where the $\Delta E_{1/2}$ values range from 0.77 to 0.85 V (see Figure 4-1 and Table 4-1). This unusually large potential separation between formation of the Au(II) porphyrin π -anion radical and dianion contrasts markedly with what is known to occur for ring-centered reductions of all other metalloporphyrins with M(II) centered metals, where $\Delta E_{1/2}$ values of 0.4 to 0.5 V are generally observed.¹ This might at first suggest a different site of electron transfer in the case of the PQ and QPQ derivatives, but the situation becomes more complex when also analyzing potentials for the first three reductions and first oxidation of the PQ_2 , PQ_3 , and PQ_4 compounds. This analysis is given in Figure 4-2, where correlations between half-wave potentials ($E_{1/2}$) and n , the number of Q groups, are presented. As seen in the figure, the first and third reductions of $\text{Au}^{\text{III}}(\text{PQ}_n)^+$ shift positively in potential by 0.14 to 0.15 V per added Q group (an easier reduction) upon going from $n = 0$ to $n = 4$, while the first oxidation shifts negatively by 0.09 V with the change in structure, *i.e.*, an easier oxidation occurs as the number of fused Q groups on the molecule is increased.

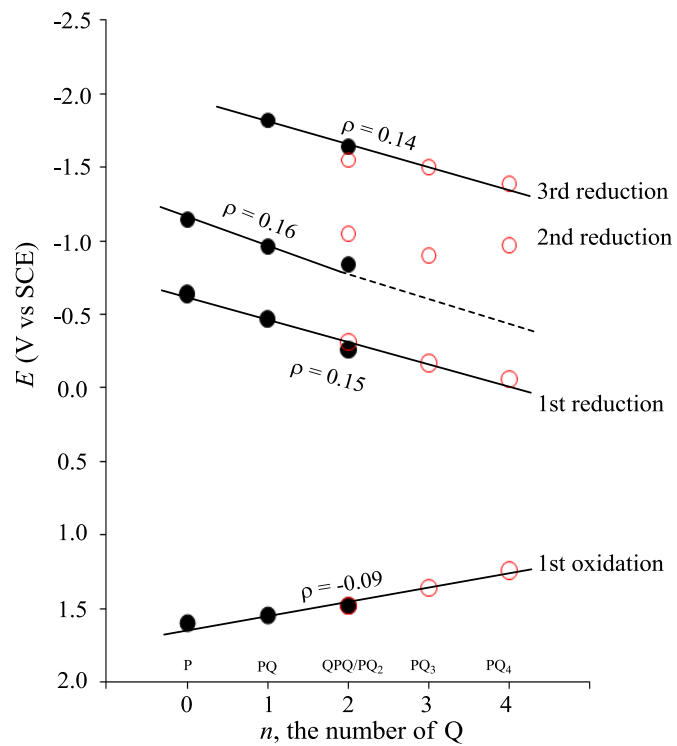


Figure 4-2. Plots of redox potentials of $\text{Au}^{\text{III}}(\text{PQ}_n)^+$ in CH_2Cl_2 vs the number of quinoxaline groups, where ● represents of P, PQ, and QPQ and ○ represents PQ_2 , PQ_3 , and PQ_4 .

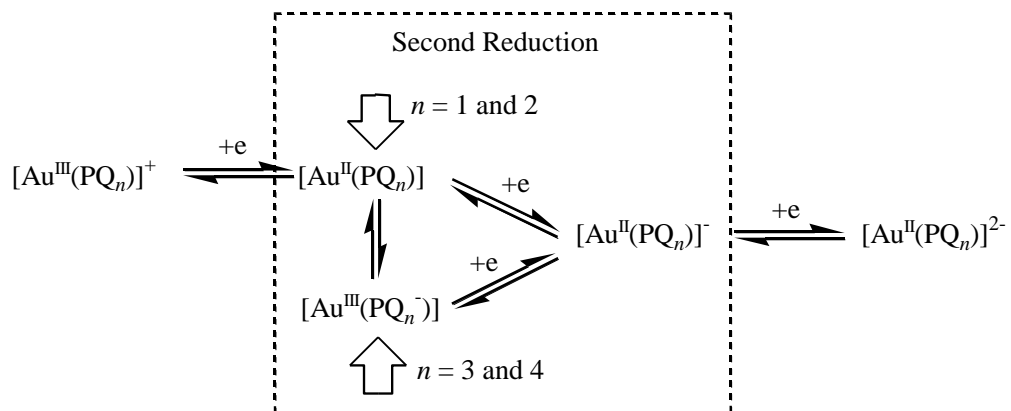
Changes in the measured $E_{1/2}$ values for oxidation and reduction of a given compound in the $\text{Au}^{\text{III}}(\text{PQ}_n)^+$ series upon going from $\text{Au}^{\text{III}}(\text{P})^+$ to $\text{Au}^{\text{III}}(\text{PQ}_4)^+$ will depend upon a number of factors, the most important of which are substituent effects of the fused Q groups on the electroreduction or electrooxidation site, changes in the size of the conjugated π -system, and changes in planarity of the macrocycle with increase in number of Q groups or change of solvent. A progressively easier reduction would be expected to occur upon increasing the number of electron-withdrawing Q groups, and an easier reduction would also be expected to occur if the size of the conjugated π -system were increased upon going from $\text{Au}^{\text{III}}(\text{P})^+$ to $\text{Au}^{\text{III}}(\text{PQ}_4)^+$. In the case of oxidation, a harder electron abstraction process (more positive potential) would be expected with increase in electron-withdrawing effect of the Q substituents, but an easier oxidation would result with an increase in size of the porphyrin π -ring system. An increased non-planarity of the porphyrin macrocycle might also lead to an easier oxidation, as has been demonstrated for a number of compounds.^{1,18-21}

The shift of $E_{1/2}$ with increase in number of Q groups for the second reduction of $\text{Au}^{\text{III}}(\text{PQ}_n)^+$ to form an Au^{II} π -anion radical is a combination of two trends. The first involves the P, PQ, and QPQ derivatives (solid points in Figure 4-2) where half-wave potentials linearly shift in a positive direction with increase in Q (slope = 0.16 V), while the second involves $\text{Au}^{\text{III}}(\text{PQ}_2)^+$, $\text{Au}^{\text{III}}(\text{PQ}_3)^+$, and $\text{Au}^{\text{III}}(\text{PQ}_4)^+$ (open points in Figure 4-2), where there is little to no significant shift in $E_{1/2}$. This suggests a change in mechanism or change in charge delocalization between the two series of compounds. Interestingly, the separation in $E_{1/2}$ between the first and third reductions of $\text{Au}^{\text{III}}(\text{PQ}_n)^+$ complexes remains

relatively constant at 1.33 to 1.38 V for all of the compounds except PQ₂, which displays a smaller separation of 1.24 V in CH₂Cl₂.

This relatively constant potential separation between the first and third reductions further emphasizes the unexpected trends in $E_{1/2}$ for the second reduction as a function of the number of Q groups on the macrocycle. As seen in Figures 4-1 and 4-2, the second macrocycle-centered reduction of Au^{II}(PQ₂)⁺, Au^{III}(PQ₃)⁺, and Au^{III}(PQ₄)⁺ become increasingly more difficult as compared to the first reduction, the absolute difference in potential between these two processes being 910 mV for Au^{III}(PQ₄)⁺ as compared to 500 mV for the same two electron transfer reactions of Au^{III}(PQ)⁺. This result is consistent with an increased negative charge being located on the macrocycle after the first metal-centered reduction of Au^{II}(PQ₂)⁺, Au^{III}(PQ₃)⁺, and Au^{III}(PQ₄)⁺, and might be accounted by a transfer of charge between the Au(II) central metal ion and the porphyrin macrocycle as shown in Scheme 4-2.

Scheme 4-2. Proposed mechanism for first three reductions of $\text{Au}^{\text{III}}(\text{PQ}_2)^+$, $\text{Au}^{\text{III}}(\text{PQ}_3)^+$, and $\text{Au}^{\text{III}}(\text{PQ}_4)^+$ in CH_2Cl_2 .



In contrast to the second reduction, a linear relationship is observed in the plot of $E_{1/2}$ vs the number of β,β' -fused Q substituents for all other reactions of $\text{Au}^{\text{III}}(\text{PQ}_n)^+$ (Figure 4-2). Similar relationships between $E_{1/2}$ and n are also seen for reductions and oxidations of the $\text{Au}^{\text{III}}(\text{PQ}_n)^+$ complexes in pyridine and THF, thus indicating that there is little to no solvent effect on the potential shifts.

4.2.2 Spectra of neutral and reduced compounds

UV-visible spectra of the different $\text{Au}^{\text{III}}(\text{PQ}_n)^+$ compounds in CH_2Cl_2 are shown in Figure 4-3. The P, PQ, and QPQ derivatives (Figure 4-3a) are each characterized by a single sharp Soret band at 415, 435 and 450 nm, respectively, while the PQ_2 , PQ_3 , and PQ_4 derivatives (Figure 4-3b) display three relatively broad Soret bands as seen in the figure. The energy of the most intense Soret band, labeled as I in Figure 4-3, and that of the two visible bands, labeled as II and III, all shift towards longer wavelengths as a function of the number of Q groups on $\text{Au}^{\text{III}}(\text{PQ}_n)^+$. This relationship is shown in Figure 4-4, where a plot of Soret band energy vs the number of Q groups, shows one linear relationship for all six compounds, and that of the two visible band shows two linear relationships, one for P, PQ, and PQ_2 and the other for PQ_2 , PQ_3 , and PQ_4 (Figure 4-4).

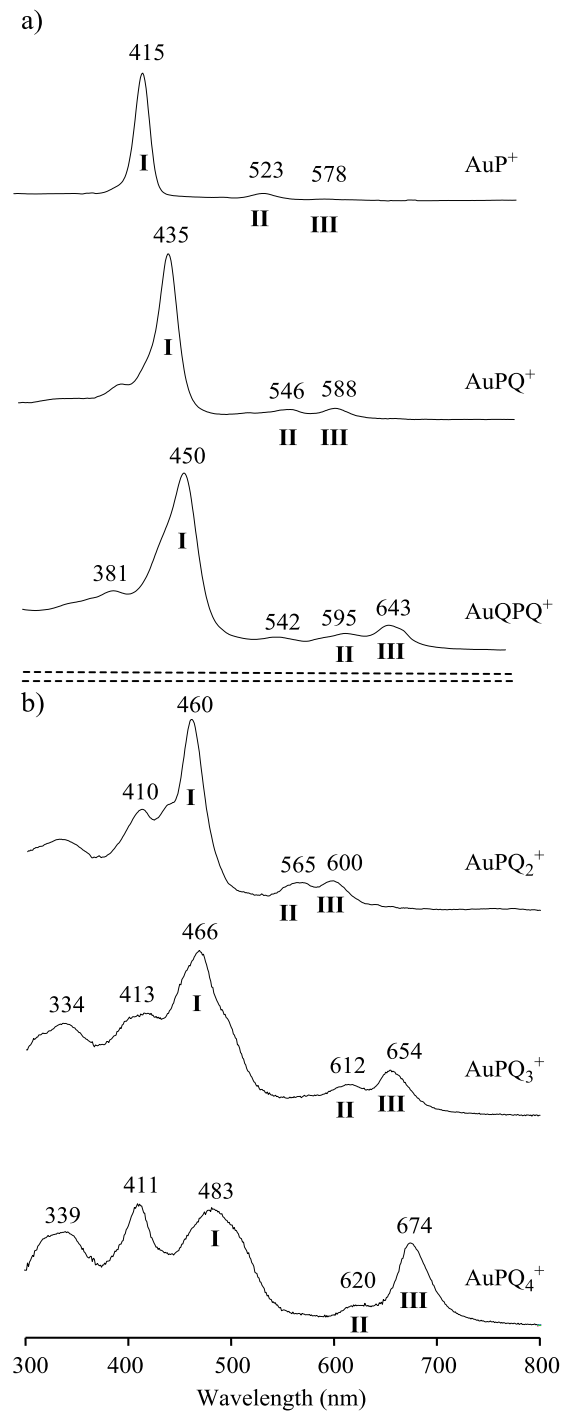


Figure 4-3. UV-visible spectra of (a) $\text{Au}^{\text{III}}(\text{P})^+$, $\text{Au}^{\text{III}}(\text{PQ})^+$, $\text{Au}^{\text{III}}(\text{QPQ})^+$ and (b) $\text{Au}^{\text{III}}(\text{PQ}_2)^+$, $\text{Au}^{\text{III}}(\text{PQ}_3)^+$, and $\text{Au}^{\text{III}}(\text{PQ}_4)^+$ in CH_2Cl_2 , 0.1 M TBAP.

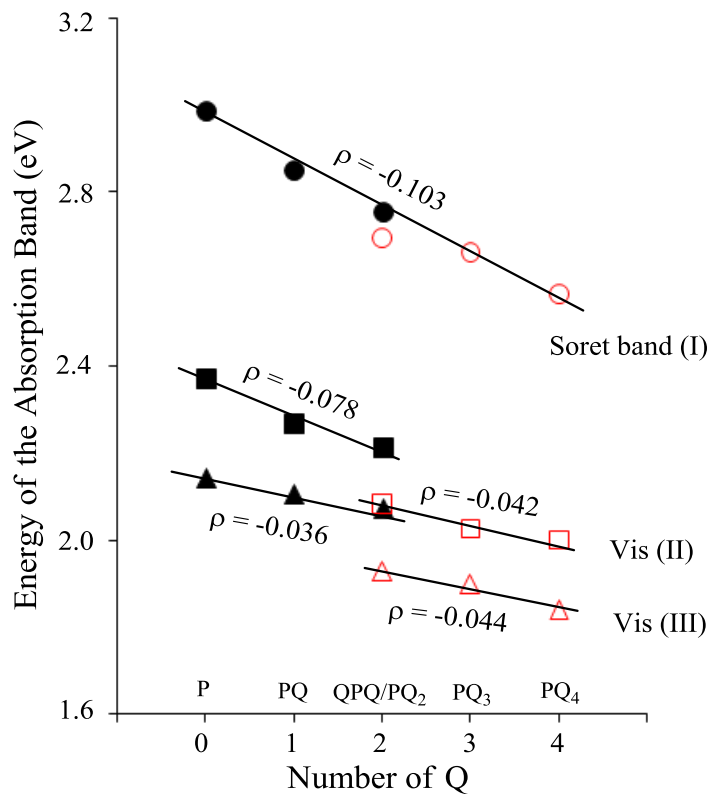


Figure 4-4. Plots of energy for the Soret and two visible bands of $\text{Au}^{\text{III}}(\text{PQ}_n)^+$ vs the number of Q groups on the macrocycle for P, PQ, and QPQ (black solid points) and PQ₂, PQ₃, and PQ₄ (red open points).

In order to evaluate possible changes in the site of electron transfer with increasing number of Q groups, the electrode reactions of $\text{Au}^{\text{III}}(\text{PQ}_2)^+$, $\text{Au}^{\text{III}}(\text{PQ}_3)^+$, and $\text{Au}^{\text{III}}(\text{PQ}_4)^+$ were monitored in CH_2Cl_2 , 0.1 M TBAP by UV-visible spectroelectrochemistry. Spectral changes obtained during the first two reductions of these three compounds are shown in Figure 4-5.

Similar evolutions in UV-visible spectra are seen during the first metal-centered reduction of the three porphyrins in CH_2Cl_2 . For example, the three Soret bands of neutral $\text{Au}^{\text{III}}(\text{PQ}_4)^+$ are red-shifted by 4-10 nm as the Au(II) complex is formed (Figure 4-5c), while the visible bands are blue-shifted by 9-18 nm during this one-electron addition process. The three Soret bands of $\text{Au}^{\text{III}}(\text{PQ}_3)^+$ are also red-shifted by 5-13 nm, while the Q bands exhibit a 14-23 nm blue-shift during the first controlled potential reduction at -0.20 V (Figure 4-5b). Several isosbestic points are seen, indicating the lack of spectrally detectable intermediates in the $\text{Au}^{\text{III}}/\text{Au}^{\text{II}}$ transition. The final spectra of singly reduced $\text{Au}^{\text{III}}(\text{PQ}_3)^+$ and $\text{Au}^{\text{III}}(\text{PQ}_4)^+$ are similar in CH_2Cl_2 to that of unreduced Pd^{II} and Zn^{II} quinoxalinoporphyrins containing the same number of Q groups. This comparison is shown in Figure 4-6 and further confirms the formation of gold(II) porphyrins after a one-electron reduction of the neutral compound.

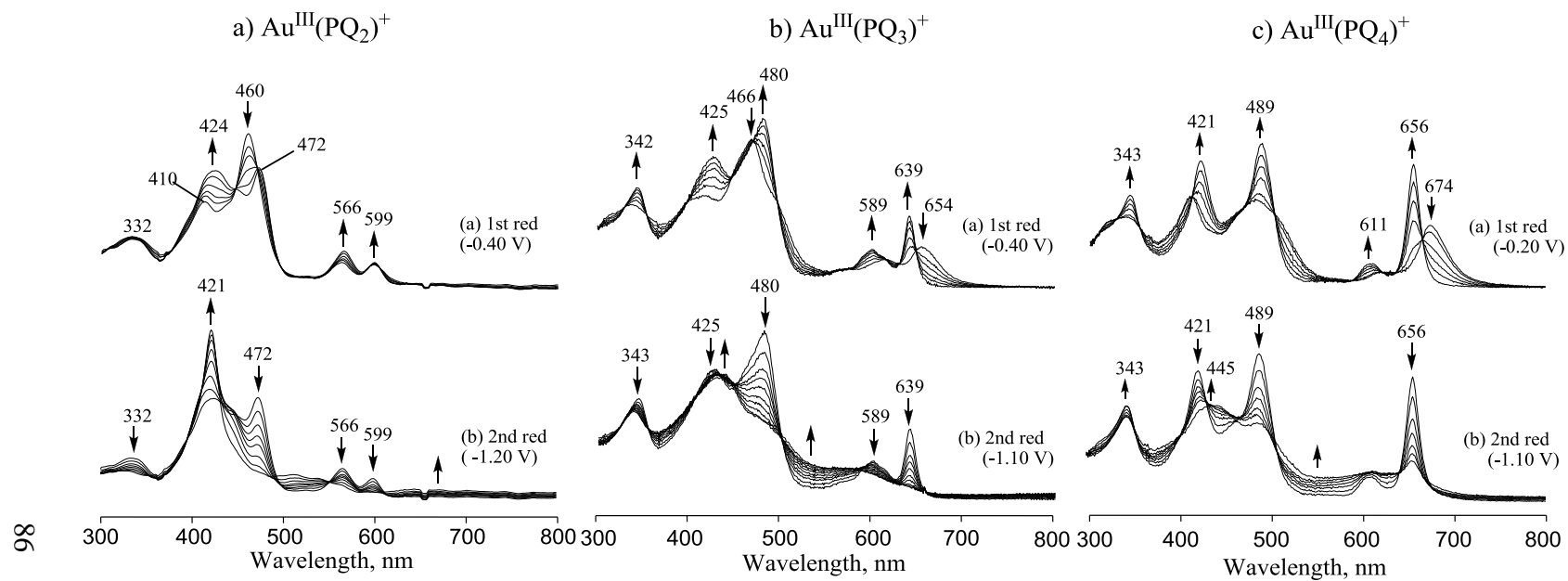


Figure 4-5. Thin-layer UV-visible spectral changes of $\text{Au}^{\text{III}}(\text{PQ}_2)\text{PF}_6$, $\text{Au}^{\text{III}}(\text{PQ}_3)\text{PF}_6$, and $\text{Au}^{\text{III}}(\text{PQ}_4)\text{PF}_6$ in CH_2Cl_2 containing 0.1 M TBAP during the reductions at indicated potential.

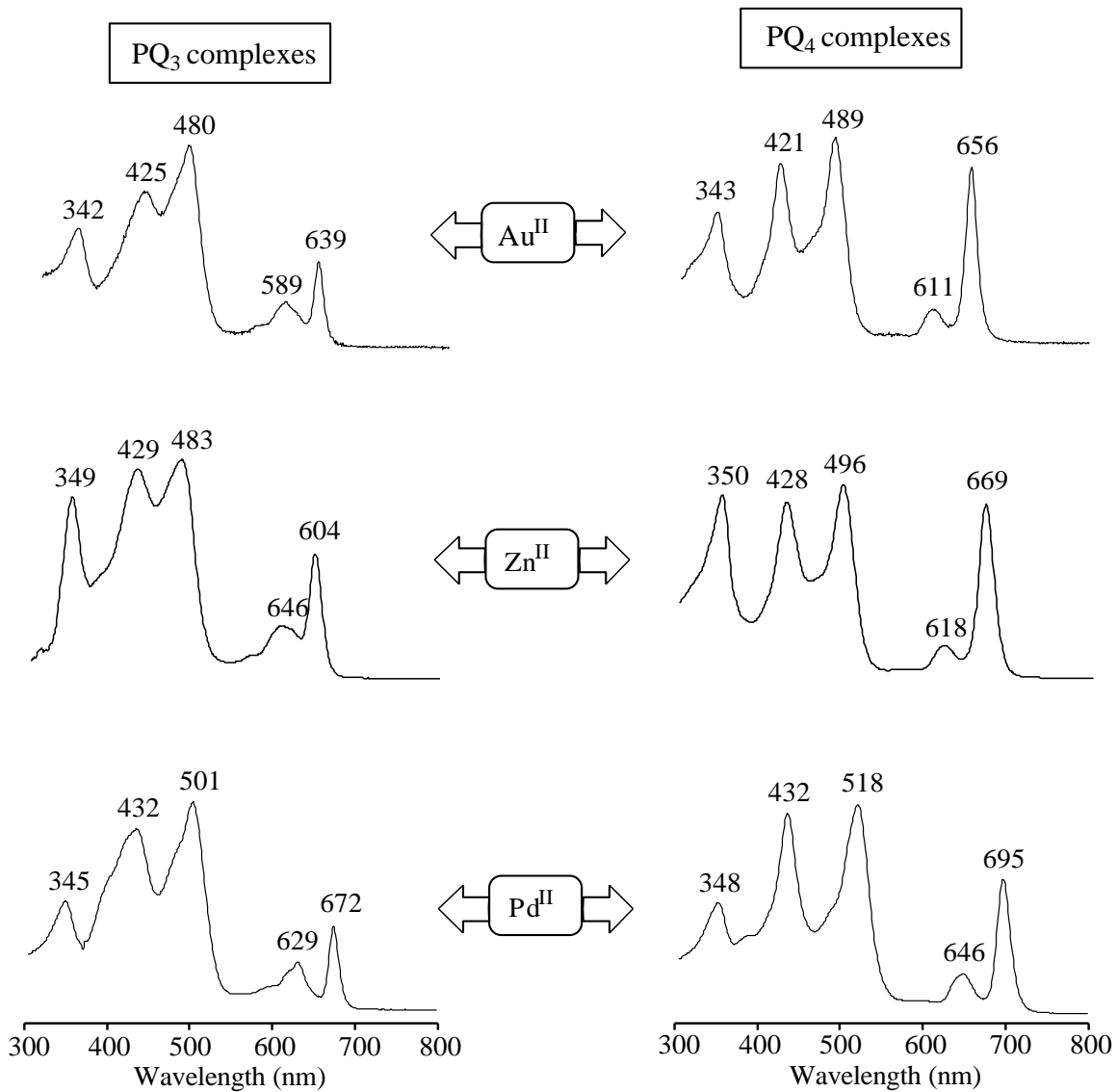


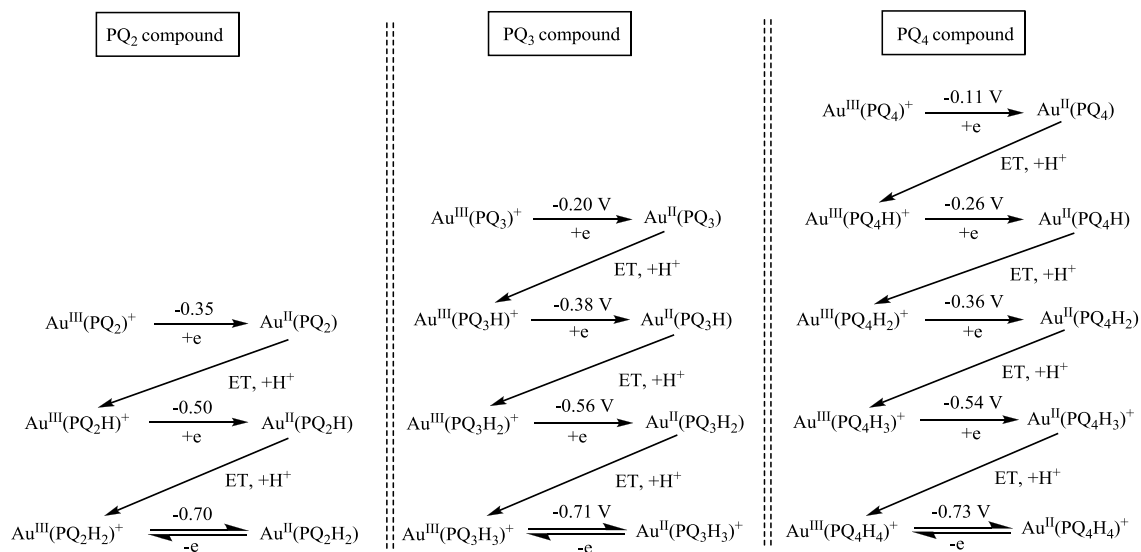
Figure 4-6. Comparisons of the UV-visible spectra of $\text{Au}^{\text{II}}(\text{PQ}_n)$, $\text{Zn}^{\text{II}}(\text{PQ}_n)$, and $\text{Pd}^{\text{II}}(\text{PQ}_n)$ ($n = 3$ and 4) in CH_2Cl_2 containing 0.1 M TBAP.

The second and third reductions of $\text{Au}^{\text{III}}(\text{PQ}_n)^+$ are proposed to occur at the porphyrin π -ring system and the decreased intensity of the Soret bands in the final spectra after reduction are consistent with this assignment. Examples of the spectral changes during the conversion of $\text{Au}^{\text{III}}(\text{PQ}_n)^+$ to its π -anion radical form are shown in Figure 4-5 for derivatives of PQ_2 , PQ_3 , and PQ_4 .

4.2.3 Electrochemistry of $\text{Au}^{\text{III}}(\text{PQ}_2)\text{PF}_6$, $\text{Au}^{\text{III}}(\text{PQ}_3)\text{PF}_6$, and $\text{Au}^{\text{III}}(\text{PQ}_4)\text{PF}_6$ in the presence of acid

The electrochemistry of $\text{Au}^{\text{III}}(\text{PQ}_2)^+$, $\text{Au}^{\text{III}}(\text{PQ}_3)^+$, and $\text{Au}^{\text{III}}(\text{PQ}_4)^+$ was also carried out in CH_2Cl_2 containing H^+ in the form of TFA. Examples of cyclic voltammograms are shown in Figure 4-7, and illustrate the significant differences in electrochemistry which result after the addition of TFA to solution. For all three quinoxalinoporphyrins, the first $\text{Au}^{\text{III}}/\text{Au}^{\text{II}}$ reduction (at $E_{1/2} = -0.31$, -0.17 , or -0.06 V in the absence of acid) becomes irreversible, and this process is followed at more negative potential by additional irreversible metal-centered reductions, as was previously reported for $\text{Au}^{\text{III}}(\text{PQ})^+$ and $\text{Au}^{\text{III}}(\text{QPQ})^+$ in acidic nonaqueous media.¹² $\text{Au}^{\text{III}}(\text{PQ}_2)^+$ undergoes two irreversible reductions followed by a reversible $\text{Au}^{\text{III/II}}$ process at a scan rate of 0.1 V/s, while $\text{Au}^{\text{III}}(\text{PQ}_3)^+$, and $\text{Au}^{\text{III}}(\text{PQ}_4)^+$ undergo three and four irreversible redox processes, respectively, followed at more negative potentials by a reversible $\text{Au}^{\text{III}}/\text{Au}^{\text{II}}$ transition. The sequential irreversible reductions are all assigned as Au(III)-centered electron transfers as shown in Scheme 4-3.

Scheme 4-3. Proposed reduction/oxidation mechanism of $\text{Au}(\text{PQ}_2)^+$, $\text{Au}(\text{PQ}_3)^+$, and $\text{Au}^{\text{III}}(\text{PQ}_4)^+$ in CH_2Cl_2 containing 2.5, 3.5 or 4.5 equivalents TFA.



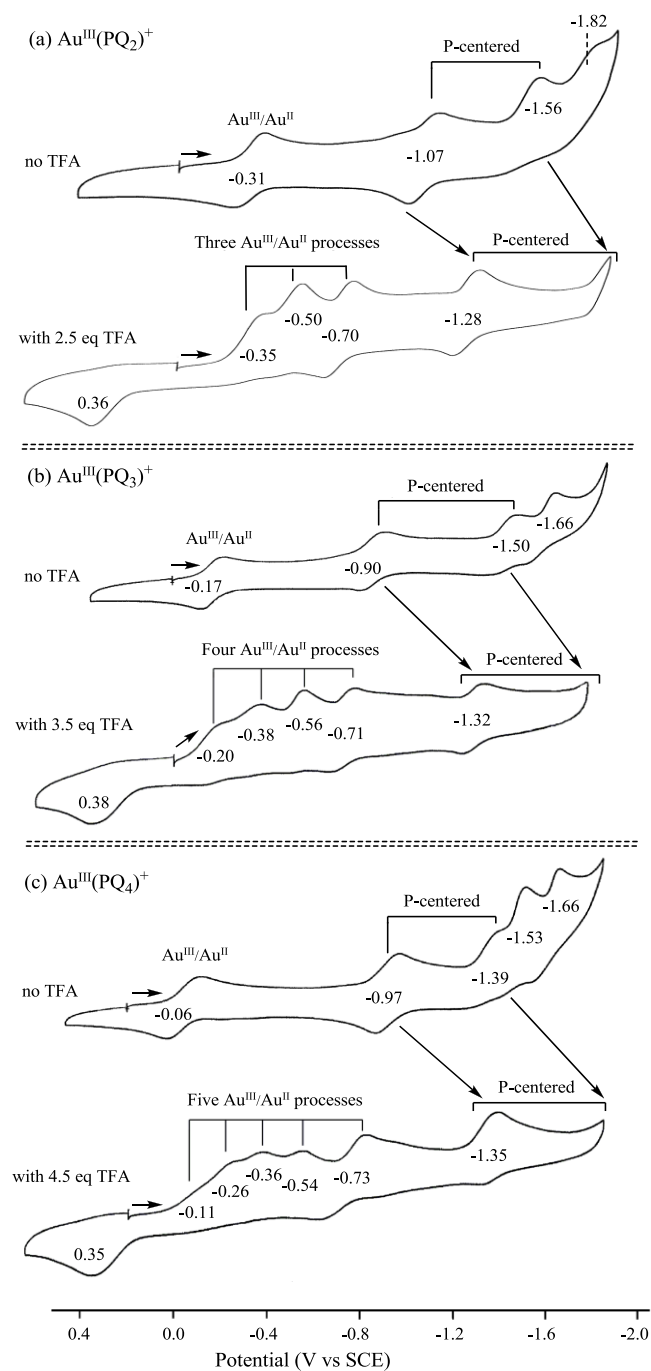


Figure 4-7. Cyclic voltammograms of (a) $\text{Au}^{\text{III}}(\text{PQ}_2)^+$, (b) $\text{Au}^{\text{III}}(\text{PQ}_3)^+$, and (c) $\text{Au}^{\text{III}}(\text{PQ}_4)^+$ in CH_2Cl_2 containing 0.1 M TBAP in the absence and presence of 2.5, 3.5, or 4.5 eq added TFA.

The potentials for each reduction of the quinoxalinoporphyrins in acidic CH_2Cl_2 are given in Schemes 4-1 and 4-3, and also summarized in Table 4-2 for three series of compounds, $\text{Au}^{\text{III}}(\text{PQ}_n)^+$, $\text{Au}^{\text{III}}(\text{PQ}_n\text{H}_n)^+$, and $\text{Au}^{\text{II}}(\text{PQ}_n\text{H}_n)$. The first series of compounds are unprotonated and the last two are fully protonated.

Several key points are evident from the data in Table 4-2, the most important of which is that the reversible potentials for reduction of the fully protonated $\text{Au}(\text{III})$ quinoxalinoporphyrins to their $\text{Au}(\text{II})$ forms are virtually independent of the number of Q groups, where $E_{1/2}$ varies over the narrow range of -0.70 to -0.73 V for the PQ_n derivatives with $n = 2, 3$ or 4 (see also last reaction in lower part of Scheme 4-3).

Similar reduction potentials are also seen for reduction of the partially protonated compounds in the PQ_2 , PQ_3 , and PQ_4 series. For example, reduction of the mono-Q protonated compound, $\text{Au}(\text{PQ}_3\text{H})^+$ is located at $E_{\text{pc}} = -0.38$ V, while an almost identical potential ($E_{\text{pc}} = -0.36$ V) is seen for the reduction of $\text{Au}(\text{PQ}_4\text{H}_2)^+$. Similar reduction potentials are also seen for $\text{Au}^{\text{II}}(\text{PQ}_2\text{H})$ (-0.50 V), $\text{Au}(\text{PQ}_3\text{H}_2)^+$ (-0.56 V), and $\text{Au}(\text{PQ}_4\text{H}_3)^+$ (-0.54 V).

Finally, the potential for reduction of the fully protonated Au^{II} derivatives of PQ_2 , PQ_3 and PQ_4 ranges from -1.28 V for $\text{Au}^{\text{II}}(\text{PQ}_2\text{H}_2)$ to -1.35 V for $\text{Au}^{\text{II}}(\text{PQ}_4\text{H}_4)$, and varies only slightly as a function of the number of Q groups on the compounds. (see Figure 4-7)

Table 4-2. Reduction Potentials (V vs SCE) of $\text{Au}^{\text{III}}(\text{PQ}_n)^+$, $\text{Au}^{\text{III}}(\text{PQ}_n\text{H}_n)^+$, and $\text{Au}^{\text{II}}(\text{PQ}_n\text{H}_n)$ in CH_2Cl_2 , 0.1 M TBAP with added TFA.^a

number of Q	unprotonated	fully protonated		reference
	$\text{Au}^{\text{III}}(\text{PQ}_n)^+$	$\text{Au}^{\text{III}}(\text{PQ}_n\text{H}_n)^+$	$\text{Au}^{\text{II}}(\text{PQ}_n\text{H}_n)$	
0	-0.64	-0.64	-1.15	12
1	-0.36 ^b	-0.60	-1.11	12
2^c	-0.29 ^b	-0.72	-1.19	12
2^d	-0.31	-0.70	-1.28	<i>tw</i>
3	-0.20	-0.71	-1.32	<i>tw</i>
4	-0.11	-0.73	-1.35	<i>tw</i>

^a1.5, 2.5, 2.5, 3.5, 4.5 equiv TFA added in solution for compounds with $n = 1-4$, respectively; potentials for PQ compound measured in PhCN. ^bIrreversible peak potential at a scan rate of 0.10 V/s. *tw* = this work. ^cThe QPQ derivative. ^dThe PQ₂ derivative.

4.2.4 Spectroelectrochemistry of $\text{Au}^{\text{III}}(\text{PQ}_2)^+$, $\text{Au}^{\text{III}}(\text{PQ}_3)^+$, and $\text{Au}^{\text{III}}(\text{PQ}_4)^+$ in the presence of acid

Thin-layer UV-visible spectroelectrochemistry was carried out in CH_2Cl_2 containing 0.1 M TBAP and added TFA to elucidate UV-visible spectra of the PQ_2 , PQ_3 , and PQ_4 derivatives in each stepwise reduced and protonated forms. Spectral changes obtained during the multiple one-electron reductions of $\text{Au}^{\text{III}}(\text{PQ}_2)^+$ and $\text{Au}^{\text{III}}(\text{PQ}_3)^+$ are shown in Figures 4-8 and 4-9, and the final UV-visible spectrum after each one electron reduction of $\text{Au}^{\text{III}}(\text{PQ}_4)^+$ are shown in Figure 4-10. The reactants and products of the $\text{Au}^{\text{III}}/\text{Au}^{\text{II}}$ processes are given in Scheme 4-3.

The unreduced Au(III) quinoxalinoporphyrins are unprotonated in CH_2Cl_2 solutions containing less than 20 equivalents of added acid, as evidenced by the UV-visible spectra. In contrast, protonation readily occurs for the electroreduced species, and this leads to characteristic shifts in the UV-vis spectra. For example, after potential reduction of $\text{Au}^{\text{III}}(\text{PQ}_3)^+$ at -0.25 V in CH_2Cl_2 containing 3.5 eq TFA (Figure 4-9a), the Soret band shifts from 466 to 452 nm and the Q band shifts from 654 to 600 nm as $\text{Au}^{\text{III}}(\text{PQ}_3\text{H})^+$ is generated as a product of the one-electron reduction and following chemical reaction. Further reduction of $\text{Au}^{\text{III}}(\text{PQ}_3\text{H})^+$ at -0.40 V in the acid containing CH_2Cl_2 solution gives a porphyrin product with a Soret band at 429 nm and a Q band at 562 nm (Figure 4-9b). This spectrum is assigned to $\text{Au}^{\text{III}}(\text{PQ}_3\text{H}_2)^+$, and is almost identical to the spectrum of $\text{Au}^{\text{III}}(\text{PQ})^+$, which has bands at 435 and 588 nm in CH_2Cl_2 .¹² The reduction of $\text{Au}^{\text{III}}(\text{PQ}_3\text{H}_2)^+$ at -0.60 V (Figure 4-9c) leads to $\text{Au}^{\text{III}}(\text{PQ}_3\text{H}_3)^+$ as a final porphyrin product ($\lambda = 409, 520$ and 640 nm), and this is followed by another $\text{Au}^{\text{III}}/\text{Au}^{\text{II}}$

process at -0.80 V (Figure 4-9d) to give the Au(II) product $\text{Au}^{\text{II}}(\text{PQ}_3\text{H}_3)$. The UV-visible spectrum of the fully protonated Au(II) porphyrin is characterized by a Soret band at 420 nm and resembles the spectrum of both $\text{Au}^{\text{II}}(\text{P})$ (420 nm)¹² and $\text{Au}^{\text{II}}(\text{PQ}_4\text{H}_4)$ (419 nm) (see Figure 4-10). Finally the reduction of $\text{Au}^{\text{II}}(\text{PQ}_3\text{H}_3)$ at -1.40 V (Figure 4-9e) results in a decreased intensity Soret band, consistent with the formation of an Au(II) porphyrin π -anion radical under the given solution conditions.

UV-visible spectra obtained before and after the first five reductions of $\text{Au}^{\text{III}}(\text{PQ}_4)^+$ in CH_2Cl_2 containing 4.5 eq TFA are shown in Figure 4-10. The stepwise products of the first four reductions and coupled chemical reactions are represented as $\text{Au}^{\text{III}}(\text{PQ}_4\text{H}_x)$, where $x = 1-4$ and the prevailing reduction mechanism is shown in Scheme 4-3. The maximum Soret band intensity of the Au(III) porphyrins is stepwise blue shifted from 483 nm for $x = 0$ (the unprotonated porphyrin) to 405 nm for $x = 4$ (the fully protonated Q_4H_4 derivative).

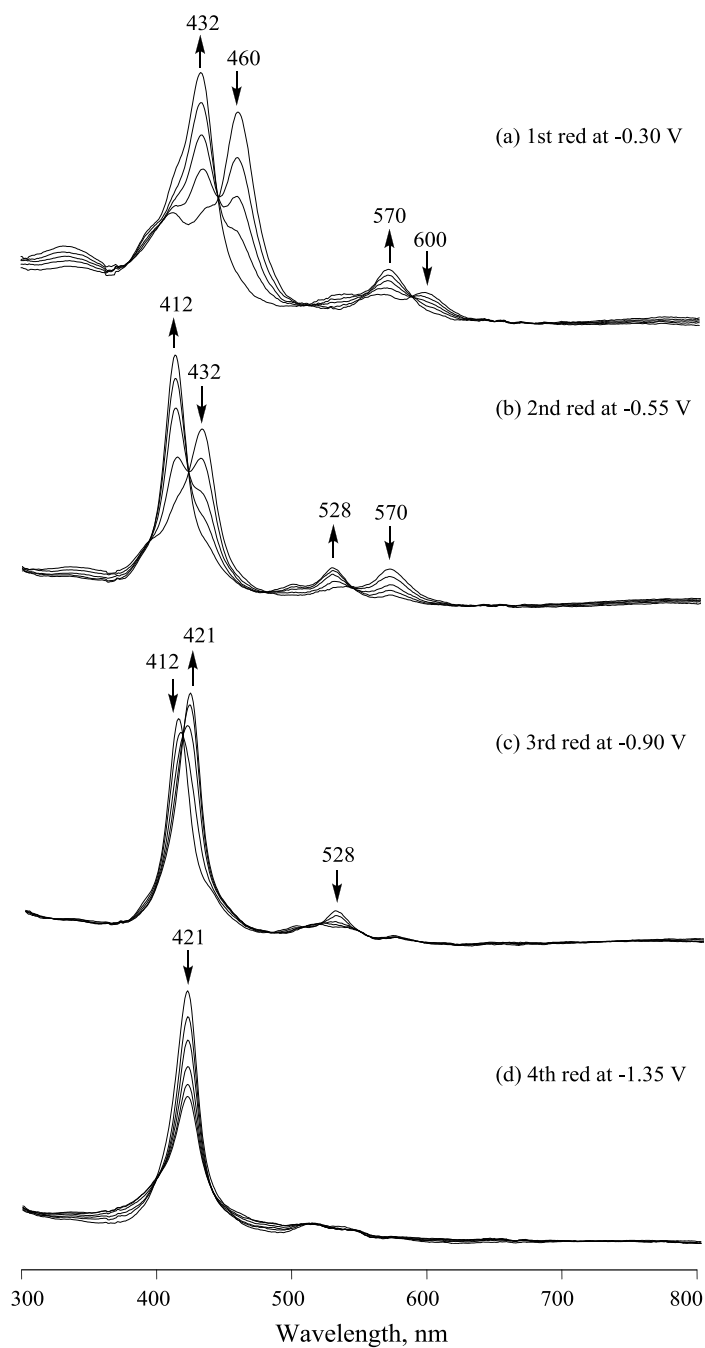


Figure 4-8. Thin-layer UV-visible spectral changes of $\text{Au}(\text{PQ}_2)^+$ during reductions at (a) -0.30 (b) -0.55, (c) -0.90, and (d) -1.35 V in CH_2Cl_2 containing 0.1 M TBAP and 2.5 eq added TFA.

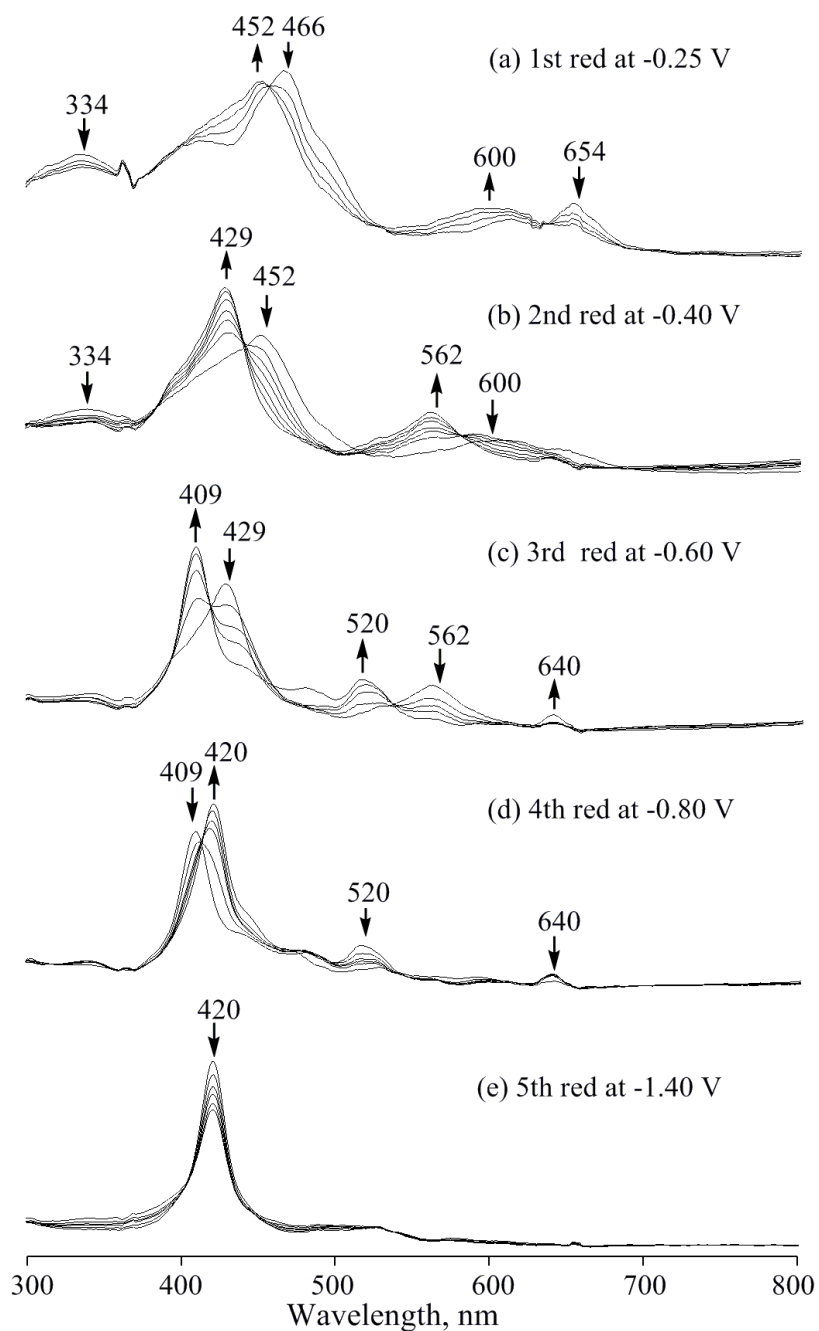


Figure 4-9. Thin-layer UV-visible spectral changes of $\text{Au}(\text{PQ}_3)^+$ during reductions at (a) -0.25 (b) -0.40, (c) -0.60, and (d) -0.80 V in CH_2Cl_2 containing 0.1 M TBAP and 3.5 eq added TFA.

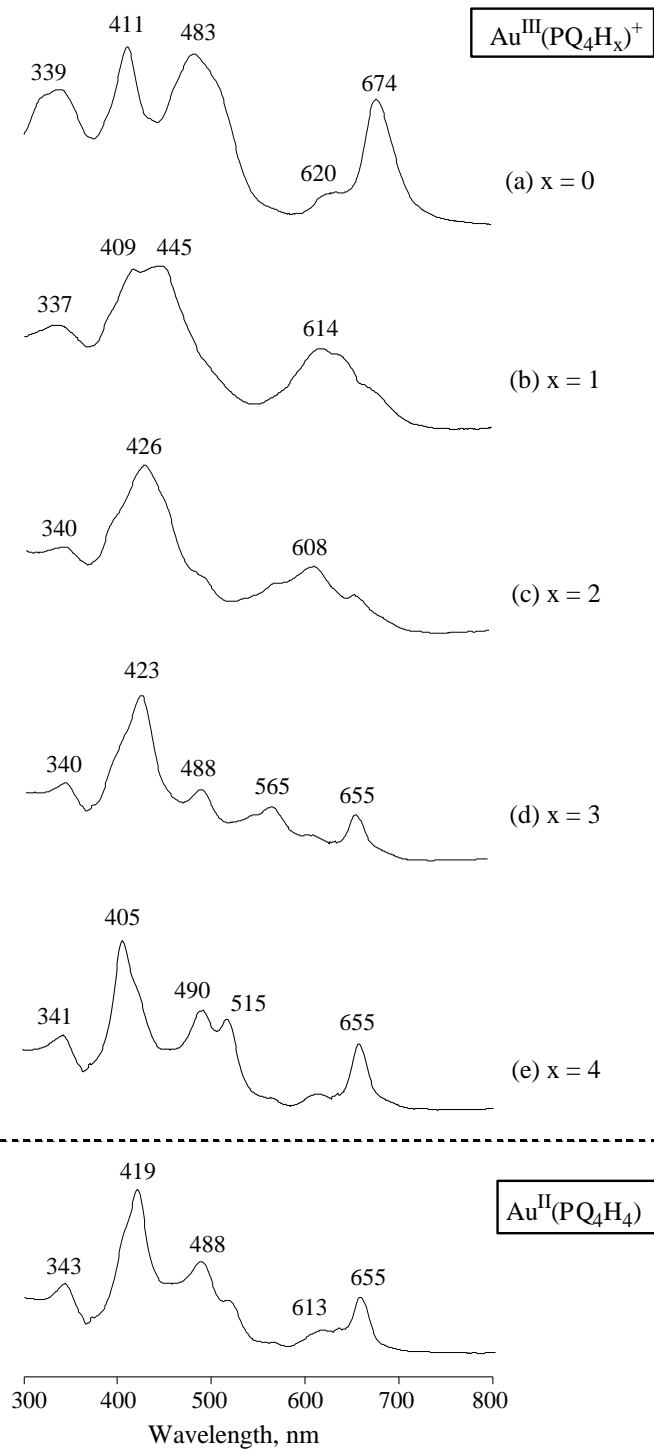


Figure 4-10. UV-visible spectra of $\text{Au}^{\text{III}}(\text{PQ}_4)^+$ and its stepwise reduction products in CH_2Cl_2 containing 0.1 M TBAP and 4.5 equivalents added TFA.

4.3 Conclusions

In summary, the electrochemical and spectroelectrochemical properties of $\text{Au}^{\text{III}}(\text{PQ}_3)^+$ and $\text{Au}^{\text{III}}(\text{PQ}_4)^+$ were examined in CH_2Cl_2 containing 0.1 M TBAP. Each porphyrin undergoes one metal-centered reduction to form the corresponding Au(II) porphyrin, and this reaction is followed by two porphyrin ring-centered reductions and one or two Q-centered reductions. Different electrochemical behavior is seen for $\text{Au}^{\text{III}}(\text{PQ}_3)^+$ and $\text{Au}^{\text{III}}(\text{PQ}_4)^+$, as compared to the related P, PQ, and QPQ derivatives. Negative shifts in reduction potentials are seen upon going from $\text{Au}^{\text{III}}(\text{QPQ})^+$ to $\text{Au}^{\text{III}}(\text{PQ}_3)^+$ to $\text{Au}^{\text{III}}(\text{PQ}_4)^+$, while positive shifts are observed upon going from the P to PQ to QPQ derivatives under the same solution conditions. All of the Au(III) quinoxalinoporphyrins in the presence of TFA will undergo multiple $\text{Au}^{\text{III}}/\text{Au}^{\text{II}}$ processes due to an internal electron transfer and protonation of the fused Q group(s) on the porphyrin macrocycle, which regenerates a new Au(III) porphyrin with a reduced and protonated quinoxaline group. The number of multiple $\text{Au}^{\text{III}}/\text{Au}^{\text{II}}$ reactions observed is one more than the number of Q groups on the compound. Thus, $\text{Au}^{\text{III}}(\text{PQ})^+$ and $\text{Au}^{\text{III}}(\text{QPQ})^+$ undergo two and three metal-centered reductions,¹² while $\text{Au}^{\text{III}}(\text{PQ}_3)^+$ undergoes four metal-centered reductions, and $\text{Au}^{\text{III}}(\text{PQ}_4)^+$ exhibits five $\text{Au}^{\text{III}}/\text{Au}^{\text{II}}$ processes in the presence of acid. The electrochemically initiated protonation of the Q-group changes not only the redox potentials of the compounds, but also their UV-visible properties, as well as the conjugation between the porphyrin ring and quinoxaline units.

4.4 References

- (1) Kadish, K. M.; Van Caemelbecke, E.; Rotal, G. In *The Porphyrin Handbook*, Kadish, K. M.; Smith, K. M.; Guillard, R., Eds, Academic Press: New York, 2000; Vol. 8, pp 1-114.
- (2) Kadish, K. M.; E, W.; Ou, Z.; Shao, J.; Santic, P. J. Ohkubo, K.; Fukuzumi, S.; Crossley, M. J. *Chem. Comm.* **2002**, 356.
- (3) Ou, Z.; Kadish, K. M.; E, W.; Shao, J.; Santic, P. J.; Ohkubo, K.; Fukuzumi, S.; Crossley, M. J. *Inorg. Chem.* **2004**, *43*, 2078.
- (4) Zhu, W.; Santic, M.; Ou, Z.; Santic, P. J.; McDonald, J. A.; Brotherhood, P. R.; Crossley, M. J.; Kadish, K. M. *Inorg. Chem.* **2010**, *49*, 1027.
- (5) Ohkubo, K.; Garcia, R.; Santic, P. J.; Khoury, T.; Crossley, M. J.; Kadish, K. M.; Fukuzumi, S. *Chem.- Eur. J.* **2009**, *15*, 10493.
- (6) Santic, P. J.; E, W.; Ou, Z.; Shao, J.; McDonald, J. A.; Cai, Z.; Kadish, K. M.; Crossley, M. J.; Reimers, J. R. *Phys. Chem. Chem. Phys.* **2008**, *10*, 515.
- (7) Ou, Z.; E, W.; Zhu, W.; Thordarson, P.; Santic, P. J.; Crossley, M. J.; Kadish, K. M. *Inorg. Chem.* **2007**, *46*, 10840.
- (8) Kadish, K. M.; E, W.; Santic, P. J.; Ou, Z.; Shao, J.; Ohkubo, K.; Fukuzumi, S.; Govenlock, L. J.; McDonald, J. A.; Try, A. C.; Cai, Z.; Reimers, J. R.; Crossley, M. J. *J. Phys. Chem. B* **2007**, *111*, 8762.
- (9) Hutchison, J. A.; Santic, P. J.; Crossley, M. J.; Nagamura, T.; Ghiggino, K. P. *Phys. Chem. Chem. Phys.* **2009**, *11*, 3478.
- (10) Armstrong, R. S.; Foran, G. J.; Hough, W. A.; D'Alessandro, D. M.; Lay, P. A.; Crossley, M. J. *Dalton Trans.* **2006**, *40*, 4805.
- (11) Fukuzumi, S.; Ohkubo, K.; Zhu, W.; Santic, M.; Khoury, T.; Santic, P. J.; E, W.; Ou, Z.; Crossley, M. J.; Kadish, K. M. *J. Am. Chem. Soc.* **2008**, *130*, 9451.
- (12) Ou, Z.; Zhu, W.; Fang Y.; Santic, P. J.; Khoury, T.; Crossley, M. J.; Kadish, K. M. *Inorg. Chem.* **2011**, *50*, 12802.
- (13) E, W.; Kadish, K. M.; Santic, P.; Khoury, T.; Govenlock, L.; Ou, Z.; Shao, J.; Ohkubo, K.; Reimers, J.; Fukuzumi, S.; Crossley, M. J. *J. Phys. Chem. A* **2008**, *112*, 556.

- (14) Ou, Z.; Zhu, W.; Santic, P.; Fang, Y.; Crossley, M.; Kadish, K. M. *J. Porphyrins Phthalocyanines* **2012**, *16*, 5.
- (15) Santic, P.; E, W.; Ou, Z.; Shao, J.; McDonald, J.; Cai, Z.; Kadish, K. M. *Phys. Chem. Chem. Phys.* **2008**, *10*, 268.
- (16) Ou, Z.; E, W.; Shao, J.; Burn, P.; Craig, S.; Robin, W.; Kadish, K. M.; Crossley, M. J. *J. Porphyrins Phthalocyanines* **2005**, *9*, 142.
- (17) Crossley, M. J.; Santic, P. J.; Walton, R.; Reimers, J. R. *Org. Biomol. Chem.* **2003**, *1*, 2777.
- (18) Kadish, K. M.; Li, J.; Van Caemelbecke, E.; Ou, Z.; Guo, N.; Autret, M.; D'Souza, F.; Tagliatesta P. *Inorg. Chem.* **1997**, *36*, 6292.
- (19) D'Souza, F.; Zandler, M. E.; Tagliatesta, P.; Ou, Z.; Shao, J.; Van Caemelbecke, E.; Kadish, K. M. *Inorg. Chem.* **1998**, *37*, 4567.
- (20) Tagliatesta, P.; Li, J.; Autret, M.; Van Caemelbecke, E.; Villard, A.; D'Souza, F.; Kadish, K. M. *Inorg. Chem.* **1996**, *35*, 5570.
- (21) Kadish, K. M.; D'Souza, F.; Villard, A.; Autret, M.; Van Caemelbecke, E.; Bianco, P.; Antonini, A.; Tagliatesta, P. *Inorg. Chem.* **1994**, *33*, 5169.

Chapter Five

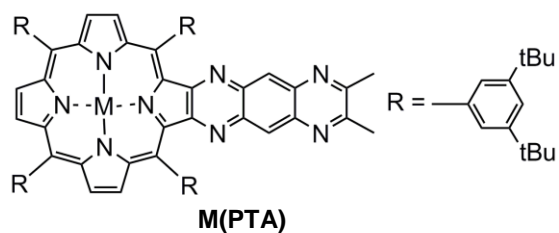
Electrochemistry of Mono- and Bis-porphyrins Containing

a β,β' -fused Tetraazaanthracene Group

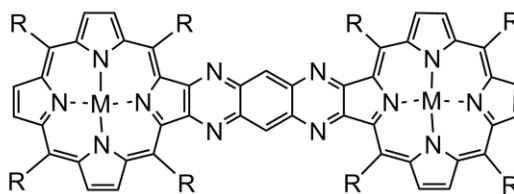
5.1 Introduction

Porphyrins and porphyrin-like compounds have unique physical and photochemical properties, suggesting their use for diverse applications in the fields of biology, medicine, and material science.¹⁻³ In this regard a number of ring-extended porphyrins have been synthesized for use as molecular wires and switches.⁴⁻¹⁴ The ‘simplest’ ring-extended derivatives among these compounds are the 5,10,15,20-tetrakis(3,5-di-tert-butylphenyl)-porphyrins containing a β,β' -fused quinoxaline (Q) or tetraazaanthracene (TA) group. These compounds, whose structures are shown in Chart 5-1, are represented as M(PQ) and M(PTA), where PQ = the dianion of 5,10,15,20,tetrakis(3,5-di-tert-butylphenyl)quinoxalino-[2,3-b]porphyrin and PTA = the dianion of 5,10,15,20,tetrakis(3,5-di-tert-butylphenyl)-6',7'-dimethyl-1',4',5',8'-tetraazaanthraceno-[2',3'-b]porphyrin. Tetraazaanthracene (TA) can also be fused to two porphyrin macrocycles, linking them in a linear fashion. These TA-linked bis-porphyrins, are also shown in Chart 5-1 and are represented as M(P)-TA-(P)M, where P is the dianion of 5,10,15,20,tetrakis(3,5-di-tert-butylphenyl)porphyrin.

(a) Investigated porphyrins

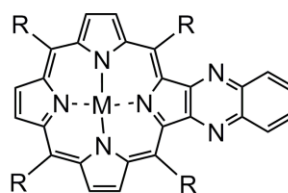


1. M = 2H; 2. M = Cu(II); 3. M = Zn(II)



4. M = 2H; 5. M = Cu(II); 6. M = Zn(II);
7. M = Ni(II); 8. M = Pd(II)

(b) Reference compounds



Q

TA

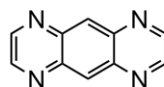
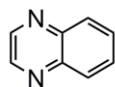


Chart 5-1. Structures of investigated porphyrins and reference compounds

Elucidating the redox potentials and spectroscopic properties of bis-porphyrins such as M(P)-TA-(P)M before and after electron transfer is important for better understanding electronic properties of those oligoporphyrins, and the data can provide key information needed for the enhanced development of applications in molecular electronics. The linking of porphyrins at their β,β' -pyrrole positions is a first step in preparing porphyrin modular units as building blocks towards a porphyrin-based molecular wire.^{4,15,16} The synthetic flexibility afforded by functionalizing the porphyrin β -pyrrolic periphery, as well as the ability to selectively metalate constituent macrocycles,^{4,17-21} offers the possibility to create molecules with pre-designed molecular functionality. β,β' -appended and linked porphyrins have been proposed as key components for applications in the area of molecular switches,¹² rectifiers,²² solar cells,²³ and in long-distance electron transfer.^{24,25} In addition, computational work on this class of molecule has laid the groundwork for understanding the experimental behavior of porphyrins in molecular wire applications.²⁶⁻²⁹ With specific reference to the β,β' -linked porphyrins, it has been shown that the bridging unit reduces the degree of delocalization within the array as compared to the Osuka porphyrin tapes,^{30,31} but not to the extent where it impairs its function as a molecular wire.³² Computational work has also shown that the molecular wire characteristics of this type of molecule are highly susceptible to tuning, either by metal chelation or chemical substitution,²⁶ which has recently been confirmed by experimental evidence.^{14,20,22}

The basic component of the many β,β' -linked porphyrin arrays proposed as molecular wires is the TA bridged porphyrin dyad,⁴ which is one focus of this current manuscript. This molecule contains the tetraazaanthracene bridging unit which confines

the appended macrocycles in a rigid coplanar arrangement. It is also a perfect model compound for understanding what role the bridge plays in mediating electronic communication between porphyrins, which theoretical work has indicated are critical in determining whether molecules of this type are viable as molecular wires.^{28,29} Extensive research has been undertaken in understanding the electronic character of the porphyrin-bridge interaction in quinoxalinoporphyrins, where delocalization of electron density upon electrochemical reduction has been demonstrated.^{7,22} It has also been shown that the electron distribution in the molecule can be altered by both metalation and through chemical substitution.¹⁴ In the current study, we have extended our previous electrochemical analyses of quinoxalinoporphyrins M(PQ)^{7,10,22} by the fusing of a larger ring system to a tetraazaanthracene-linked porphyrin monomer M(PTA), and we have investigated its electronic character conjointly with its π -conjugated bis-porphyrin parent.

Our laboratories have earlier reported the electrochemistry of M(P)-TA(P)M where M = H₂⁴, Mn(III),⁹ or Co(II).¹⁰ All three bis-porphyrins show a rich electrochemistry in nonaqueous media, with electron transfer reactions occurring in some cases at the conjugated π -ring system of the two macrocycles and in others at the central metal ions. However, to our knowledge, no electrochemical properties of monoporphyrins with a β,β' -fused TA group have been reported in the literature, nor is detailed information available on the electrochemistry of TA-linked bis-porphyrins containing a non-electroactive central metal ion where all redox reactions would involve only the conjugated π ring system of the macrocycle or the TA linker. Both points are addressed in the present study for two types of compounds, M(PTA) where M = H₂, Cu(II), or Zn(II), and M(P)-TA-(P)M where M = H₂, Cu(II), Zn(II), Ni(II), and Pd(II). As

will be demonstrated, a strong interaction between the two electroactive macrocycles of the bis-porphyrin is observed. The effect of the fused electroactive TA group and central metal ion on the redox potentials, UV-visible spectra, and porphyrin-porphyrin interaction across the TA-bridge are discussed.

5.2 Results and Discussion

5.2.1 Electrochemistry of mono-porphyrins

5.2.1.1 Free-base porphyrin, H₂(PTA)

The electrochemistry of H₂(PTA) in nonaqueous media is similar in many respects to that which has been previously described for H₂(PQ) under similar solution conditions.^{7,22} By way of example, cyclic voltammograms for H₂(P), H₂(PQ), and H₂(PTA) in PhCN, 0.1 M TBAP are shown in Figure 5-1. The free-base porphyrin without the fused Q or TA group, H₂(P), undergoes two reversible one-electron additions which are porphyrin-ring centered, and lead to the stepwise formation of a π -anion radical and dianion, respectively. Two porphyrin ring-centered reductions are also obtained for H₂(PQ) ($E_{1/2} = -1.08$ and -1.31 V) and H₂(PTA) ($E_{1/2} = -0.93$ and -1.13 V), and as seen from the figure, both sets of reductions are shifted positively with respect to $E_{1/2}$ values for H₂(P). The positive shift in $E_{1/2}$ amounts to 110 mV for the first reduction upon going from H₂(P) to H₂(PQ) and another 150 mV shift occurs upon going from H₂(PQ) to H₂(PTA). This is consistent with the larger conjugated π -ring system of the PTA complex, leading to a more facile reduction.

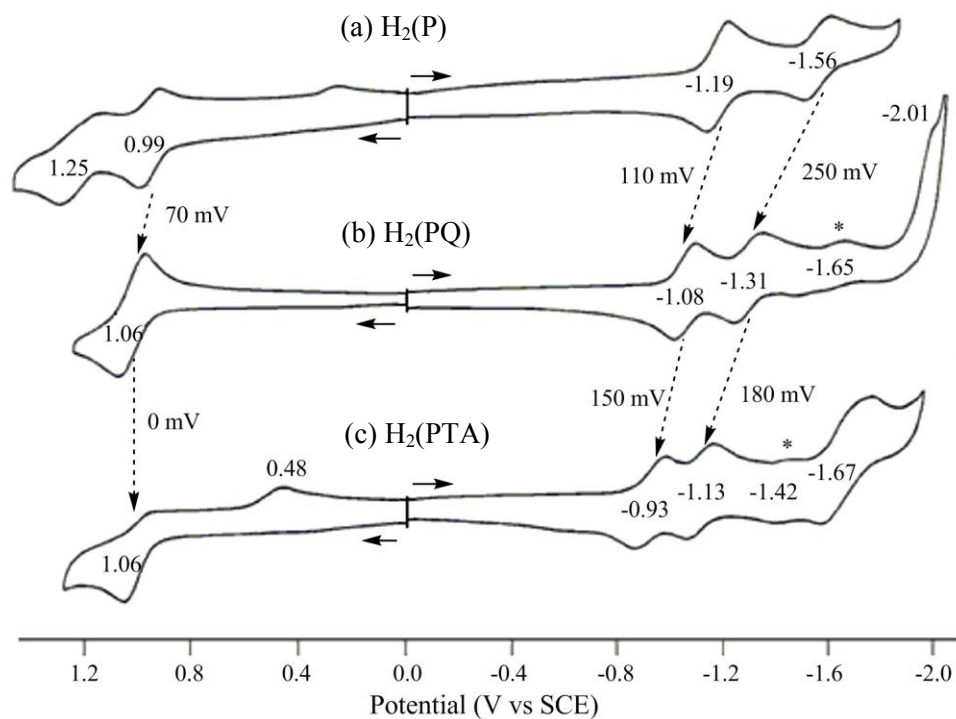


Figure 5-1. Cyclic voltammograms of $H_2(P)$, $H_2(PQ)$, and $H_2(PTA)$ in PhCN containing 0.1 M TBAP. Scan rate = 0.1 V/s. The reductions labelled with an asterisk are associated with a 'side reaction' involving a protonated form of the reduced porphyrin.

Two additional redox processes are also seen in the cyclic voltammograms of $H_2(\text{PTA})$ and $H_2(\text{PQ})$ at more negative potentials. The first, at $E_{1/2} = -1.42$ V (PTA) or -1.65 V (PQ), is labeled with an asterisk in Figure 5-1, and has a reduced peak current as compared to the first two one-electron additions. This process is not observed for $H_2(\text{P})$ up to the negative potential limit of the PhCN solvent (-2.00 V vs SCE), nor is it observed for $H_2(\text{PTA})$ or $H_2(\text{PQ})$ when pyridine is used as the electrochemical solvent. This result and related data in the literature on protonated $M(\text{PQ})$ derivatives^{10,33} suggest that similar protonated forms of $H_2(\text{PTA})$ and $H_2(\text{PQ})$ are formed in the PhCN solvent after an initial reduction at the porphyrin conjugated macrocycle.

The reduction of $H_2(\text{PTA})$ at $E_{1/2} = -1.67$ is assigned as a TA-centered multi-electron transfer. This reversible process is located at almost the same half-wave potential of -1.65 to -1.73 V in CH_2Cl_2 , PhCN, and pyridine (see Figure 5-2 and Table 5-1), and is characterized by a maximum peak current which is higher than the first one-electron reduction by a factor of 2.4 (PhCN) to 3.0 (py). According to cyclic voltammetric theory, the peak current of a reversible process is proportional to $n^{3/2}$ where n is the number of electrons transferred.³⁴ Thus the overall data in Figures 5-1 and 5-2 are consistent with two initial stepwise one-electron additions to the conjugated π -ring system of $H_2(\text{PTA})$ followed, at more negative potentials, by a global two-electron addition which involves the TA group of the porphyrin.

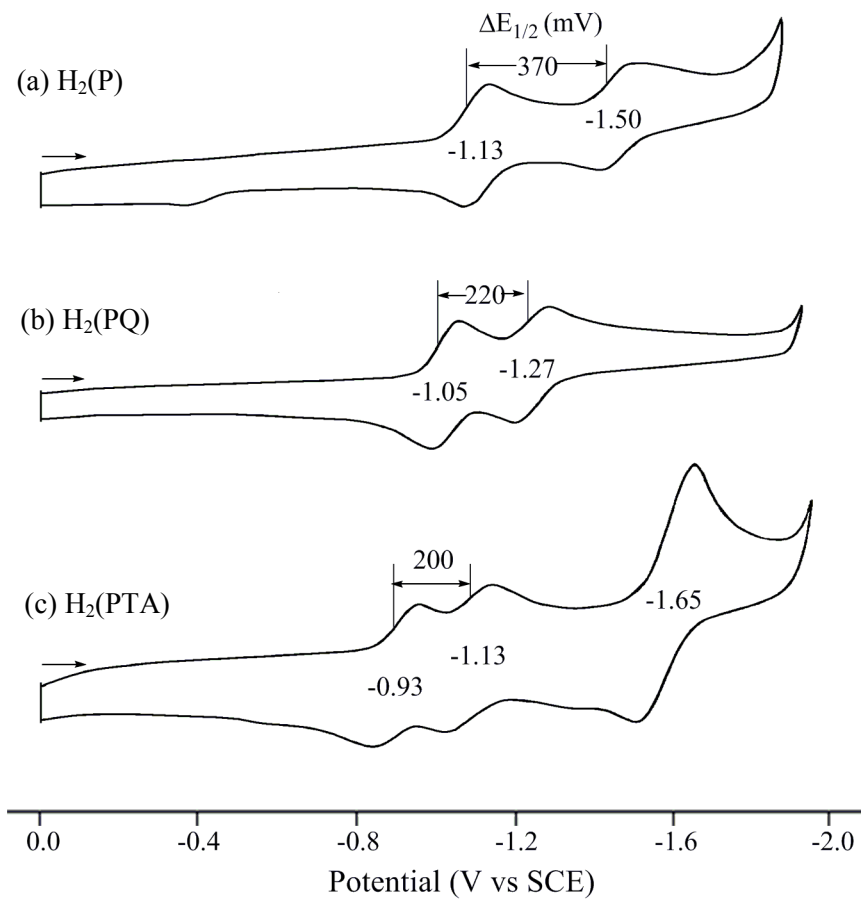


Figure 5-2. Cyclic voltammograms of $H_2(P)$, $H_2(PQ)$, and $H_2(PTA)$ in pyridine containing 0.1 M TBAP.

The potential separation ($\Delta E_{1/2}$) between the reversible π -ring centered reductions of the three related free-base porphyrins, H₂(P), H₂(PQ), and H₂(PTA), vary with the macrocyclic structure. This separation equals 200 mV for H₂(PTA) ($E_{1/2} = -0.93$ and -1.13 V), 230 mV for H₂(PQ) ($E_{1/2} = -1.08$ and -1.31 V) and 370 mV for H₂(P) ($E_{1/2} = -1.19$ and -1.56 V), all in PhCN (see Figure 5-1). Virtually the same potential separations between the first two reversible reductions of the three related porphyrins are seen in pyridine (Figure 5-2). This trend in $\Delta E_{1/2}$ (PTA < PQ < P) is consistent with the size of the π -system in the three compounds, *i.e.* the larger the conjugated π -system, the easier it is to add a second electron, and consequently the smaller the separation between formation of a porphyrin π -anion radical and a dianion.

Comparisons might also be made between half-wave potentials for the reduction of H₂(PTA) and the bis-quinoxalinalporphyrin, H₂(QPQ), which were earlier investigated in CH₂Cl₂.²² The first reduction of H₂(QPQ) occurs at $E_{1/2} = -1.03$ V in CH₂Cl₂, which compares to an $E_{1/2} = -1.05$ V for H₂(PTA) (see Table 5-1) under the same solution conditions. The $E_{1/2}$ for the first reduction of H₂(P) in CH₂Cl₂ is -1.22 V.⁷ Thus, the fusion of a single TA group to the free-base porphyrin seems to have a similar effect in shifting $E_{1/2}$ values towards a more facile reduction, as does the β,β -fusion of two Q groups trans to each other on the same macrocycle.

Table 5-1. Half-wave potentials (V vs SCE) of mono-porphyrins M(PTA), M(PQ)^a and M(P)^a, where M = H₂, Cu or Zn in different solvents containing 0.1 M TBAP.

solvent	cpd	oxidation			P-centered reduction			TA-centered reduction	HOMO-LUMO gap (V) ^e
		2nd	1st	$\Delta E(\text{mV})$	1st	2nd	$\Delta E(\text{mV})$		
CH ₂ Cl ₂	H ₂ (PTA)	<i>b</i>	0.99	-	-1.05	-1.19	140	-1.73 ^c	2.04
py	H ₂ (PTA)	<i>b</i>	<i>b</i>	-	-0.93	-1.13	200	-1.65	--
PhCN	H ₂ (PTA)	1.68 ^c	1.06	-	-0.93	-1.13 ^d	200	-1.67	1.99
	H ₂ (PQ)	1.06	1.06	0	-1.08	-1.31	230	--	2.14
	H ₂ (P)	1.25	0.99	260	-1.19	-1.56	370	--	2.18
	Cu(PTA)	1.19	1.01	180	-0.92	-1.37 ^d	300	-1.70	1.93
	Cu(PQ)	1.14	0.98	160	-1.09	-1.55	460	--	2.07
	Cu(P)	1.26	0.96	300	-1.28	-1.75	470	--	2.24
	Zn(PTA)	1.04	0.84	200	-1.00	-1.40	400	-1.69	1.84
	Zn(PQ)	1.04	0.84	200	-1.19	-1.58 ^c	390	--	2.03
	Zn(P)	1.09	0.77	320	-1.34	-1.73	390	--	2.11

^aData taken from reference 7. ^bNot observed up to positive potential limit of solvent. ^cIrreversible peak potential at scan rate of 0.10 V/s. ^dAn additional process is observed at -1.42 V for M = 2H and -1.22 V for M = Cu in PhCN. ^eThe potential difference between the first oxidation and first reduction.

UV-visible spectral data for the neutral and electroreduced forms of $H_2(PTA)$ are shown in Figure 5-3. The neutral porphyrin, $H_2(PTA)$, is characterized by a Soret band at 428 and two visible bands at 540 and 611 nm in PhCN. During the first controlled-potential reduction at -1.05 V in a thin-layer cell, the Soret band at 428 nm increases slightly in intensity, while the visible band at 611 nm disappears and a new visible band grows in at 515 nm (Figure 5-3a). These spectral changes are reversible and the original UV-visible spectrum could be regenerated when the potential is set back to 0.0 V and reoxidation occurs. The spectrum of singly reduced $H_2(PTA)$ is similar to that of neutral $H_2(P)$, which has a Soret band at 424 nm and a visible band at 518 nm in PhCN. This suggests some localization of the added electron on the fused TA part of the molecule and an associated interruption in conjugation between the π system of the TA group and the π -ring system of the porphyrin in singly reduced $H_2(PTA)$. A similar argument has been made for singly reduced $M(PQ)$ compounds, whose UV-visible spectra often resemble spectra of the neutral $M(P)$ complexes in the same solvent.⁷ However, it should be noted that a broad visible band is also seen at 729 nm for singly reduced $H_2(PTA)$. This band is characteristic of a porphyrin π -anion radical and is not present in the spectrum of neutral $H_2(P)$.

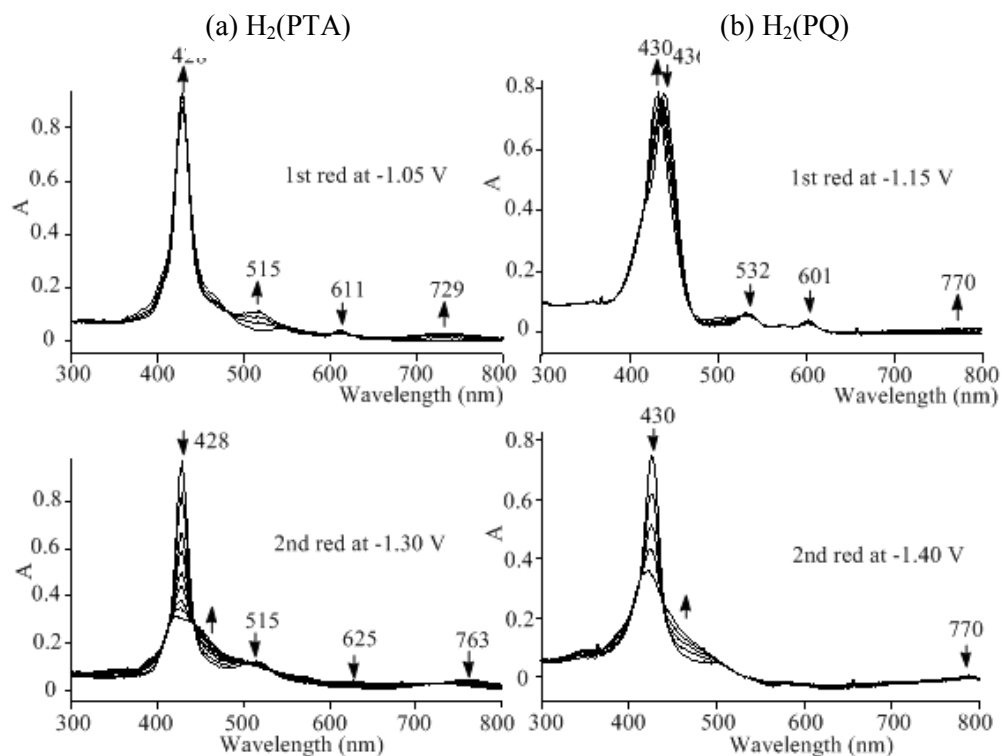


Figure 5-3. UV-visible spectral changes obtained during the first two controlled potential reductions of (a) H₂(PTA) and (b) H₂(PQ) at the indicated potential in PhCN, 0.1 M TBAP.

The strong Soret band of singly reduced $H_2(PTA)$ at 428 nm and the two visible bands at 515 and 729 nm (Figure 3a) all decrease in intensity when the applied potential is set at -1.30 V, thus indicating the formation of a porphyrin dianion in solution. Similar spectral changes as in Fig. 3a are seen during the stepwise controlled potential reduction of $H_2(PQ)$ to its π -anion radical in the first step and porphyrin dianion in the second (Figure 3b).

As reported in the literature, the potentials for electrooxidation of $H_2(PQ)$ and $H_2(QPQ)$, vary little as compared to $E_{1/2}$ values for oxidation of the parent metalloporphyrin not containing the fused quinoxaline group, $M(P)$.^{7,22} The same lack of sensitivity to the β,β' -fused TA group also occurs in the case of $H_2(PTA)$, which undergoes a one-electron abstraction in PhCN at virtually the same potential as for oxidation of $H_2(PQ)$ (see Figure 5-1). The main difference between the two compounds, however, is in the stability of the electrogenerated radical cation. This form of the porphyrin is relatively stable in the case of $[H_2(PQ)]^{+\bullet}$, but not in the case of $[H_2(PTA)]^{+\bullet}$ which undergoes a rapid chemical reaction in solution to generate a new species which is reduced on the return sweep at $E_{pc} = 0.48$ V for a scan rate of 0.1 V/s.

The observation of a homogenous chemical reaction following electrogeneration of $[H_2(PTA)]^{+\bullet}$ parallels what is seen for a number of other free-base porphyrins and corroles in CH_2Cl_2 or PhCN, namely a conversion of the cation radical to its protonated form, where one or two protons from the solution are added at the central nitrogens of the macrocycle.³⁵⁻³⁷ This topic, although interesting, is only tangential to the scope of the present study on TA-linked porphyrins and is not described in further detail.

5.2.1.2 Metalated porphyrins, M(PTA), where M = Cu(II) or Zn(II)

Cu(PTA) and Zn(PTA) exhibit two oxidations and three reductions in PhCN containing 0.1 M TBAP (Figure 5-4). Both oxidations occur at the conjugated macrocycle, and generate the porphyrin π -cation radical and dication at potentials virtually identical to $E_{1/2}$ values for the two ring-centered oxidations of M(PQ), where M = Cu or Zn (see Table 5-1). The UV-visible spectral changes obtained during these processes differ little from what has been reported during oxidation of M(PQ) or M(P) complexes with the same metal ion.

The first two reductions of Cu(PTA) and Zn(PTA) in Figure 5-4 are also assigned to porphyrin ring-centered reactions, while the last process at $E_{1/2} = -1.70$ V (Cu) and -1.69 V (Zn) is proposed to be TA-centered and located at a similar $E_{1/2}$ value as for reduction of H₂(PTA) in PhCN, pyridine, or CH₂Cl₂ (see Table 5-1). The two M(PTA) compounds are also easier to reduce than the corresponding M(P) and M(PQ) derivatives with the same metal ions. For example, the first reductions of Cu(PTA) ($E_{1/2} = -0.92$ V) and Zn(PTA) ($E_{1/2} = -1.00$ V) are shifted positively by 170 mV and 190 mV, respectively, in PhCN as compared to the first reduction of Cu(PQ) ($E_{1/2} = -1.09$ V) and Zn(PQ) ($E_{1/2} = -1.19$ V)⁷ in the same solvent. As seen in Table 5-1, there is little change in the oxidation potentials with change in macrocyclic structure, while the reduction of M(PTA) is easier than the reduction of M(PQ) or M(P). Because of this, the HOMO-LUMO gap ($\Delta E_{1/2}$) decreases in the following order: M(P) > M(PQ) > M(PTA), *i.e.*, $\Delta E_{1/2} = 2.24$ V for Cu(P), 2.07 V for Cu(PQ), and 1.93 V for Cu(PTA) (see Table 5-1).

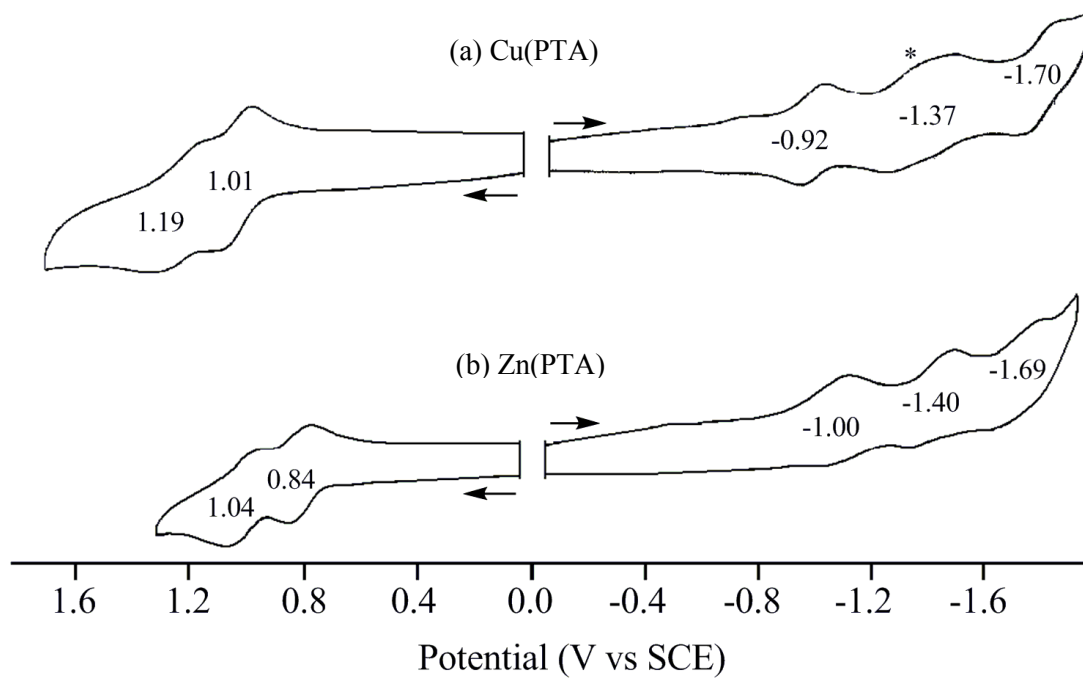


Figure 5-4. Cyclic voltammograms of (a) Cu(PTA) and (b) Zn(PTA) in PhCN containing 0.1 M TBAP. Scan rate = 0.1 V/s. The reduction labeled with an asterisk is associated with a 'side reaction' involving a protonated form of the reduced porphyrin.

The UV-visible spectral changes obtained during the first two reductions of Zn(PTA) and Cu(PTA) in PhCN, 0.1 M TBAP are shown in Figure 5-5, and parallel what is observed for H₂(PTA) (Figure 5-3a). The more facile reduction of M(PTA) as compared to M(PQ), suggests an initial electron addition to the conjugated macrocycle but, unlike a porphyrin ring-centered reduction, the UV-visible spectrum shows no loss in intensity of the Soret band and exhibits only a small shift in λ_{max} upon reduction. This is consistent with substantial electron density being shifted to the TA group in the singly reduced species, along with possible protonation, as also occurs in the case of electroreduced M(PQ)^{II} and M^{IV}(PQ) derivatives.^{10,33} Upon further reduction of Cu(PTA) and Zn(PTA) at -1.50 V in the thin-layer cell, the Soret band of the singly reduced porphyrin substantially decreases in intensity (Figure 5-5), and this is consistent with a porphyrin dianion being formed in the second electron addition at this potential.

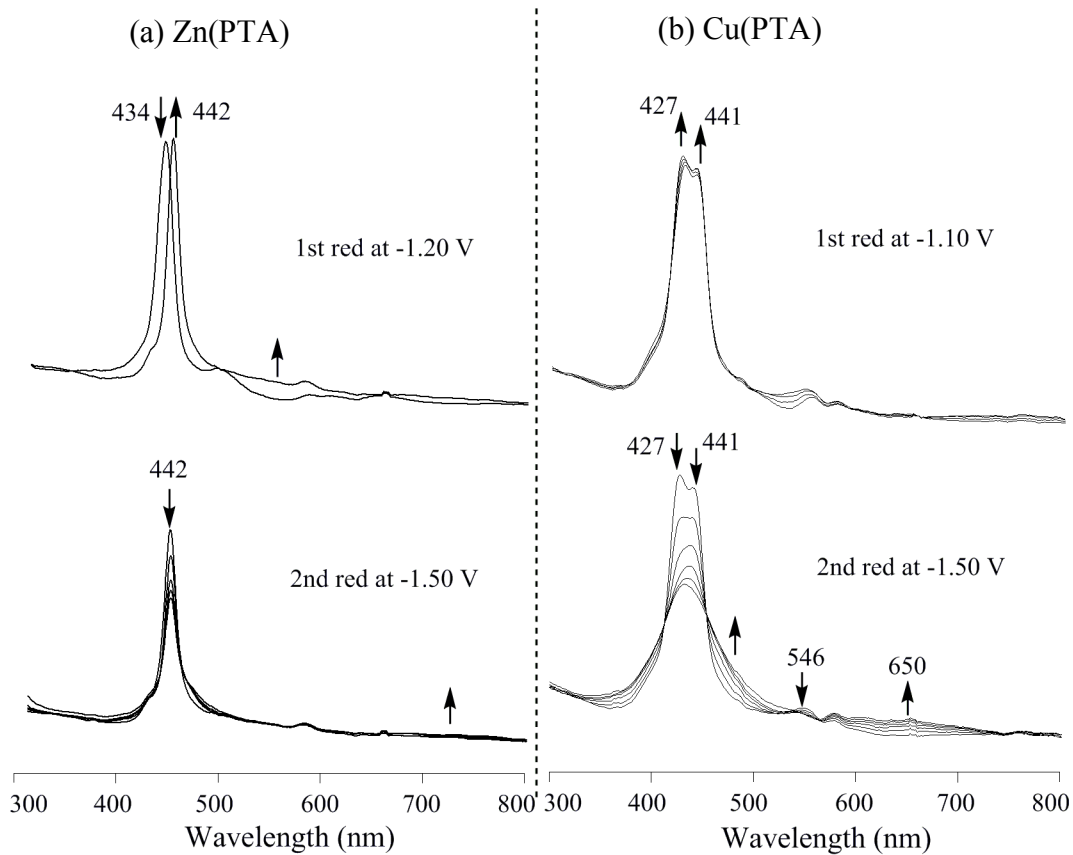


Figure 5-5. UV-visible spectral changes obtained during controlled potential reductions of (a) Zn(PTA) and (b) Cu(PTA) at the indicated potential in PhCN, 0.1 M TBAP.

5.2.2 Electrochemistry of TA-linked bis-porphyrins

5.2.2.1 Free-base bis-porphyrin, H₂(P)-TA-(P)H₂

Free-base TA-linked porphyrins were earlier shown to undergo four reductions⁴ in CH₂Cl₂ containing 0.1 M TBAPF₆, but a follow up study with spectroscopic monitoring of these redox reactions has never reported. The structurally similar TA-linked free-base porphyrin characterized in the current work also exhibits four one-electron reductions in CH₂Cl₂, PhCN, or pyridine containing 0.1 M TBAP. The best solubility is obtained in pyridine where well-defined processes at $E_{1/2} = -0.78, -1.01, -1.21, \text{ and } -1.43 \text{ V}$ are seen as shown in Figure 5-6. The solubility of the bis-porphyrin is much lower in PhCN and CH₂Cl₂ than in pyridine, but similar half-wave potentials could be measured in these latter two solvents, and these values are listed in Table 5-2.

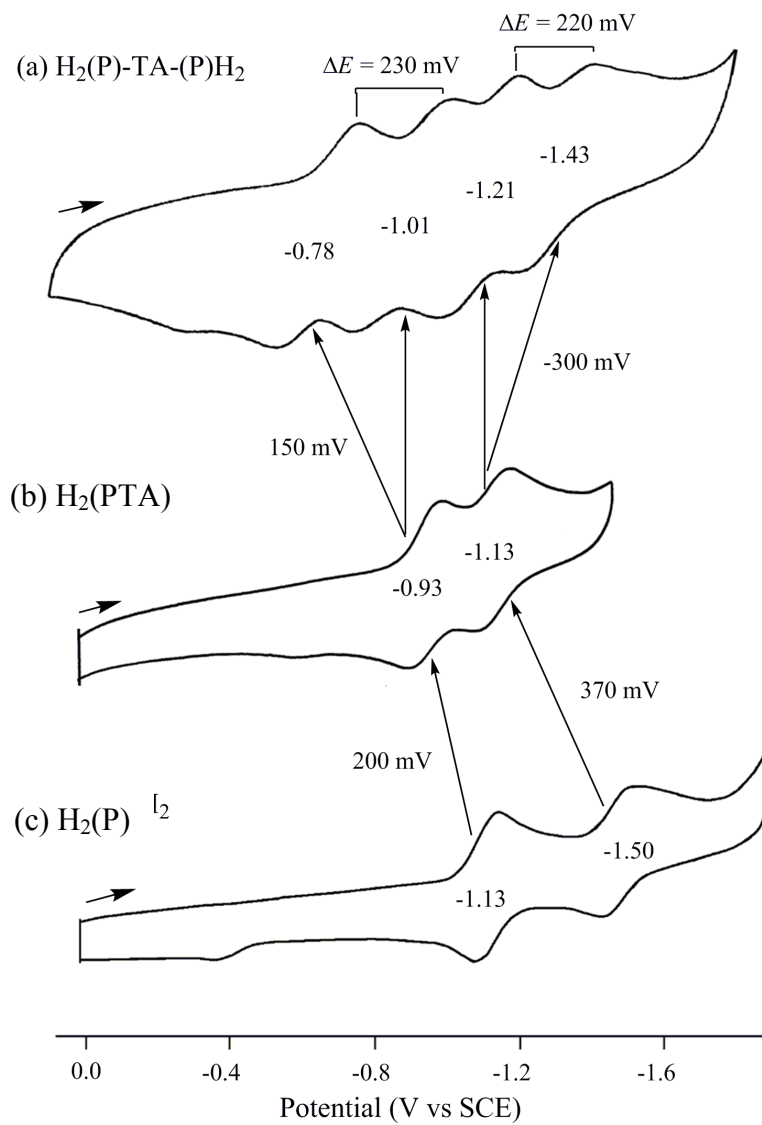


Figure 5-6. Cyclic voltammograms showing porphyrin ring-centered reductions of (a) $\text{H}_2(\text{P})$, (b) $\text{H}_2(\text{PTA})$, and (c) $\text{H}_2(\text{P})\text{-TA-(P)H}_2$ in pyridine containing 0.1 M TBAP.

Table 5-2. Half-wave potentials (V vs SCE) of bis-porphyrins M(P)-TA-(P)M in different solvents containing 0.1 M TBAP.

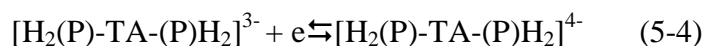
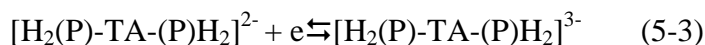
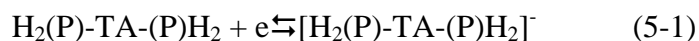
solvent	M	oxidation		reduction						$E(1ox-1red)^a$
		2 nd	1 st	1 st	2 nd	$E(1r-2r)$	3 rd	4 th	$E(3r-4r)$	
PhCN	2H	1.05 ^c	1.05 ^c	-0.80	-1.03	0.23	-1.29	-1.46	0.17	1.85
	Ni		1.06 ^c	-0.93	-1.18	0.25	-1.41	--	--	1.99
	Cu	1.20 ^c	1.00 ^c	-0.70	-1.18	0.48	-1.47	-1.92 ^b	0.45	1.70
	Zn	1.04 ^c	0.84 ^c	-0.83	-1.33 ^b	0.50	-1.48 ^c	-1.83 ^b	0.35	1.67
	Pd	1.42 ^c	1.14 ^c	-0.70	-1.20	0.50	-1.45	-1.87 ^b	0.42	1.84
	Co ^d	1.30	1.10	-0.59	-0.73	0.14	-1.42	-1.91 ^b	0.49	1.69
py	2H			-0.78	-1.01	0.23	-1.21	-1.43	0.22	--
	Zn			-0.79	-1.12 ^b	0.33	-1.31	-1.69 ^b	0.38	--
CH ₂ Cl ₂	2H	1.46 ^b	1.11 ^b	-0.89	-1.07	0.18	-1.28	-1.55	0.27	2.00
	Zn	1.24 ^b	0.78 ^c	-0.89	-1.37	0.48	-1.64 ^b	-1.91 ^b	0.27	1.67

^aThe potential difference between the first oxidation and first reduction (HOMO-LUMO gap).

^bIrreversible peak potential at a scan rate of 0.1 V/s. ^cTwo overlapping one-electron oxidations.

^dData taken from reference 10. The first two reductions are metal-centered electron transfer processes.

The first two reductions of $\text{H}_2(\text{P})\text{-TA-(P)H}_2$ give a bis- π -anion radical after the stepwise addition of one electron to each macrocycle of **4** (Eqs 5-1 and 5-2). These reductions occur at separate half-wave potentials as expected for two equivalent interacting redox centers. The next two reductions of **4** (Eqs 5-3 and 5-4) then give the bis-porphyrin bis-dianion as a final product of an overall four electron additions, and these reductions also occur at separate half-wave potentials.



The absolute difference in potential between the first two reductions of the TA-linked dyad **4** (Eqs 5-1 and 5-2) gives a measure of the interaction between the two equivalent TA-linked macrocycles. The larger the separation, the larger the interaction. The measured value of $\Delta E_{1/2}$ is 230 mV in pyridine, 230 mV in PhCN, and 180 mV in CH_2Cl_2 (see Table 5-2), and these values can be compared to separations which range from 150 to 300 mV for interacting redox centers of bis-porphyrins³⁸ and bis-corrole^{39,40} dyads linked in a face-to-face arrangement. The next two reductions of $\text{H}_2(\text{P})\text{-TA-(P)H}_2$ generate the bis-porphyrin bis-dianion as a final product. The potentials for these reductions in pyridine are located at $E_{1/2} = -1.21$ and -1.43 V (Figure 5-6c) and the separation between these two processes ($\Delta E_{1/2}$) amounts to 220 mV in pyridine, 170 mV in PhCN and 270 mV in CH_2Cl_2 (Table 5-2).

Also shown in Figure 5-6 are cyclic voltammograms of the mono-porphyrins, $\text{H}_2(\text{P})$ and $\text{H}_2(\text{PTA})$. Each mono-porphyrin undergoes two reversible one-electron

reductions. The first gives a porphyrin π -anion radical and the second a porphyrin dianion. It is easier to generate the half-reduced π -anion radical of $\text{H}_2(\text{P})\text{-TA-(P)H}_2$ ($E_{1/2} = -0.78$ V) than to generate the fully reduced π -anion radical of $\text{H}_2(\text{PTA})$ (-0.93 V) or $\text{H}_2(\text{P})$ (-1.13 V). In contrast, all other reductions of **4** are located at more negative potentials (harder reductions) as compared to the same electron transfer processes of $\text{H}_2(\text{PTA})$.

UV-visible spectra obtained during the first two controlled potential reductions of $\text{H}_2(\text{P})\text{-TA-(P)H}_2$ in PhCN are shown in Figure 5-7. The unreduced bis-porphyrin has a split Soret band at 428 and 459 nm, which decreases in intensity during the first one-electron addition at a controlled potential of -0.95 V. The 'half reduced' $\text{H}_2(\text{P})\text{-TA-(P)H}_2$ porphyrin generated at this potential is characterized by less intense 428 and 549 nm bands (Figure 5-7a) which change little in position or intensity when a more negative potential of -1.20 V is applied to generate the bis-porphyrin bis- π -anion radical as a final product. The final spectrum of doubly reduced $\text{H}_2(\text{P})\text{-TA-(P)H}_2$ (Figure 5-7b) is quite similar to that of singly reduced $\text{H}_2(\text{PTA})$ (Figure 5-3a), *i.e.* both spectra have a Soret band at 428 nm and a broad near-IR band at similar wavelengths.

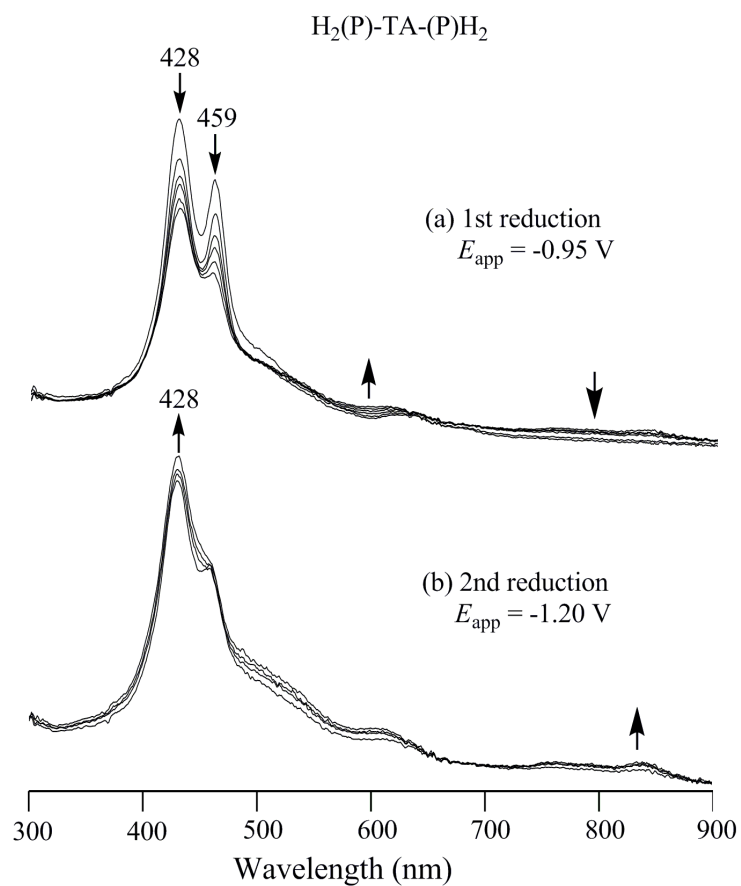


Figure 5-7. UV-visible spectral changes of $H_2(P)-TA-(P)H_2$ during reductions in PhCN containing 0.1 M TBAP.

5.2.2.2 Metalated TA-linked bis-porphyrins

The investigated M(P)-TA-(P)M derivatives are similar to the TA-linked free-base porphyrin in that they also exhibit four reductions in nonaqueous media. A summary of the measured half-wave potentials in PhCN, pyridine, and CH₂Cl₂ is given in Table 5-2. Examples of cyclic voltammograms are shown in Figure 5-8, along with the corresponding mono-porphyrin, M(P), having the same Cu(II) or Zn(II) central metal ion. As seen from this figure, each ring-centered reduction of M(P) is split into two one-electron transfer processes, giving four separate one-electron additions, as also occurs for H₂(P)-TA-(P)H₂ (see Figure 5-6 and Eqs 5-1 to 5-4). The difference in $E_{1/2}$ between the first two reductions of the three metalated bis-porphyrins is about 500 mV as compared to a much smaller separation of 230 mV in the case of H₂(P)-TA-(P)H₂ (see Table 5-2). This is consistent with a stronger interaction between the two equivalent porphyrin redox centers in the metalated forms of M(P)-TA-(P)M, as compared to free-base H₂(P)-TA-(P)H₂.

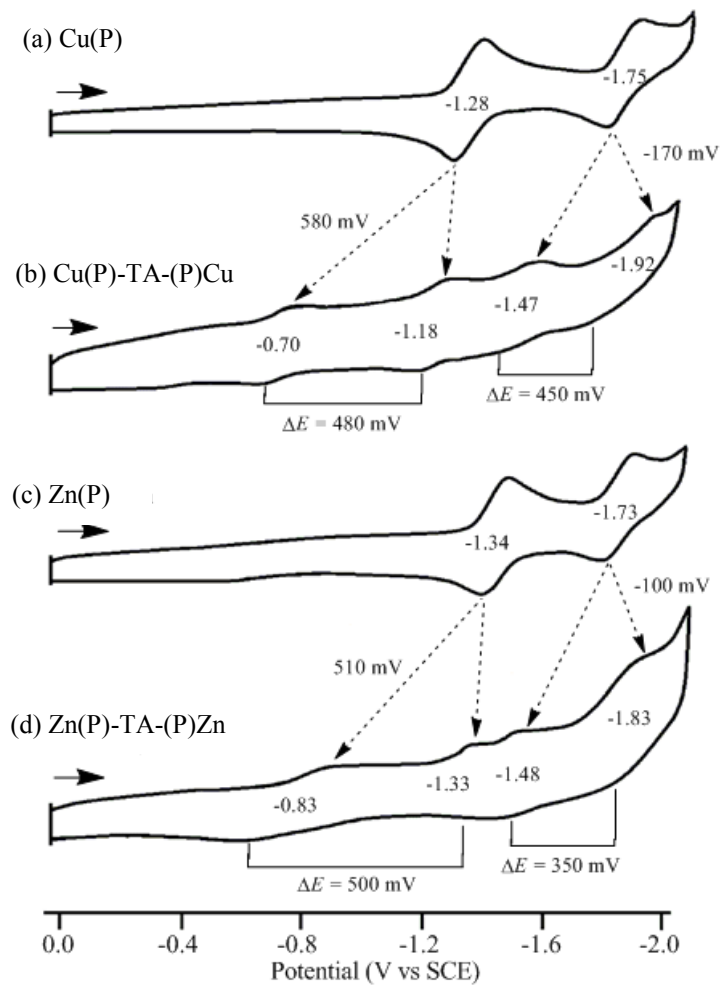


Figure 5-8. Cyclic voltammograms showing reductions of M(P) and M(P)-TA-(P)M in PhCN containing 0.1 M TBAP.

The potentials for reduction of Co(P)-TA-(P)Co, which were reported in an earlier study,¹⁰ are also included in Table 5-2. The $\Delta E_{1/2}$ between the first two reductions of the bis-cobalt(II) porphyrin is much smaller (140 mV) than in the case of the TA-linked free-base or metalated derivatives, consistent with a much weaker interaction between the two equivalent redox centers of the Co(II) bis-porphyrin. However, the third and fourth reductions of Co(P)-TA-(P)Co are separated by 490 mV, which is the same $\Delta E_{1/2}$ as for the first two ring-centered reductions of the Zn^{II}, Pd^{II} and Cu^{II} bis-porphyrins (~500 mV, see Table 5-2). The first two reductions of Co(P)-TA-(P)Co involve a Co^{II}/Co^I process, while the next two reductions are macrocycle-centered, as is also the case for M(P)-TA-(P)M, where M = Cu(II), Zn(II) or Pd(II).

Spectral changes obtained during the first two reductions of M(P)-TA-(P)M in PhCN in a thin-layer cell are illustrated in Figure 5-9. The Soret bands of the neutral compounds decrease in intensity upon the first one-electron addition at -0.90 V but then increase again in intensity during the second electron addition to the bis-porphyrin. A comparison of the spectral data in Figure 5-9 with that for the mono-porphyrin Cu(PTA) in Figure 5-7b suggests that the first one-electron addition to M(P)-TA-(P)M occurs at the conjugated π -ring system, while the second electron addition gives a bis-porphyrin, bis- π -anion radical with substantial electron density having been transferred to the bridging TA group.

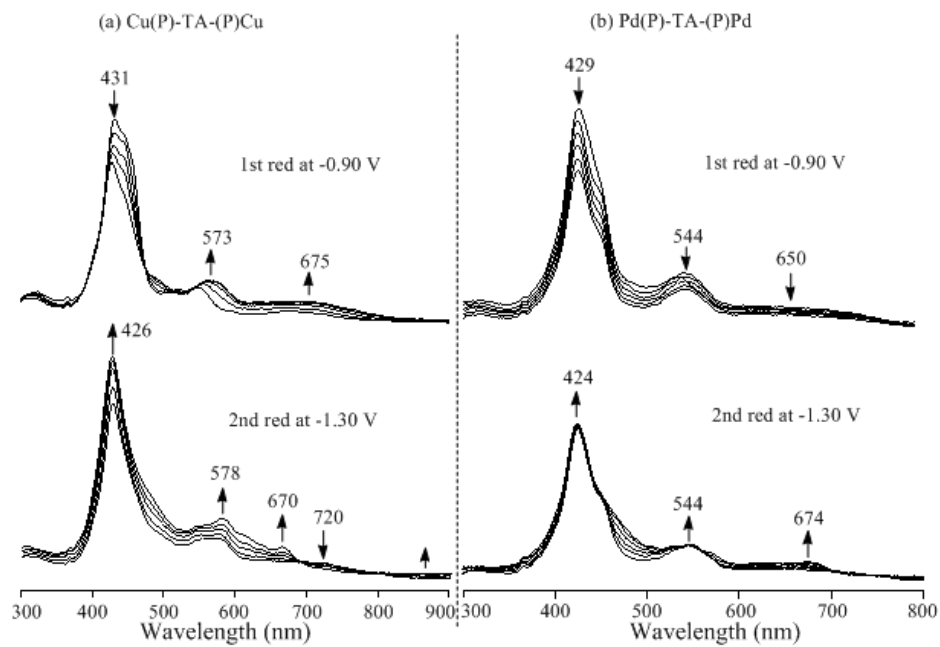


Figure 5-9. UV-visible spectral changes during the controlled potential reductions of (a) Cu(P)-TA-Cu(P) and (b) Pd(P)-TA-(P)Pd in PhCN, 0.1 M TBAP.

5.3 Conclusions

The three M(P)-TA-(P)M complexes undergo two oxidations in PhCN. Half-wave potentials for these processes are listed in Table 5-2, and are almost identical as $E_{1/2}$ values for oxidation of the related PQ and PTA monoporphyrins.⁷ However, the oxidation peak currents of M(P)-TA-(P)M are in each case almost twice as high as those for the first reduction of the same compound, consistent with both macrocycles in the bis-porphyrin undergoing a one-electron abstraction at the same half-wave potential. This result is consistent with what was previously reported for the related TA-linked bis-cobalt porphyrin,¹⁰ and can be interpreted as an electrooxidation involving two equivalent but non-interacting redox centers.

The same interpretation can be given on the basis of the UV-visible spectral changes which occur during controlled potential oxidation of the metalated bis-porphyrins. These spectra can be compared to the spectra obtained during electrooxidation of Cu(PTA) and Zn(PTA) under the same solution conditions. As indicated above, the two oxidations of the TA-linked bis-porphyrins each involve two overlapping one-electron abstractions leading to formation of bis-cation radicals and bis-dications which have the same spectral characteristics as the π -cation radicals and dications of the mono-porphyrins.

5.4 References

- (1) Martínez-Díaz, M.; Torres, T. In *Handbook of Porphyrin Science*; Kadish, K. M.; Smith, K. M.; Guillard, R. Eds. World Scientific: Singapore, 2010; Vol. 10, p 141.
- (2) Duclairoir, F.; Marchon, J. In *Handbook of Porphyrin Science*; Kadish, K. M.; Smith, K. M.; Guillard, R. Eds. World Scientific: Singapore, 2010; Vol. 10, p 245.
- (3) Ethirajan, M.; Patel, N.; Pandey, R. In *Handbook of Porphyrin Science*; Kadish, K. M.; Smith, K. M. and Guillard R. Eds. World Scientific: Singapore, 2010; Vol. 4, p 249.
- (4) Crossley, M.; Burn, P. *J. Chem. Soc., Chem. Commun.* **1987**, 39.
- (5) Lu, T.; Reimers, J.; Crossley, M.; Hush, N. *J. Phys. Chem.* **1994**, 98, 11878.
- (6) Crossley, M.; Santic, P.; Walton, R.; Reimers, J. *Org. Biomol. Chem.* **2003**, 2777.
- (7) Ou, Z.; E, W.; Shao, J.; Burn, P.; Sheehan, C.; Walton, R.; Kadish, K. M.; Crossley, M. *J. Porphyrins and Phthalocyanines.* **2005**, 9, 142.
- (8) Beavington, R.; Burn, P. *J. Chem. Soc., Perkin Trans. 1*, **2000**, 1231.
- (9) Armstrong, R.; Foran, G.; Hough, W.; D'Alessandro, D.; Lay, P.; Crossley, M. *J. Dalton Trans.* **2006**, 4805.
- (10) Zhu, W.; Santic, M.; Ou, Z.; Santic, P.; McDonald, J.; Brotherhood, P.; Crossley, M.; Kadish, K. M. *Inorg. Chem.* **2010**, 49, 1027.
- (11) Flamigni, L.; Marconi, G.; Johnston, M. *Phys. Chem. Chem. Phys.* **2001**, 3, 4488.
- (12) Sendt, K.; Johnston, L.; Hough, W.; Crossley, M.; Hush, N.; Reimers, J. *J. Am. Chem. Soc.* **2002**, 124, 9299.
- (13) Hutchison, J.; Bell, T.; Ganguly, T.; Ghisellini, K.; Langford, S.; Lokan, N.; Paddon-Row, M. *J. Photochemistry and Photobiology A: Chemistry.* **2008**, 197, 220.
- (14) Santic, P.; E, W.; Ou, Z.; Shao, J.; McDonald, J.; Cai, Z.; Kadish, K. M.; Crossley, M.; Reimers, J. *Phys. Chem. Chem. Phys.* **2008**, 10, 515.
- (15) Crossley, M.; Govenlock, L.; Prashar, J. *J. Chem. Soc., Chem. Commun.* **1995**, 2379.
- (16) Crossley, M.; Burn, P. *J. Chem. Soc., Chem. Commun.* **1991**, 1569.

- (17) Crossley, M.; Burn, P.; Langford, S.; Prashar, J.; Stark, G. *J. Chem. Soc., Chem. Commun.* **1991**, 1567.
- (18) Crossley, M.; King, L.; Newsom, I.; Sheehan, C. *J. Chem. Soc., Perkin Trans. 1.* **1996**, 2675.
- (19) Crossley, M.; Sheehan, C.; Khoury, T.; Reimers, J.; Santic, P. *New J. Chem.* **2008**, 340.
- (20) Kadish, K. M.; E, W.; Santic, P.; Ou, Z.; Shao, J.; Ohkubo, K.; Fukuzumi, S.; Govenlock, L.; McDonald, J.; Try, A.; Cai, Z.; Reimers, J.; Crossley, M. *J. Phys. Chem. B* **2007**, *111*, 8762.
- (21) Crossley, M.; Harding, M.; Tansey, C. *J. Org. Chem.* **1994**, 4433.
- (22) E, W.; Kadish, K.; Santic, P.; Khoury, T.; Govenlock, L.; Ou, Z.; Shao, J.; Ohkubo, K.; Reimers, J.; Fukuzumi, S.; Crossley, M. *J. Phys. Chem. A* **2008**, *112*, 556.
- (23) Eu, S.; Hayashi, S.; Umeyama, T.; Matano, Y.; Araki, Y.; Imahori, H. *J. Phys. Chem. C* **2008**, *112*, 4396.
- (24) Crossley, M.; Santic, P.; Hutchison, J.; Ghiggino, K. *Org. Biomol. Chem.* **2005**, *3*, 852.
- (25) Hutchison, J.; Santic, P.; Crossley, M.; Nagamura, T.; Ghiggino, K. *Phys. Chem. Chem. Phys.* **2009**, *11*, 3478.
- (26) Carroll, R.; Gorman, C. *Angew. Chem. Int. Ed.* **2002**, *41*, 4378.
- (27) Hush, N.; Reimers, J.; Hall, L.; Johnston, L.; Crossley, M. *Ann. N. Y. Acad. Sci.* **1998**, 852, 1.
- (28) Lü, T.; Reimers, J.; Crossley, M.; Hush, N. *J. Phys. Chem.* **1994**, *98*, 11878.
- (29) Reimers, J.; Hall, L.; Crossley, M.; Hush, N. *J. Phys. Chem. A* **1999**, *103*, 4385.
- (30) Tsuda, A.; Osuka, A. *Science*, **2001**, *293*, 79.
- (31) Aratani, N.; Osuka, A. In *Handbook of Porphyrin Science*, Kadish, K. M.; Smith, K. M.; Guilard, R. Eds. Press: World Scientific, New Jersey, 2010; Vol.1, p 1.
- (32) Reimers, J.; Hush, N.; Crossley, M. *J. Porphyrins and Phthalocyanines* **2002**, *6*, 795.

- (33) Ou, Z.; E, W.; Zhu, W.; Thordarson, P.; Sintic, P.; Crossley, M.; Kadish, K. M. *Inorg. Chem.* **2007**, *46*, 10840.
- (34) Bard, A.; Faulkner, L. *Electrochemical Methods* (2nd Ed.), Press: John Wiley & Sons, Inc. 2001.
- (35) Inisan, C.; Saillard, J.; Guilard, R.; Tabard, A.; Le, M. *New J. Chem.* **1998**, *22*, 823.
- (36) Ou, Z.; Shen, J.; Shao, J.; E, W.; Galezowski, M.; Gryko, D.; Kadish, K. M. *Inorg. Chem.* **2007**, *46*, 2775.
- (37) Shen, J.; Shao, J.; Ou, Z.; E, W.; Koszarna, B.; Gryko, D.; Kadish, K. M. *Inorg. Chem.* **2006**, *45*, 2251.
- (38) Le, M.; Her, M.; Collman, J.; Kim, K.; Hendricks, N.; Helm, S. *J. Electroanal. Chem.* **1987**, *234*, 277.
- (39) Guilard, R.; Jerome, F.; Barbe, J.; Gros, C.; Ou, Z.; Shao, J.; Fischer, J.; Weiss, R.; Kadish, K. M. *Inorg. Chem.* **2001**, *40*, 4856.
- (40) Guilard, R.; Gros, C.; Barbe, J.; Espinosa, E.; Jerome, F.; Tabard, A.; Latour, J.; Shao, J.; Ou, Z.; Kadish, K. M. *Inorg. Chem.* **2004**, *43*, 7441.

Chapter Six

Electrochemically Driven Intramolecular Oxidative Aromatic Coupling as a Pathway Towards π -Extended Ni Porphyrins

6.1 Introduction

Highly conjugated porphyrins, by nature of their electronic and redox properties, have attracted attention as conducting materials, near-IR dyes, nonlinear optical materials, or photosensitizers for photodynamic therapy (PDT) of cancer tissues or *in vivo* studies.^{1,6} Ring extension of the porphyrins will lead to a significant modification of the compound's optical features, redox characteristics, and the HOMO-LUMO energy gap.

The relationship between the structure of porphyrinoids and their spectroscopic and photophysical properties is a complex issue.⁷⁻⁹ Over the last two decades considerable attention has been devoted to studies involving the π -conjugation of porphyrins. These materials display significant changes in their optical and electrochemical properties when compared with native porphyrins. Among other changes, π -extension of a porphyrin chromophore usually leads to a bathochromic shift in its absorption (and hence emission) spectrum.¹⁰ The diverse class of π -extended porphyrinoid molecules has attracted much attention because of their fundamental, theoretical interest, as well as because of the opportunities they offer in technology and medicine that arises from their linear and non-linear optical properties.¹¹⁻²⁰ The π -electron system of a porphyrin macrocycle can be extended by peripheral substituents at the *meso*-positions, or by the addition of one or more fused polycyclic ring systems.²¹⁻²⁸ The magnitude of this alteration depends more on the type of conjugation than on the actual number of double/triple bonds or aromatic rings added.²⁹ In last two decades three fundamental papers showed that it is possible to prepare porphyrins fused with other porphyrins or with aromatic hydrocarbons at both the

meso and β - positions of the macrocycle.³⁰⁻³² These discoveries have opened up new avenues that were quickly followed by other researchers.³⁰⁻³⁴

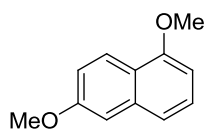
Over time, it was observed that the synthesis of π -extended porphyrins *via* intramolecular oxidative coupling usually requires activation of the aromatic subunits (for example by introducing alkoxy groups).³⁵⁻⁴⁰

Oxidative aromatic coupling has recently become a popular method for the π -extension of a porphyrin.⁴¹⁻⁴⁷ The first example of a porphyrin fused with naphthalene was reported by Cammidge and co-workers in 2005.⁴⁸ In principle, any aromatic unit located at the *meso*-position of a porphyrin and possessing high electron density should be able to form analogous products via oxidative aromatic coupling, which was proven in a seminal contribution by Anderson *et al.*⁴⁹

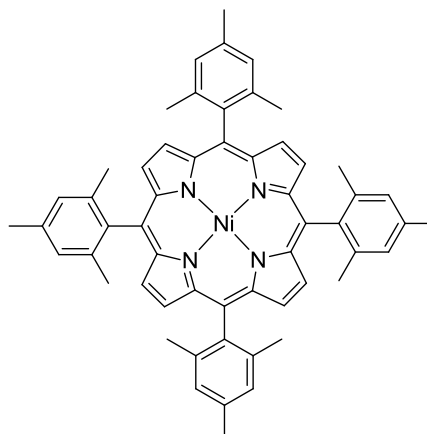
Previous studies³⁵⁻⁴⁰ (most notably by Osuka and Anderson)^{30,37-40,42,44,47} and general knowledge of aromatic oxidative coupling both indicate that the planned concept can only be realized if the naphthalene-porphyrin bears an electron-donating substituent at a suitable position.⁴⁹⁻⁵⁵ In the course of our studies involving an elucidation of relationships between the output of oxidative aromatic coupling reactions, the nature of the oxidizing agent, and the central metal cation, we were able to establish a protocol for oxidative coupling leading to a *meso*, β -naphthalene-fused porphyrinoid **4** (see Chart 6-1) in high yield without contamination from chlorinated side-products using $\text{Fe}(\text{ClO}_4)_3 \cdot \text{H}_2\text{O}$.⁵⁶ Unfortunately, the described procedure is sensitive to solvents and oxidant quality and not general for diverse *meso*-substituted porphyrinoids. Because of these drawbacks, we were led to consider the use of electrochemical methods as a possible alternative in solving mechanistic issues. Such an approach was pioneered by

Smith and co-workers who described the first electrosynthesis of porphyrins from a,c-biladienes.^{57,58} Recently an elegant approach towards cyclo[n]pyrroles *via* electrochemical intermolecular oxidative coupling was presented by Bucher and Sessler.^{59,60} Electrochemically mediated aromatic oxidative coupling has also been applied for other substrates.⁶¹⁻⁶³

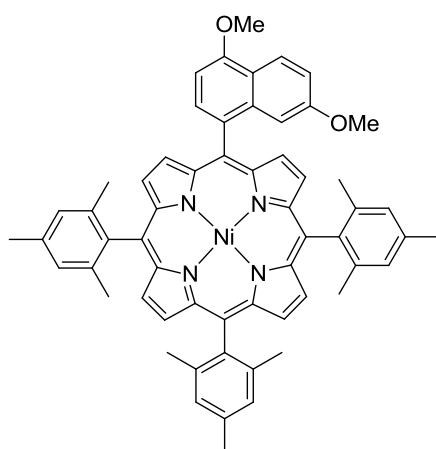
Another motivation to perform this study came from the fact that a major roadblock to enhancing the synthesis of π -extended porphyrins *via* intramolecular oxidative coupling requires a better understanding of the mechanism of these reactions. Specifically it is pivotal to know which moiety (porphyrin or the second aromatic system) is first attacked by the oxidant to form an electrophilic radical-cation. An answer to this and similar questions will help explain the apparently contradictory observations such as: (a) the participation of units which are by no means electron-rich⁶⁴ and (b) the difficulty with carrying out oxidative aromatic coupling on an already partially fused porphyrin^{49, 65-67} where product decomposition is observed in cases when multiply electron-rich hydrocarbons are fused with the central macrocyclic ring.⁶⁵ Electrochemically mediated aromatic oxidative coupling is the only way to establish these mechanistic details. In our initial study of this problem, we have chosen a Ni(II) porphyrin with an extended π system which was previously prepared using chemical oxidation. We assumed that having such a standard in hand would allow us to unequivocally establish the order of steps in the synthetic process. Herein we report the results of our study.



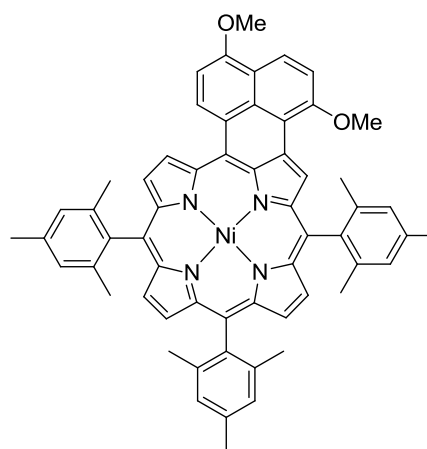
2, 6-di-OMe-Naphthalene 1



TMP-Ni 2



Open-Ni 3



Fused-Ni 4

Chart 6-1. Structures of the Investigated Compounds

6.2 Results and Discussion

The investigated compounds **1-4** were examined as to their electrochemical behavior in CH_2Cl_2 and PhCN containing 0.1 M tetrabutylammonium perchlorate (TBAP); and the measured half-wave or peak potentials for reduction and oxidation of each compound are summarized in Table 6-1. The site of electron transfer for each redox reaction is also given in the table, with assignments being based on the measured spectral changes, measured $E_{1/2}$ values and previous assignments of electron transfer site given in the literature for related compounds.⁶⁵⁻⁶⁷ Cyclic voltammograms for these compounds are shown in Figure 6-1.

Table 6-1. Half-wave or peak potentials (V vs SCE) and proposed site of electron transfer for redox reactions of investigated porphyrins in CH₂Cl₂ and PhCN containing 0.1 M TBAP. Scan rate = 0.1 V/s.

solvent	cpd #	naphth- alene	oxidation			reduction	
			Ni ^{II/III}	ring		ring	
			<i>E</i> _{1/2}	2 nd	1 st	1 st	2 nd
CH ₂ Cl ₂	1	1.33 ^a					
	2			1.38 ^a	1.02	-1.60 ^a	
	3		1.64 ^a	1.15	1.02	-1.47 ^a	
	4		1.55	1.02	0.67	-1.24	-1.84 ^a
PhCN	1	1.36 ^a					
	2			1.14	1.14	-1.30	
	3		1.63 ^a	1.14	1.14	-1.24	
	4		1.55	1.00	0.74	-1.20	-1.80 ^a

^a peak potential at a scan rate of 0.1 V/s.

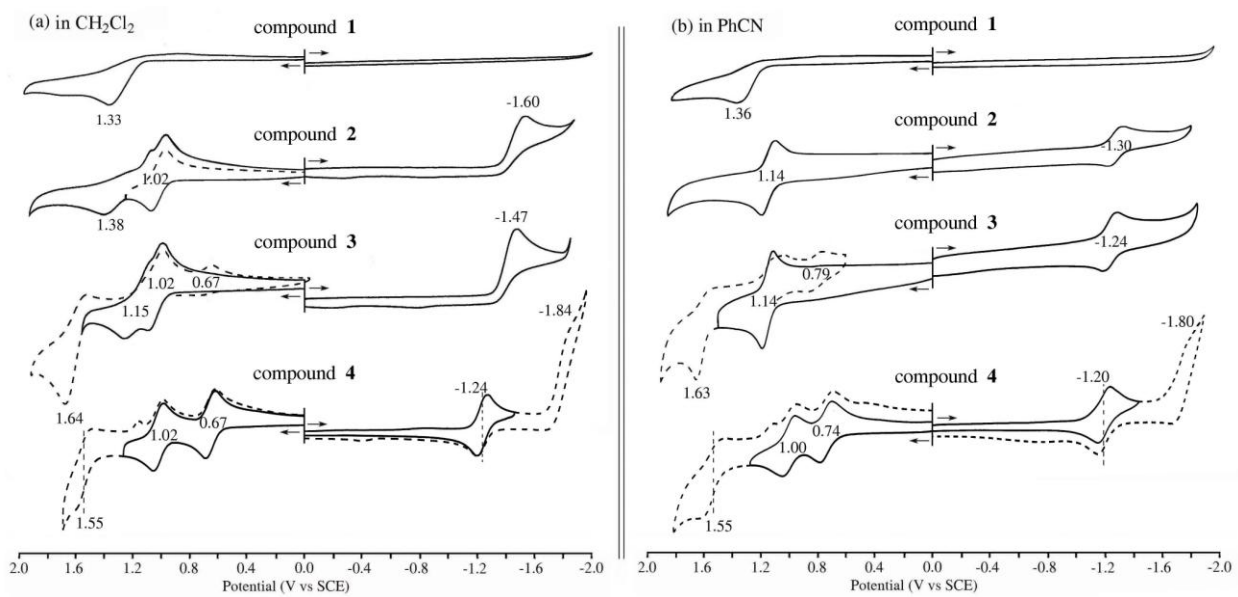


Figure 6-1. Cyclic voltammograms of **1-4** in (a) CH_2Cl_2 and (b) PhCN containing 0.1 M TBAP. Scan rate = 0.1V/s.

6.2.1 Reduction of Ni(II) porphyrins

Many Ni(II) porphyrins undergo two one-electron reductions in nonaqueous media to form π -anion radicals and dianions^{68, 69} and this is also the case for compound Fused-Ni **4** in PhCN or CH₂Cl₂. However, other Ni(II) porphyrins show just one reduction due to a limited negative potential range of the utilized solvent, the presence of a macrocycle with highly electron-donating substituents, or the occurrence of a chemical reaction between the electroreduced porphyrin and the solvent. The latter situation occurs for compounds TMP-Ni **2** and Open-Ni **3** which exhibit just a single reduction which is reversible in PhCN but irreversible in CH₂Cl₂. The singly reduced porphyrins TMP-Ni **2** and Open-Ni **3** both react with CH₂Cl₂, as was reported for many related nickel porphyrins where the transient formation of a CH₂Cl sigma-bonded species may be generated.^{65,66} In contrast, most singly reduced nickel porphyrins are stable in PhCN, as is the case for the currently investigated compounds where the product can be assigned as a Ni(II) porphyrin π -anion radical.

6.2.2 Oxidation of Ni(II) porphyrins

The first two oxidations of most Ni(II) porphyrins generally lead to a porphyrin π -cation radical and dication, but the absolute potential difference between these two redox processes will be highly variable, and will depend upon the solvent, the substituents on the macrocycle, and the anion of the supporting electrolyte.^{68,69} Two well-separated one-electron oxidations are observed for some Ni(II) porphyrins, while others undergo two overlapping one-electron oxidations at the same potential.^{68,69} As seen in Figure 6-1, these two extremes of electrochemical reactivity are observed for the three nickel porphyrins investigated in the current study. Compounds TMP-Ni **2**, Open-Ni **3**, and Fused-Ni **4** exhibit two well-separated one-electron oxidations in CH₂Cl₂, while only compound Fused-Ni **4** displays this behavior in PhCN. In contrast, an overall two-electron oxidation to give the Ni(II) porphyrin dication occurs at $E_{1/2} = 1.14$ V for compounds **2** and **3** in this solvent.

A third reversible oxidation has been reported for some Ni(II) porphyrins,⁶⁹ and this is also the case for compounds Open-Ni **3** and Fused-Ni **4** in both solvents. The third oxidation involves a one-electron transfer and formation of a Ni(III) porphyrin dication. Because of the very positive potential for this metal-centered reaction, it is often hard to detect, but for compound Fused-Ni **4**, the third oxidation is easily observed and located at $E_{1/2} = 1.55$ V in both solvents.

All three oxidations of Fused-Ni **4** are more facile as compared to the same reaction for compound Open-Ni **3**. This is because compound Fused-Ni **4** has an expanded π -conjugated system which leads to a negative shift in $E_{1/2}$ for formation of the Ni(II) π cation radical. The magnitude of the potential shift is largest for the first ring-centered

reaction which shifts by 350-400 mV (depending upon solvent), smaller for the second oxidation which shifts by 130-140 mV, and smallest for the third, metal-centered process which shifts by only 80-90 mV upon going from compound Open-Ni **3** to compound Fused-Ni **4**. The absolute potential difference between the reversible second and third oxidations of Fused-Ni **4** ($\Delta|Ox_3 - Ox_2|$) ranges from 530 to 550 mV in CH₂Cl₂ and PhCN (see Figure 6-1) and this is consistent with reported 500 ~ 730 mV potential differences between similar redox reactions of other nickel porphyrins which exhibit a Ni(II)/Ni(III) process at positive potentials.^{68, 69}

The third oxidation of Open-Ni **3**, at $E_p = 1.63$ - 1.64 V, is slightly more difficult than the third oxidation of Fused-Ni **4**, which occurs at $E_p = 1.59$ V in PhCN and CH₂Cl₂, and this process is also assigned to generation of a Ni(III) porphyrin. In compound Open-Ni **3** the reaction is irreversible due to the occurrence of a coupled chemical reaction which occurs after the electron transfer. This reaction is related to the electrochemical generation of Fused-Ni **4** as discussed in later sections of the manuscript.

As seen in Figure 6-1, the irreversible oxidation of 1,6-dimethoxynaphthalene (cpd **1**) is located at $E_p = 1.33$ - 1.36 V, either by itself (top voltammogram in Figure 6-1) or in a solutions also containing **2** (figure not shown). No oxidations are observed in this potential region for compound **3** in CH₂Cl₂ or PhCN, which implies that the naphthalene group shows no electrochemical activity when it is attached to the *meso*-position of this Ni(II) porphyrin. This observation proves that the electrochemically generated radical-cation located on the porphyrin macrocycle attacks the neighboring dimethoxynaphthalene unit, forming a C-C bond (and not *vice versa*).

6.2.3 Spectral monitoring of reduction in thin-layer cell

The three Ni porphyrins were also characterized by UV-vis spectroelectrochemistry. Examples of the spectral changes which occur during controlled potential reduction and oxidation of Open-Ni **3** and Fused-Ni **4** in PhCN are illustrated in Figures 6-2 and 6-3.

Figure 6-2 compares the spectral changes for Open-Ni **3** and Fused-Ni **4** during the first one-electron reduction in PhCN. The neutral porphyrin Fused-Ni **4** in this solvent is characterized by a Soret band at 487 nm (molar absorptivity, $\epsilon = 9.6 \times 10^4 \text{ L mol}^{-1} \text{ cm}^{-1}$), a shoulder at 462 nm, and a visible band at 654 nm ($\epsilon = 3.8 \times 10^4 \text{ L mol}^{-1} \text{ cm}^{-1}$). The neutral porphyrin Open-Ni **3** has an intense Soret band at 419 nm ($\epsilon = 22.6 \times 10^4 \text{ L mol}^{-1} \text{ cm}^{-1}$) and a weak visible band at 529 nm ($\epsilon = 2.8 \times 10^4 \text{ L mol}^{-1} \text{ cm}^{-1}$). The ring-expanded Fused-Ni **4** has a slightly more intense visible band than Open-Ni **3**, but it has a much weaker Soret band than the compound with a non-expanded porphyrin macrocycle. This is consistent with known spectral characteristics of ring-expanded porphyrins;^{70,71} the Soret band becomes weaker while the visible band becomes more intense as the size of the π -conjugated system increases.

During the first one-electron reduction of Fused-Ni **4** (Figure 6-2a), the bands at 462, 487, and 654 nm decrease in intensity, while new bands grow in at 338, 419, 509, and 722 nm. For compound Open-Ni **3** (Figure 6-2b), the Soret and Q bands of the neutral compound both decrease in intensity as the first reduction proceeds and a new weak, and very broad, band appears at 642 nm. Both sets of spectral changes can be assigned to a ring-centered addition of one electron to form a porphyrin π -anion radical. Of note, however, is the fact that the spectrum of singly-reduced Open-Ni **3** does not

have an intense band close to 722 nm, as does singly-reduced Fused-Ni **4** (labeled as [Fused-Ni]⁻) and this absorption, in the case of Fused-Ni **4**, can then be used as a marker band for the radical anion of the naphthalene-fused Ni(II) porphyrin.

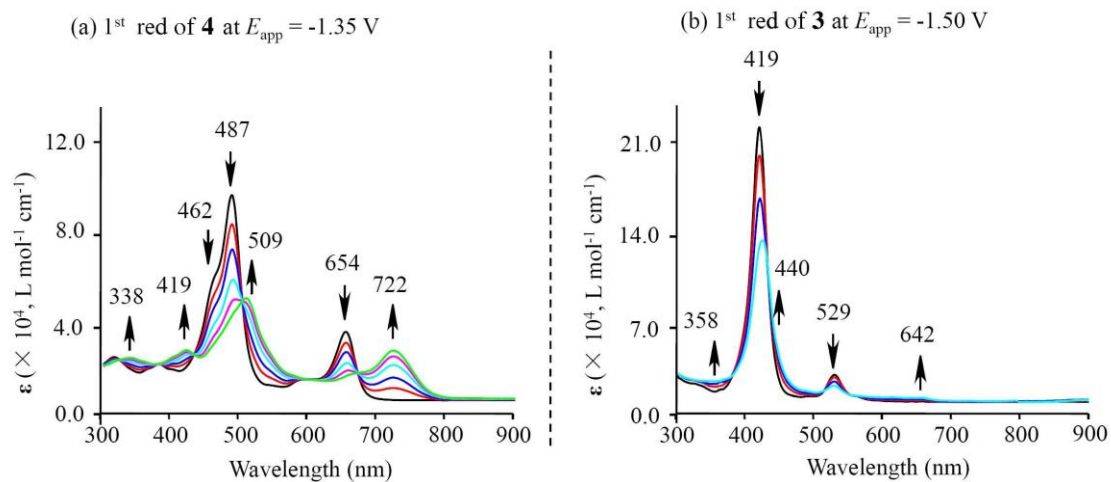


Figure 6-2. UV-visible spectral changes of (a) Fused-Ni **4** and (b) Open-Ni **3** during the controlled potential reduction at in PhCN containing 0.1 M TBAP.

6.2.4 Spectral monitoring of oxidation in thin-layer cell

Figure 6-3 presents the spectral changes which occur during the three stepwise one-electron oxidations of Fused-Ni **4** in PhCN (see cyclic voltammogram of the compound in Figure 6-4). During the first controlled potential oxidation at 0.90 V, the 462, 487, and 654 nm bands all decrease in intensity while a strong new band grows in at 741 nm. The final spectrum after the first one electron oxidation also has a moderate intensity band at 490 nm and two weak, broad, bands at 410 and 554 nm. This spectrum is shown in Figure 6-3a and corresponds to the porphyrin π -cation radical product of compound Fused-Ni **4**. The 741 nm band in the π -cation radical spectrum of compound Fused-Ni **4** is not seen in the spectrum of singly oxidized Open-Ni **3** (see Figure 6-4b) and is assigned as a marker band for the cation radical of the singly oxidized naphthalene-fused Ni(II) porphyrin.

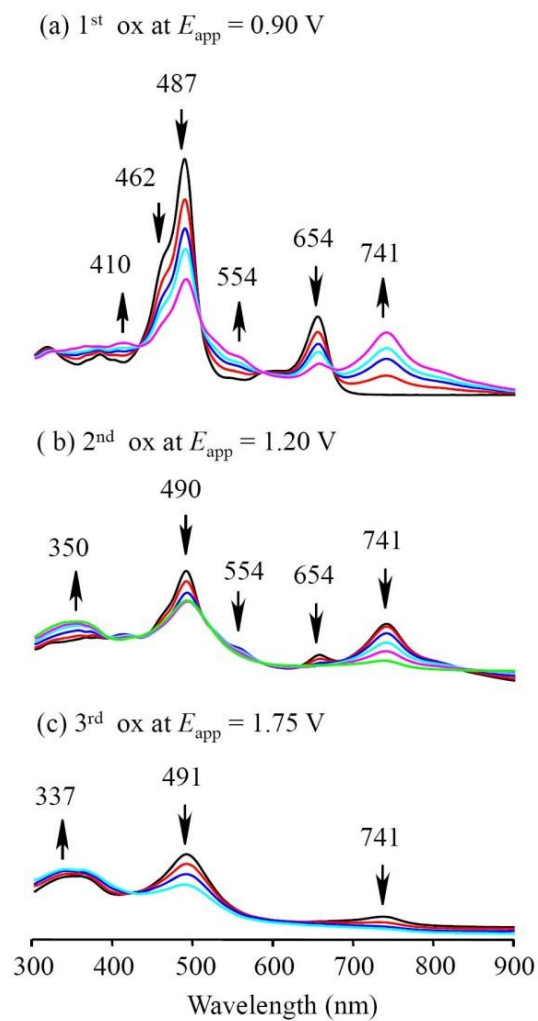


Figure 6-3. UV-visible spectral changes of Fused-Ni **4** during the controlled potential oxidations at (a) 0.90 V, (b) 1.20 V, and (c) 1.75 V in PhCN containing 0.1 M TBAP.

When the potential of singly oxidized Fused-Ni **4** was switched from 0.90 to 1.20 V (Figure 6-3b), the 741 nm marker band of the cation radical disappears, consistent with the formation of a Ni(II) dication in the thin-layer cell. This species is characterized by weak bands at 350 and 491 nm. Finally, the Ni(III) porphyrin dication of Fused-Ni **4** was electrogenerated by switching the controlled potential from 1.20 to 1.75 V; this triply oxidized species has two very weak bands at 337 and 491 nm.

The dimethoxynaphthalene group is electron-rich, and the effect of this substituent on half-wave potentials for reduction or oxidation of the porphyrin should be similar to that of a compound having only mesityl groups. This can be seen by comparing reversible half-wave potentials for the first one-electron oxidation of compounds TMP-Ni **2** and Open-Ni **3** in PhCN (see cyclic voltammograms in Figure 6-1b). When one of the four mesityl groups on the *meso*-positions of compound TMP-Ni **2** is replaced by a dimethoxynaphthalene group to form compound Open-Ni **3**, the half-wave potential for the reversible two-electron oxidation remains unchanged at $E_{1/2} = 1.14$ V in PhCN. In contrast, when the dimethoxynaphthalene group is fused onto the porphyrin macrocycle, as in compound Fused-Ni **4**, a large negative shift in potential for the first oxidation is observed. This is shown by the cyclic voltammograms in Figure 6-1 where the initial reversible one-electron oxidation of Fused-Ni **4** occurs at $E_{1/2} = 0.67$ V (CH_2Cl_2) or 0.74 V (PhCN) (as compared to 1.02 and 1.14 V for oxidation of compound Open-Ni **3** in CH_2Cl_2 and PhCN, respectively). The second one-electron abstraction of Fused-Ni **4** is also reversible in the two solvents and located at $E_{1/2} = 1.00$ V in PhCN as compared to $E_{1/2} = 1.14$ V for the second oxidation of Open-Ni **3** in the same solvent.

In a previous study of Pt porphyrins with π -expanded macrocycles, we reported that ring expansion results in a considerable raising of the macrocycle HOMO levels but induces only small changes in the LUMO levels of the π -ring system.⁷¹ As a result of the more facile ring oxidations, the measured HOMO-LUMO gap decreases as the size of the π -conjugated system is increased. This is also seen for compound Fused-Ni **4** in PhCN where the reversible first reduction potential of -1.20 V is only slightly easier than the reversible first reduction of Open-Ni **3** at -1.24 V and the HOMO-LUMO gap decreases from 2.38 V for Open-Ni **3** to 1.94 V for Fused-Ni **4**.

Of critical importance is the fact that compound Open-Ni **3** shows a new reversible redox couple located at $E_{1/2} = 0.67$ V (in CH₂Cl₂) or $E_{1/2} = 0.79$ V (in PhCN), after scanning the potential to values positive of the third oxidation where the Ni(III) porphyrin dication is electrogenerated. The formation of the new peak on the return negative potential scan is shown by a dashed line in the cyclic voltammograms of Figure 6-1. The $E_{1/2}$ of 0.67 V for the new peak in CH₂Cl₂ is identical to $E_{1/2}$ for the first oxidation of Fused-Ni **4** in this solvent, and similar oxidation potentials are also seen for the relevant processes of Open-Ni **3** and Fused-Ni **4** in PhCN. These results prove that a chemical transformation occurs after oxidation of compound Open-Ni **3**, with an oxidized compound Fused-Ni **4** being generated as a product of the reaction at the electrode surface. In a previous study⁵⁶ we demonstrated that compound Fused-Ni **4** could be synthesized by chemically oxidizing Open-Ni **3** and a similar electrosynthesis of Fused-Ni **4** appears to have occurred in the electrooxidation of compound Open-Ni **3**. In order to further prove this hypothesis and to better understand the electrooxidation processes of Open-Ni **3**, the spectra of each oxidation product was characterized by *in*

situ thin-layer spectroelectrochemistry. The results of these measurements are discussed below.

6.2.5 Fusion of π ring system and conversion of Open-Ni to Fused-Ni during oxidation

Figure 6-4a illustrates thin-layer cyclic voltammograms of Open-Ni **3** in PhCN using different potential sweep ranges. As in the case of “regular” cyclic voltammetry, the first two oxidations of Open-Ni **3** occur in a single step two electron transfer at $E_{1/2} = 1.10$ V. The oxidative coupling reaction occurs when the scan is reversed at 1.35 V, but the new redox couple of Fused-Ni **4** at 0.74 V has very small current (top voltammogram of Figure 6-4a). In contrast, a new well-defined new reduction and reoxidation process is seen at $E_{1/2} = 0.74$ V when the potential scan in the thin-layer cell is reversed at a more positive potential of 1.75 V (middle CV of Figure 6-4a). Furthermore, when the positive potential scan was held at 1.35 V for 5 minutes and then reversed, two reversible redox couples were obtained at $E_{1/2} = 1.02$ and 0.74 V (lower CV of Figure 6-3a). As seen in Figure 6-1 and Table 1, the potentials of the two new redox couples generated in the thin layer cell after the second or third oxidation of Open-Ni **3** are almost identical to half wave potentials for the first two oxidations of Fused-Ni **4** in the same solvent/supporting electrolyte system.

Figure 6-4b shows the UV-visible spectral changes which occur during the stepwise oxidations of Open-Ni **3** at the indicated potentials. The neutral compound Open-Ni **3** in PhCN is characterized by an intense Soret band at 419 nm and a weak band at 530 nm. When the potential is held at 1.35 V for 4-7 min, the initial bands at 419 and 530 nm disappear while two weak new bands of the product grow in at 350 and 490 nm (Figure

6-4b); further oxidation at an applied potential of 1.75 V leads, after 2 minutes of electrolysis, to a spectrum having bands at 350 and 490 nm (lower left spectrum in Figure 6-4b). These latter spectral changes are almost the same as those which occur during the second and the third oxidations of Fused-Ni **4** (see Figure 6-3b).

The reverse spectral changes in Figure 6-4b unambiguously confirm the formation of doubly oxidized Fused-Ni **4**, which is then reduced to the neutral compound Fused-Ni **4** when a controlled potential of 0.00 V is applied to the thin-layer cell. Two electrons are added stepwise during controlled potential reduction of the electrogenerated dication at 0.00 V, giving in the first step a spectrum with bands at 488 and 739 nm and then, in the second step, a final reduction product which is characterized by a split Soret band at 463 and 487 nm and a visible band at 655 nm. A 739 nm band was earlier assigned as a marker band for the radical cation of the naphthalene-fused Ni porphyrin. This band is seen in the first step during reduction at 0.0 V (top right spectrum in Figure 6-4), and the spectrum of the final product after further reduction is identical to that of the neutral compound Fused-Ni **4** (see spectrum in lower right on Figure 6-4b).

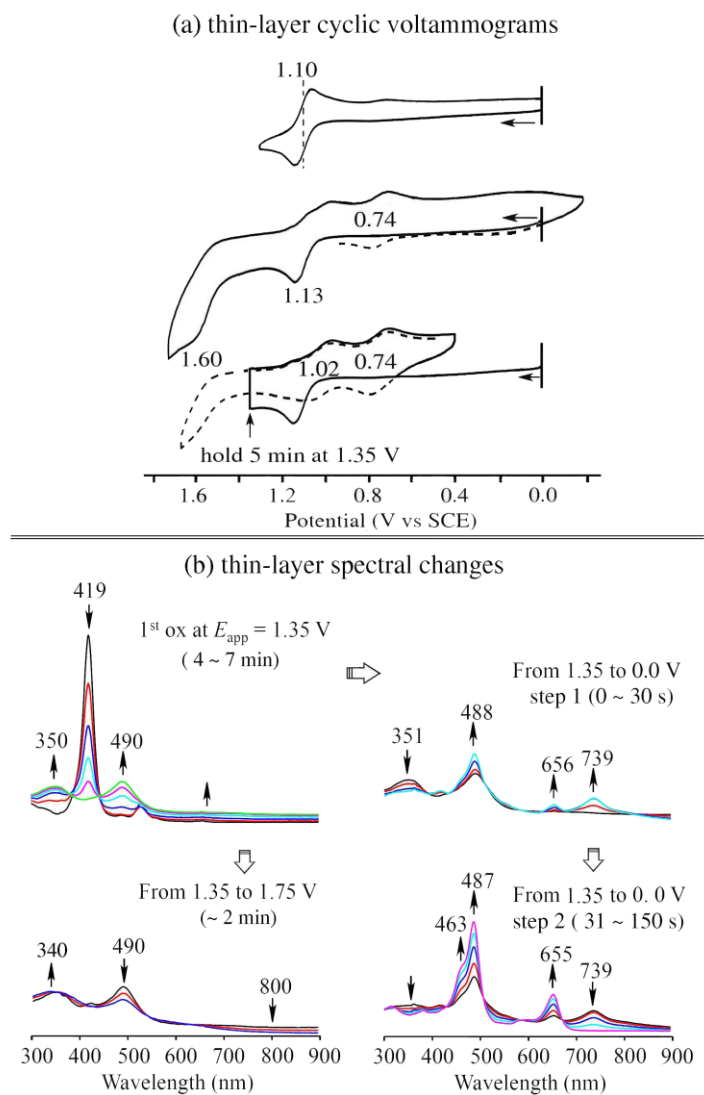
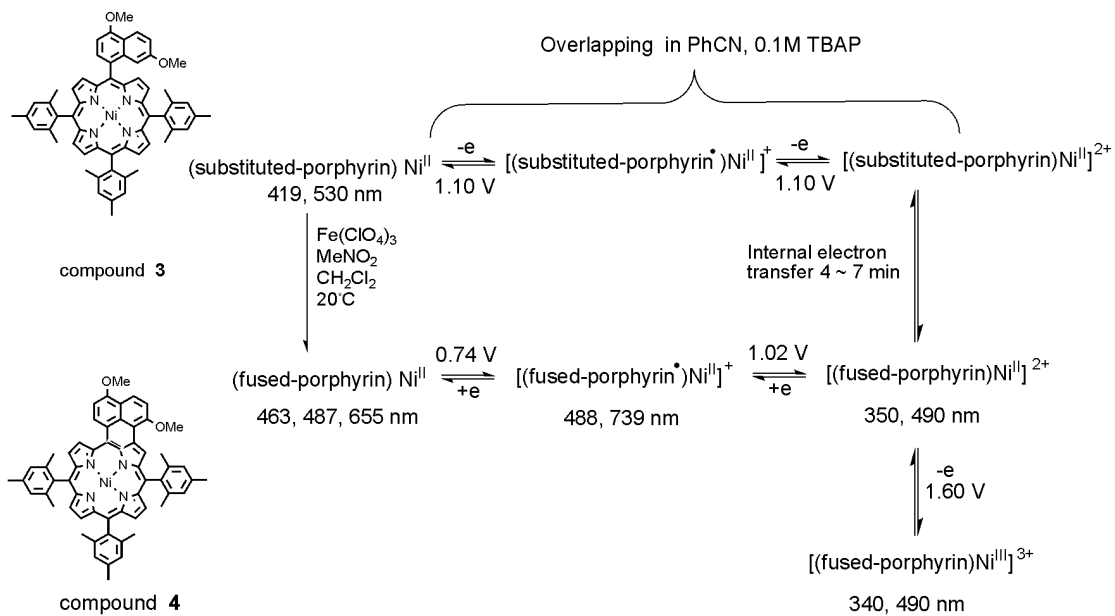


Figure 6-4. (a) Thin-layer cyclic voltammograms of Open-Ni **3** in PhCN containing 0.1 M TBAP at a scan rate of 20 mV/s and (b) stepwise UV-visible spectral changes of Open-Ni **3** during the indicated applied potential under the same solution conditions.

The electrochemical and spectroelectrochemical data are thus self-consistent, indicating that compound Fused-Ni **3** is first oxidized to a dication ($[\text{Open-Ni}]^{2+}$) *via* a two one-electron abstractions, after which $[\text{Open-Ni}]^{2+}$ converts to $[\text{Fused-Ni}]^{2+}$ by an internal electron transfer process. Based on the results obtained from electrochemistry, thin-layer spectroelectrochemistry and the literature,⁷² a proposed reaction mechanism in PhCN is presented in Scheme 6-1. The conversion of Open-Ni **3** and Fused-Ni **4** is not limited to PhCN, as a solvent and similar electrochemical and spectroelectrochemical results are also obtained in CH_2Cl_2 .

Scheme 6-1. Proposed mechanism for the reversible conversion between compound Open-Ni **3** and Fused-Ni **4**.



6.3 Conclusions

In conclusion, an electrochemical approach to synthesis of the π -extended porphyrin Fused-Ni **4** allowed us to avoid the use of harsh reaction conditions, such as the need for adding iron(III) or molybdenum(V) salts which are a hallmark of these chemical methods. More importantly, by electrochemical and spectroelectrochemical studies, we have proven that a radical-cation is initially formed on the porphyrin ring, following its reaction with the linked dimethoxynaphthalene moiety. This observation will enable the design of suitable architectures for the future synthesis of π -extended porphyrins by both electrochemical and chemical methods. Another appealing aspect of an electrochemically based synthetic method is that it allows the reaction conditions to be easily varied. For instance, under conditions of the electrolysis, it is possible to adapt an oxidation potential which specifically suits the redox properties of a given porphyrinic precursor, and to also study the effects of various metals placed into the macrocyclic core. In summary, the currently described electrosynthetic method describes a new and simple way to produce π -extended porphyrins, which should permit control of electronic interactions, and thus enable one to more closely control and tune the physical properties of these type macrocycles.

6.4 References

- (1) Vinogradov, S. A.; Wilson, D. F. *J. Chem. Soc., Perkin Trans. 2*, **1995**, 103.
- (2) Chen, P.; Dvornikov, A. S.; Nakashima, M.; Roach, J. F.; Alabran, D. M.; Rentzepis, P. M. *J. Phys. Chem.* **1996**, *100*, 17507.
- (3) Chou, J. H.; Kosal, M. E.; Nalwa, H. S.; Rakow, N. A.; Suslick, K. S. in *The Porphyrin Handbook*, Kadish, K. M.; Smith K. M.; Guillard, R., Eds.; Academic Press, San Diego, CA, **2000**, Vol. 6, p. 43.
- (4) Fronczek, F. R. Hao E.; Vicente, M. G. H. *J. Org. Chem.*, **2006**, *71*, 1233.
- (5) Bonnett, R. *Chem. Soc. Rev.* **1995**, *24*, 19.
- (6) Boyle, R.W.; Dolphin, D. *Photochem. Photobiol.* **1996**, *64*, 469.
- (7) Anderson, H. L. *Chem. Commun.* **1999**, 2323.
- (8) Schwab, P. F.; Levin M. D.; Michl, J. *Chem. Rev.* **1999**, *99*, 1863.
- (9) Pschirer, N. G.; Kohl, C.; Nolde, F.; Qu J.; Müllen, K. *Angew. Chem. Int. Ed.* **2006**, *45*, 1401.
- (10) Sessler, J. L.; Seidel, D. *Angew. Chem. Int. Ed.* **2003**, *42*, 5134.
- (11) Nath, M.; Pink, M.; Zaleski, J. M. *J. Am. Chem. Soc.* **2005**, *127*, 478.
- (12) Sprutta, N.; Swiderska M.; Latos-Grażyński, L. *J. Am. Chem. Soc.* **2005**, *127*, 13108.
- (13) Anand, V. G.; Saito, S.; Shimizu S.; Osuka, A. *Angew. Chem. Int. Ed.* **2005**, *44*, 7244.
- (14) Khoury T.; Crossley, M. J. *Chem. Commun.* **2007**, 4851.
- (15) Lash, T. D.; Colby, D. A.; Idate, A. S.; Davis, R. N. *J. Am. Chem. Soc.* **2007**, *129*, 13800.
- (16) Esdaile, L. J.; Jensen, P.; McMurtrie, J. C.; Arnold, D. P. *Angew. Chem. Int. Ed.* **2007**, *46*, 2090.
- (17) Boyle R. W.; Fox, S. *Chem. Commun.* **2004**, 1322.
- (18) Gill, H. S.; Harujanz, M.; Santamaria, J.; Finger I.; Scott, M. J. *Angew. Chem. Int. Ed.* **2004**, *43*, 485.
- (19) Fronczek, F. R.; Hao E.; Vicente, M. G. H. *J. Org. Chem.* **2006**, *71*, 1233.

- (20) Collins, H. A.; Khurana, M.; Moriyama, E.; Mariampillai, H. A.; Dahlstedt, E.; Balaz, M.; Kuimova, M. K.; Drobizhev, M.; Yang, V. X. D.; Phillips, D.; Rebane, A.; Wilson B. C.; Anderson, H. L. *Nat. Photonics* **2008**, *2*, 420.
- (21) Chang, C. K.; Bang, N. J. *Org. Chem.* **1995**, *60*, 7030.
- (22) Fumoto, Y.; Uno, H.; Murashima, T.; Ono, N. *Heterocycles*, **2001**, *54*, 705.
- (23) Lindsey, J. S. in *The Porphyrin Handbook*; Kadish K. M.; Smith, K. M.; Guillard, R., Eds.; Academic Press: San Diego, CA, **2000**, Vol. 1, pp 45.
- (24) Wilson; G. S.; Anderson, H. L. *Synlett* **1996**, 1039.
- (25) Finikova, O.; Cheprakov, A.; Beletskaya, Z.; Vinogradov, S. *Chem. Commun.* **2001**, 261.
- (26) Ono, N.; Hironaga, H.; Ono, K.; Kaneko, S.; Murashima, T.; Ueda, T.; Tsukamura, C.; Ogawa, T. *J. Chem. Soc. Perkin Trans. 1*, **1996**, 417.
- (27) Lash, T. D.; Chandraseker, P. A.; Osuma, T.; Chaney S. T.; Spence, J. D. *J. Org. Chem.* **1998**, *63*, 8455.
- (28) Ito, S.; Ochi, N.; Uno, H.; Murashima T.; Ono, N. *Chem. Commun.* **2000**, 893.
- (29) Sahoo, A. K.; Mori, S.; Shinokubo H.; Osuka, A. *Angew. Chem. Int. Ed.* **2006**, *45*, 7972.
- (30) Tsuda, A.; Furuta, H.; Osuka, A. *Angew. Chem. Int. Ed.* **2000**, *39*, 2549.
- (31) Sugiura, K.; Matsumoto, T.; Ohkouchi, S.; Naitoh, Y.; Kawai, T.; Takai, Y.; Ushiroda, K.; Sakata, Y. *Chem. Commun.* **1999**, 1957.
- (32) Yamane, O.; Sugiura, K.; Miyasaka, H.; Nakamura, K.; Fujimoto, T.; Kaneda, T.; Sakata Y.; Yamashita, M. *Chem. Lett.* **2004**, *33*, 40.
- (33) Diev, V.; Hanson, K.; Zimmerman, J. D.; Forrest S. R.; Thompson, M. E. *Angew. Chem. Int. Ed.*, **2010**, *49*, 5523.
- (34) Ahn, T. K.; Kim, S.; Kim, D. Y.; Noh, S. B.; Aratani, N.; Ikeda, C.; Osuka, A.; Kim, D. *J. Am. Chem. Soc.*, **2006**, *128*, 1700.
- (35) Sanienda, A. *Zeitschrift fuer Naturforschung, Teil B: Anorganische Chemie, Organische Chemie, Biochemie, Biophysik, Biologie* **1967**, *22*, 1107-1111.

- (36) Bucher, C.; Buda, M. in *the Handbook of Porphyrin Science*, Kadish, K. M.; Smith, K. M.; Guillard, R., Eds.; World Scientific, Singapore, **2012**, Vol. 17, pp. 240.
- (37) Anderson, H. L.; Davis, N. L. S.; Pawlicki, M. *Org. Lett.* **2008**, *10*, 3945.
- (38) Anderson, H. L.; N. Davis, L. S.; Thompson, A. L. *Org. Lett.* **2010**, *12*, 2124.
- (39) McKeown, N. B.; Makhseed, S.; Msayib, K. J.; Ooi, L. L.; Helliwell M.; Warren, J. E. *Angew. Chem. Int. Ed.* **2005**, *44*, 7546.
- (40) Sahoo, K.; Nakamura, Y.; Aratani, N.; Kim, K. S.; Noh, S. B.; Shinokubo, H.; Kim D.; Osuka, A. *Org. Lett.* **2006**, *8*, 4144.
- (41) Lewtak, J. P.; Gryko, D. T. *Chem. Commun.* **2012**, *48*, 10069.
- (42) Kim D.; Osuka, A. *Acc. Chem. Res.* **2004**, *37*, 735.
- (43) Ono, N.; Yamada, H.; Okujima, T. in *the Handbook of Porphyrin Science*, Kadish, K. M.; Smith, K. M.; Guillard, R., Eds; World Scientific, Singapore, **2009**, vol. 2, p 1.
- (44) Tsuda A.; Osuka, A. *Science* **2001**, *293*, 79.
- (45) Tsuda, A.; Osuka, A. *Adv. Mater.* **2002**, *14*, 75.
- (46) Pereira, A. M. V. M.; Richeter, S.; Jeandon, C.; Gisselbrecht, J.-P.; Wytko, J.; Ruppert, R. *J. Porphyrins Phthalocyanines* **2012**, *16*, 464-478.
- (47) Kim, D.; Osuka, A.: Single-molecule photophysical properties of various directly linked porphyrin arrays, in *Multiporphyrin arrays*, Kim, D., Ed.; Pan Stanford Publishing, Singapore, **2012**, p 1-54.
- (48) Hughes, D. L.; Cammidge, A. N.; Scaife, P. *J. Org. Lett.* **2005**, *7*, 3413.
- (49) Davis, N. L. S.; Thompson, A. L.; Anderson, H. L. *J. Am. Chem. Soc.* **2011**, *133*, 30.
- (50) Whiting, D. A. *In Comprehensive Organic Synthesis*, **1991**, vol. 3, pp. 659.
- (51) Dohi, T.; Ito, M.; Morimoto, K.; Iwata M.; Kita, Y. *Angew. Chem., Int. Ed.* **2008**, *47*, 1301.
- (52) Dwight, T. A.; Rue, N.; Charyk, R. D.; Josselyn, R.; DeBoef, B. *Org. Lett.* **2007**, *9*, 3137.

- (53) Kalyani, D.; Deprez, N. R.; Desai, L. V.; Sanford, M. S. *J. Am. Chem. Soc.* **2005**, *127*, 7330.
- (54) Wang, K.; Lu, M.; Yu, A.; Zhu X.; Wang, Q. *J. Org. Chem.* **2009**, *74*, 935.
- (55) Sarhan, A. A. O.; Bolm, C. *Chem. Soc. Rev.* **2009**, *38*, 2730.
- (56) Lewtak, J. P.; Gryko, D.; Bao, D.; Sebai, E.; Vakuliuk, O.; Ścigaj, M.; Gryko, D. *T. Org. Biomol. Chem.* **2011**, *9*, 8178.
- (57) Jeyakumar, D.; Snow, K. M.; Smith, K. M. *J. Am. Chem. Soc.* **1988**, *110*, 8562.
- (58) Wijesekera, T. P.; Dolphin, D. *Chemtracts: Org. Chem.* **1990**, *3*, 375.
- (59) Buda, M.; Iordache, A.; Bucher, C.; Moutet, J.-C.; Royal, G.; Saint-Aman, E.; Sessler, J. L. *Chem. Eur. J.* **2010**, *16*, 6810.
- (60) Bui, T.-T.; Iordache, A.; Chen, Z.; Roznyatovskiy, V.V.; Saint-Aman, E.; Lim, J. M.; Lee, B. S.; Ghosh, S.; Moutet, J.-C.; Sessler, J. L.; Kim, D.; Bucher, C. *Chem. Eur. J.* **2012**, *18*, 5853.
- (61) Hammerich, O.; Parker, V. D. *Acta Chem. Scand.* **1982**, *B36*, 519.
- (62) Schäfer, H. J. Electrolytic oxidative coupling, in *Organic Electrochemistry*, 4th ed. (eds. H. Lund, O. Hammerich), Marcel Dekker, New York, **2001**, p 883-967.
- (63) Kirste, A.; Elser, B.; Schnakenburg, G.; Stecker, F.; Waldvogel, S. R. *J. Am. Chem. Soc.* **2012**, *134*, 3571-3576.
- (64) Eu, S.; Hayashi, S.; Tanaka, M.; Matano, Y.; Umeyama T.; Imahori, H. *Chem. Commun.*, **2007**, *20*, 2069.
- (65) Kadish, K. M.; Franzen, M. M.; Han, B.; Araullo-Madams, C.; Sazou, D. *J. Am. Chem. Soc.* **1991**, *113*, 512.
- (66) Kadish, K. M.; Franzen, M. M.; Han, B.; Araullo-Madams, C.; Sazou, D. *Inorg. Chem.* **1992**, *31*, 4399.
- (67) Lewtak, J. P.; Węclawski, M.; Gryko, D. T.; unpublished results.
- (68) Kadish, K. M.; Caemelbecke, V.; E.; Royal, G., in *The Porphyrin Handbook: Electron Transfer*, Kadish, K. M.; Smith, K. M.; Guillard, R., eds.; Academic Press: San Diego, CA, 2000; Vol. 8.
- (69) Kadish, K. M.; Van Caemelbecke, E.; Boulas, P.; D'Souza, F.; Vogel, E.; Kisters, M.; Medforth, C. J.; Smith, K. M. *Inorg. Chem.* **1993**, *32*, 4177.

- (70) Kadish, K. M.; Lin, M.; Van Caemelbecke, E.; De Stefano, G.; Medforth, C. J.; Nurco, D. J.; Nelson, N. Y.; Krattinger, B.; Muzzi, C. M.; Jaquinod, L.; Xu, Y.; Shyr, D. C.; Smith, K. M.; Shelnut, J. A. *Inorg. Chem.* **2002**, *41*, 6673.
- (71) Chen, P.; Finikova, O. S.; Ou, Z.; Vinogradov, S. A.; Kadish, K. M. *Inorg. Chem.* **2012**, *51*, 6200.
- (72) Gouterman, M. *J. Mol. Spectrosc.* **1961** *6*, 138

Chapter Seven

Facile Electrosynthesis of π -Extended Zn(II), In(III), Ir(III),

and Free-Base Porphyrins

7.1 Introduction

Both π -expanded¹ and π -extended porphyrins²⁻⁸ have been widely used as building blocks for supramolecular and organic materials chemistry. Altering the conjugation pathway in a porphyrin can lead to profound changes in the compound's electrochemical properties, as well as in their linear and non-linear optical properties, examples being an increased absorption of light in the NIR region of the spectrum, an increase in second hyperpolarizability, and larger two-photon absorption cross-sections as compared with the native porphyrins.⁹⁻¹⁶ These features of highly conjugated porphyrins have been the object of intense investigation.^{9,10,17-25} The magnitude of the modification of the porphyrin's optical features, their redox characteristics, and the energy difference between the highest occupied molecular orbital (HOMO) and lowest unoccupied molecular orbital (LUMO) depends more on the type of conjugation than on the actual number of double or triple bonds added to the macrocycle.¹⁷⁻²⁶

The coordination chemistry of π -extended porphyrins (i.e. porphyrins consisting of four pyrrole units connected with four methine bridges, but possessing additional conjugated double or triple bonds and/or aromatic rings), is generally the same as that of the porphyrin before π extension of the macrocycle, since the cavity size is often the same in the two series of compounds. Moreover, comparative studies from the groups of Osuka, Anderson, Lash, and others have proven that attaching additional aromatic units simultaneously at the β and *meso* positions of a porphyrin macrocycle is 'economically' the most efficient way to red-shift the absorption spectrum.^{10,12-14,27-34}

The intrinsically high electron-density of porphyrins is responsible for the fact that oxidative aromatic coupling³⁵ has recently become the most popular method for π -

extension of these compounds.^{2-8,37} In this regard, the early studies by Osuka and co-workers were further extended by Anderson and others, who demonstrated that the formation of C-C bonds between the adjacent unit and the macrocyclic core^{2,12-14,16,28} could be accomplished using various one-electron oxidants when the electron-rich aromatic unit is located at the *meso*-position of the macrocycle. Although numerous aromatic hydrocarbons and heterocycles have been fused over the last 20 years, many challenges still remain, the most important of which is an unpredictability of the reaction outcome, contamination from mono-chlorinated by-products (FeCl₃),¹⁶ and the lack of a successful fusion reaction with free-base porphyrin derivatives. As a matter of fact, despite the publication of over a hundred manuscripts on the topic, only Zn-, Cu-, and Ni-complexes of porphyrins have been successfully oxidatively coupled.^{2-8,17-26}

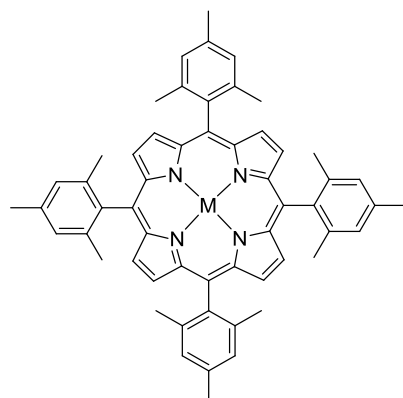
Electrochemically driven oxidative aromatic coupling is a useful method which can afford products on the electrode surface without contamination.³⁹⁻⁴⁶ This approach was first applied to the synthesis of porphyrinoids by Sessler and Bucher.⁴⁷⁻⁴⁸ More recently, studies from our own laboratories revealed that it is possible to perform intramolecular oxidative coupling of a naphthalene group with a porphyrin macrocycle to form a π -extended product after electrochemical oxidation and subsequent reduction of the chemically generated species in nonaqueous media.⁴⁹⁻⁵⁰ In the above study, the *meso*-naphthalene substituted Ni(II)-porphyrin was first oxidized by two electrons to give a porphyrin π dication, after which a fast intramolecular electron transfer occurred to form a dication radical of the π -extended porphyrin. This naphthalene-fused porphyrin dication was then re-reduced by two electrons to give the desired neutral π -extended porphyrin product.

In order to develop new materials based on π -extended porphyrins for applications in electronics and photonics, there is a need to understand and establish the degree of communication, which occurs between the conjugated porphyrin ring and the added fused group, in this case naphthalene. There is also a need to finely control the redox properties of porphyrins with such π extended systems and to ascertain the generally of the electrochemically induced fusion process for free-base porphyrins and porphyrins possessing different central metal ions and metal ions in different oxidation states.

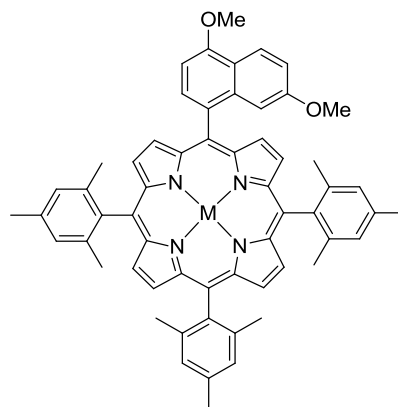
We envisioned that the electrosynthesis reaction described in our initial study for fusion of a nickel porphyrin⁴⁹ would also occur for porphyrins containing a variety of metal ions, as well as for the free-base porphyrins where chemically induced fusion reactions have yet to be demonstrated. If this occurred, the electrosynthesis process would not only duplicate results obtained by chemical methods using one-electron oxidants,^{2,12-14,16,38} but it would also allow us to generate new compounds not easily accessible with classical chemical synthetic methods. As a test of this hypothesis, we set ourselves the goal to perform the electrosynthesis of π extended porphyrins for four types of compounds: an easily oxidizable four coordinate zinc(II) porphyrin which we wished to directly electrosynthesize as a π -extended derivative without having to remove the Zn(II) central metal ion; a five coordinate indium(III)-porphyrin, which possess a relatively high oxidation potential; a six coordinate Ir(III) porphyrin which also possesses a high oxidation potential, and a free-base porphyrin; the latter of which has proven all but impossible to synthesis in its π -extended form from 'regular' free-base porphyrins using chemical methods. The clear advantage of electrochemical synthesis in the case of

free-base porphyrins is that one can then insert numerous central metal ions into the π -extended free-base macrocycle in order to generate a variety of complexes for use in a specific desired application.

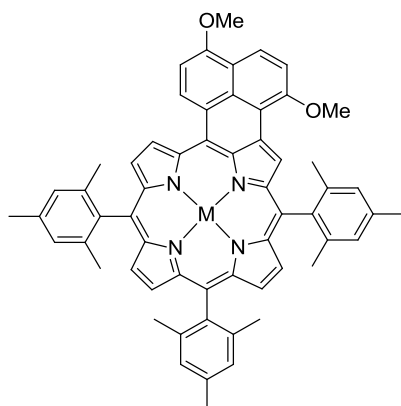
Finally, as part of the current study, we have elucidated the electrochemistry and spectroscopic properties of the electrosynthesized π -extended porphyrins in nonaqueous media containing tetra-*n*-butylammonium perchlorate (TBAP). These data are then compared to that for the same series of porphyrins which were synthesized by classical chemical methods. For the convenience of the reader, the shorthand notation and structures of the compounds examined in the current chapter are given in Chart 7-1.



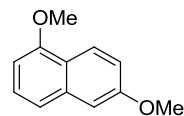
TMP M = H₂
TMP-Zn M = Zn
TMP-InCl M = InCl
TMP-Ir(CO)Cl M = Ir(CO)Cl



Open-H₂ M = H₂
Open-Zn M = Zn
Open-InCl M = InCl
Open-Ir(CO)Cl M = Ir(CO)Cl



Fused-H₂ M = H₂
Fused-Zn M = Zn
Fused-InCl M = InCl
Fused-Ir(CO)Cl M = Ir(CO)Cl



2,6-di-OMe-naphthalene

Chart 7-1. Structure of investigated porphyrins.

7.2 Results and Discussion

7.2.1 UV-vis spectra

Table 7-1 lists UV-vis spectral data of the investigated compounds with TMP, Open, and Fused macrocycles in CH₂Cl₂ containing 0.1 M TBAP. The TMP and Open macrocycle derivatives all have a strong Soret band between 418 to 428 nm in CH₂Cl₂, with some of the compounds having a shoulder at 400-405 nm. The metallated derivatives of these macrocycles also exhibit two bands from 513-601 nm in CH₂Cl₂ while four Q bands are seen for free-base TMP-H₂ due to its low symmetry.⁵¹ The replacement of one mesityl unit with a 4,7-dimethoxynaphthalen-1-yl substituent does not significantly affect the absorption spectra, and only a slight shift of λ_{max} is observed because of the similar electron-donating effect of the naphthalene and mesityl groups.

In agreement with previous studies,^{16,49-50} the π -extended naphthalene-fused porphyrins have strikingly different absorption spectra as compared to the TMP derivatives with the same central metal ions. The Fused porphyrins possess three to four split absorption peaks in the Soret band region (between 300 to 500 nm), with the strongest absorption located between 476 to 495 nm in CH₂Cl₂; this band is strongly red-shifted as compared to “regular” meso-aryl substituted porphyrins. The metallated Fused porphyrins also have three Q (visible) band absorptions, as seen in the Experimental section and in Table 7-1. There is an increased absorption in the Q band region which comes from an elongation of π -conjugation and the loss of symmetry splitting in the π - π^* levels.⁵¹ In addition to an increased intensity of the Q bands there is also a reduced HOMO-LUMO gap and a broadening of the absorption peaks.⁵¹

Table 7-1. UV-vis spectral data of neutral investigated porphyrins in CH₂Cl₂, 0.1 M TBAP.

Ring	M	Soret bands (nm)				Visible bands (nm)			
TMP	H ₂	400 ^{sh}	418			514	547	592	648
	Zn	400 ^{sh}	421			513	549	-	
	Ni	-	415			528	561		
	InCl	405 ^{sh}	425			561	599	-	
	Ir(CO)Cl	-	421			533	567	-	
Open	H ₂	400 ^{sh}	423			516	550	592	648
	Zn	400 ^{sh}	422			513	550	-	
	Ni		417			529	562		
	InCl	404 ^{sh}	428			562	601		
	Ir(CO)Cl	-	424			534	567		
Fused	H ₂	386	418	452	480	568	617	643	709
	Zn	380	421	463	488	556	622	-	672
	Ni	379	-	460	486	550	586		672
	InCl	383	426	469	495	564	606	-	688
	Ir(CO)Cl	378	-	464	489	555	595	-	672

7.2.2 Electrochemistry of chemically synthesized porphyrins

The electrochemistry of each compound in the three series of porphyrins with different macrocycles was carried out in both benzonitrile (PhCN) and dichloromethane (CH_2Cl_2) containing 0.1 M tetra-*n*-butylammonium perchlorate (TBAP) as supporting electrolyte. Cyclic voltammograms (CV) of the four chemically synthesized π -extended porphyrins in CH_2Cl_2 are shown in Figure 7-1.

As shown in the figure, the electrochemistry of the porphyrins with a fused naphthalene ring is well defined. Each compound undergoes two reversible one-electron reductions and two reversible one electron oxidations, with a similar HOMO-LUMO gap of 1.74 to 1.79 V and a similar potential separation between the first and second reductions of about 0.48 V. The easiest to reduce and hardest to oxidize porphyrin contains an In(III) central metal ion, while the hardest to reduce and easiest to oxidize porphyrin contains Zn^{II} or $\text{Ir}^{\text{III}}\text{COCl}$ which, quite surprisingly, display almost identical current voltage curves, suggesting identical sites of electron transfer at the conjugated porphyrin π -ring system. This is discussed later in the manuscript and is not the case for the TMP and A_3B type derivatives with these two central metal ions.

Similar electrochemical behavior is seen for the four chemically synthesized π -extended porphyrins in CH_2Cl_2 and PhCN; examples of cyclic voltammograms in the later solvent are shown in Figure 7-2 along with voltammograms of the TMP derivatives having the same central metal ions. Measured half-wave or peak potentials for reduction and oxidation of the TMP and fused porphyrins in PhCN are summarized in Table 7-2. These tables also include data for the related starting compounds with a single *meso*-naphthalene group (see structures in Chart 7-1).

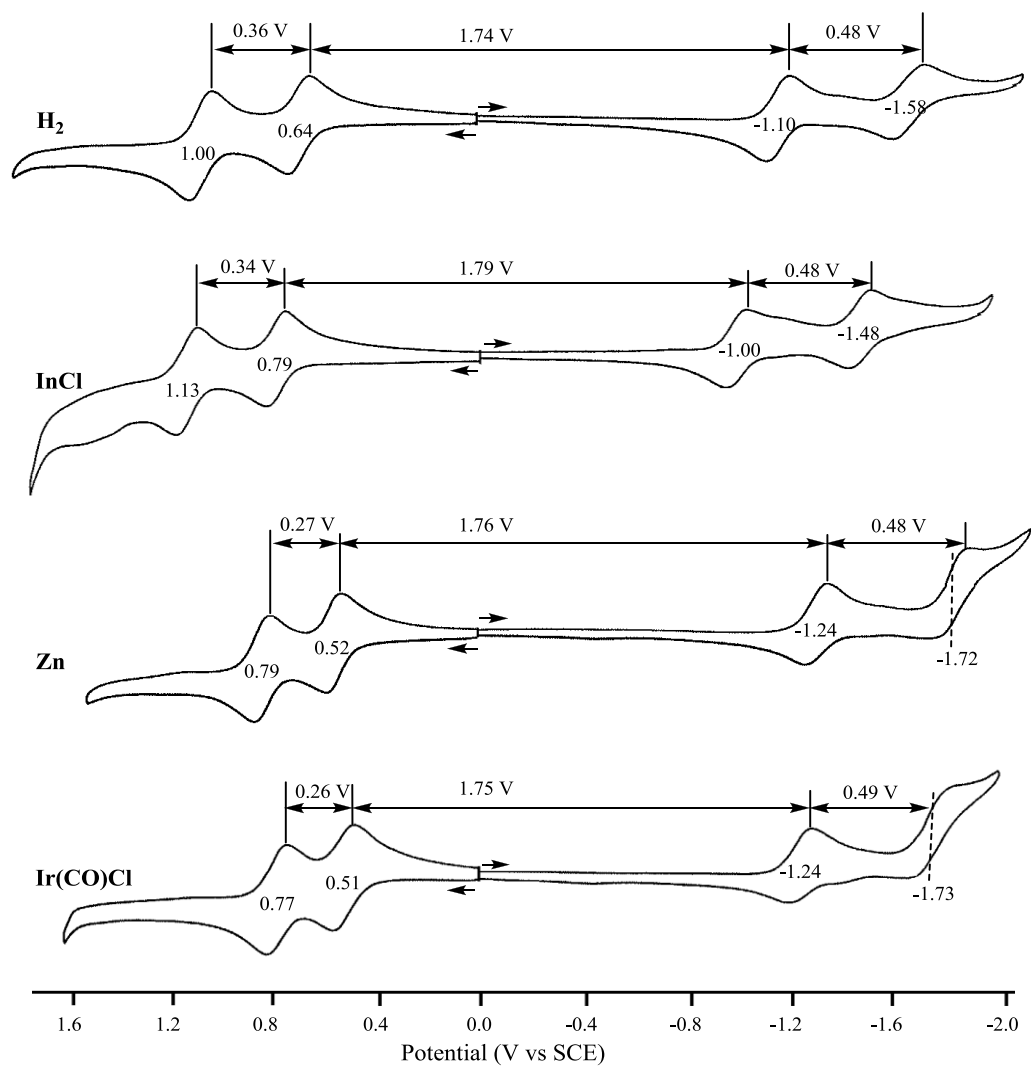


Figure 7-1. Cyclic voltammograms of the chemically synthesized π -extended porphyrins in CH_2Cl_2 , 0.1 M TBAP. The $\Delta E_{1/2}$ between the various redox progresses is also given in the figure.

The reductions and oxidations of the investigated porphyrins are reversible in all three series of compounds, thus enabling an evaluation of how changing one mesityl substituent on TMP to a *meso*-4,7-dimethoxynaphthalen-1-yl group will affect the redox potentials for addition and abstraction of one electron. Although the electron donating effect of the mesityl and naphthalene groups are similar,⁵² the potentials for both reduction and oxidation of the A₃B-porphyrins is, in most cases, slightly easier than that for reduction or oxidation of the TMP, A₄ type, species with the same central metal ions (see Figure 7-2).

Table 7-2. Half-wave or peak potentials (V vs SCE) in PhCN, containing 0.1 M TBAP.

M	Ring	Oxidation		Reduction		H-L gap (V)
		2 nd	1 st	1 st	2 nd	
H ₂	TMP	1.41	1.12	-1.19	-1.69	2.31
	Open	1.24 ^b	1.10	-1.19	-1.68	2.29
	Fused	1.01	0.71	-1.08	-1.56	1.79
Zn	TMP	1.18	0.82	-1.38	-	2.20
	Open	1.12	0.81	-1.36	-1.85	2.17
	Fused	0.85	0.53	-1.25	-1.71	1.78
Ni ^a	TMP	1.14	1.14	-1.30	-	2.44
	Open	1.14	1.14	-1.24	-1.84	2.38
	Fused	1.00	0.74	-1.20	-1.80 ^b	1.94
InCl	TMP	1.57	1.24	-1.05	-1.58	2.29
	Open	1.40 ^b	1.21	-1.01	-1.55	2.22
	Fused	1.13	0.85	-0.97	-1.46	1.82
Ir(CO)Cl	TMP	1.64	1.27	-1.17	-1.39	2.44
	Open	1.43 ^b	1.22	-1.15	-1.74	2.37
	Fused	0.85	0.53	-1.23	-1.69	1.76

^aData taken from ref 49, ^bpeak potential at a scan rate of 0.1 V/s.

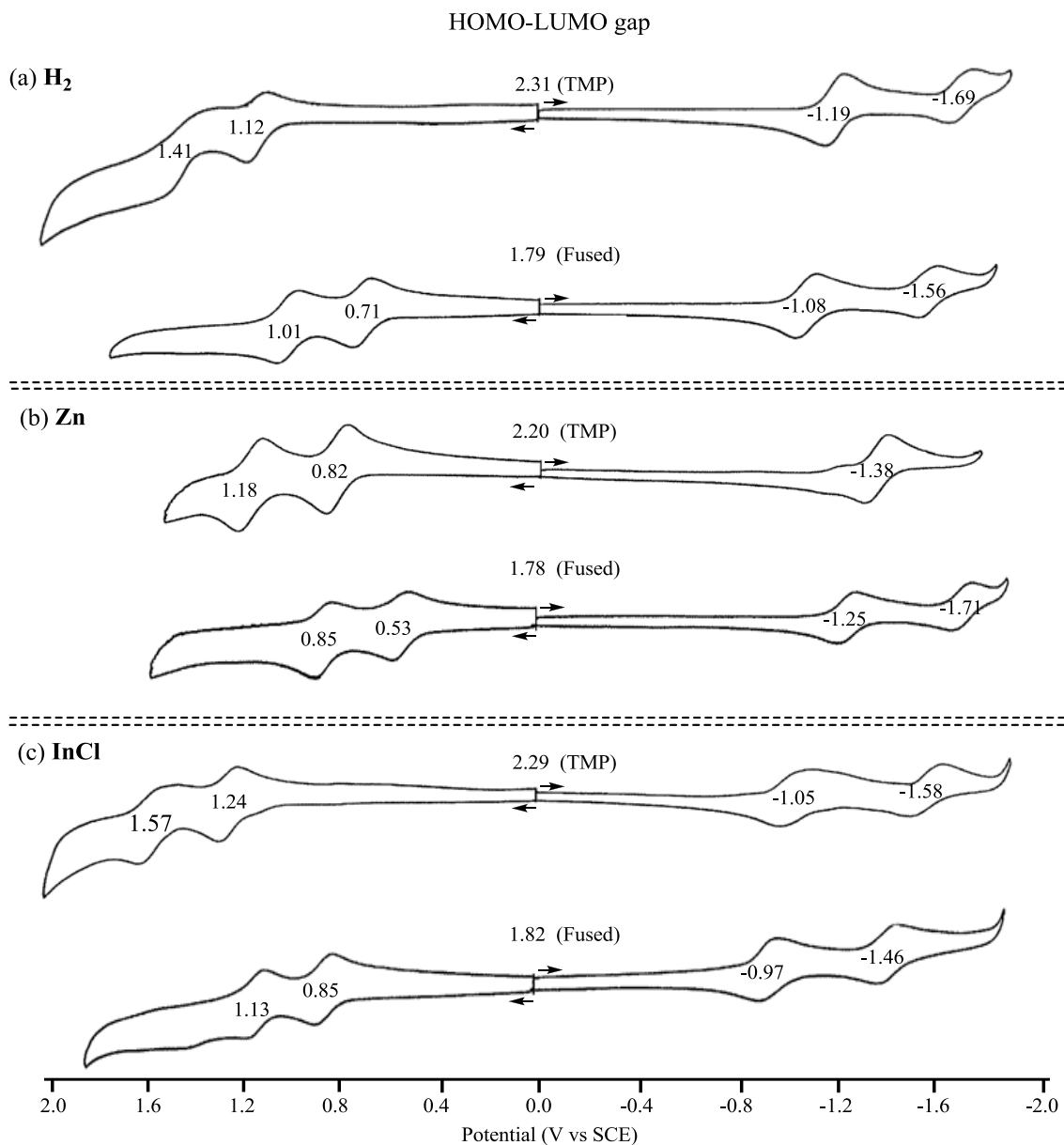


Figure 7-2. Cyclic voltammograms illustrating the reduction and oxidation of porphyrins with TMB and fused macrocycles in PhCN, 0.1 M TBAP. The $\Delta E_{1/2}$ between the two reversible redox processes (the HOMO-LUMO gap) is also given in the figure.

An examination of the electrochemical data in Table 7-2 and Figure 7-2 shows that the difference in $E_{1/2}$ between the first reduction of the TMP and Open-porphyrins with the same central metal ion ranges from 0.0 mV in the case of H_2 to 60 mV in the case of $M = Ni^{II}$. A similar difference in potential is seen for the first oxidation, where the $E_{1/2}$ values vary from 0.0 mV in the case of Ni^{II} (data taken from reference 49), to 50 mV in the case of $Ir(CO)Cl$. The HOMO-LUMO gap, defined as the absolute difference in $E_{1/2}$ between the first ring-centered oxidation and first ring-centered reduction, is thus smaller for the A_3B compounds than for the A_4 derivatives by 20-70 mV as seen in Table 7-2 (PhCN).

The similarity in the first reduction and first oxidation potentials of compounds having the TMP and Open macrocycles is related to the similar substituent effects of the trimesityl and naphthalene groups and to the similar sites of electron transfer, which in this case is the conjugated π -ring system of the porphyrin. Similar potentials are not observed for the second oxidation of the TMP and Open macrocycle compounds, where much larger differences are observed suggesting different sites of electron transfer for this reaction in the two series of compounds. The $\Delta E_{1/2}$ between the TMP and Open porphyrin derivatives ranges from 170-210 mV in the case of the free-base, $InCl$, and $Ir(CO)Cl$ compounds to 60 mV in the case of the $Zn(II)$ complexes. As will be described in the following electroynthesis section, the doubly oxidized Open porphyrin can be described as a diradical where the first electron is abstracted from the porphyrin π -ring system and the second from the electroactive naphthalene group. Once the second oxidation occurs to give the diradical, a coupling is observed, leading to an irreversible second oxidation in each case.

Large differences in potentials are also observed when comparing oxidations and reductions of the TMP derivatives to those with a π -extended system. This is shown graphically in Figure 7-2 for three of the examined π -extended porphyrins where the first reduction is easier by 80-130 mV and the first oxidation easier by 290-410 mV as compared to the related TMP derivatives with the same central metal ion.

In summary, the HOMO-LUMO gap of the fused-porphyrins (1.76-1.83 V) is about 600 mV smaller than that of tetramesitylporphyrins (2.20-2.44 V) or the A₃B-porphyrins with a single *meso*-4,7-dimethoxynaphthalen-1-yl group (2.17-2.37 V). The oxidation is more affected by ring fusion than reduction. This is consistent with previous studies involving expanded Pt porphyrins⁵³ and a Ni⁴⁹⁻⁵⁰ porphyrin where ring expansion results in a considerable raising of the macrocycle HOMO levels but induces only small changes in the LUMO levels of the π -ring system. Finally, it is interesting to point out that the average HOMO-LUMO gap of about 1.78 V for the four fused porphyrins investigated in the present study is exactly the same HOMO-LUMO gap as reported for a Pt tetraphenyl tetranaphthylporphyrin under the same solution conditions.⁵³

7.2.2.1 Ir(CO)Cl compounds. Special mention should be made of Fused-Ir(CO)Cl which differs substantially from the TMP and Open macrocycle derivatives of Ir(CO)Cl whose behavior is well characterized for related compounds in the literature, two examples being (TPP)Ir(CO)Cl⁵⁴ and (OEP)Ir(CO)Cl.⁵⁴

The electroreduction of (TPP)Ir^{III}COCl and (OEP)Ir^{III}COCl in nonaqueous solvents proceeds *via* two, one-electron transfer reductions to give as a final product, an Ir(I) porphyrin. The first one electron reduction of these compounds generates an Ir(III) porphyrin π -anion radical and this is followed by the addition of a second electron and

transfer of charge from the porphyrin π ring system to the metal center as described in the literature. The first reduction of (TPP)Ir(CO)Cl is located at -1.15 V in CH₂Cl₂ or PhCN⁵⁴ and this potential is virtually identical to the $E_{1/2}$ for the first reduction of TMP-Ir(CO)Cl and Open-Ir(CO)Cl (See Figure 7-3 and Table 7-2). The UV-visible spectrum obtained after electroreduction of (TPP)Ir(CO)Cl in PhCN has a Soret band at 397 nm as compared to 421 nm for the neutral compound. A similar shift in λ_{\max} from 423/424 nm to 403 nm is observed after reduction of TMP-Ir(CO)Cl and Open-Ir(CO)Cl under similar solution conditions (Figures 7-3a, 7-3b). In each case, the reduction products are assigned as due to Ir(I) porphyrin.

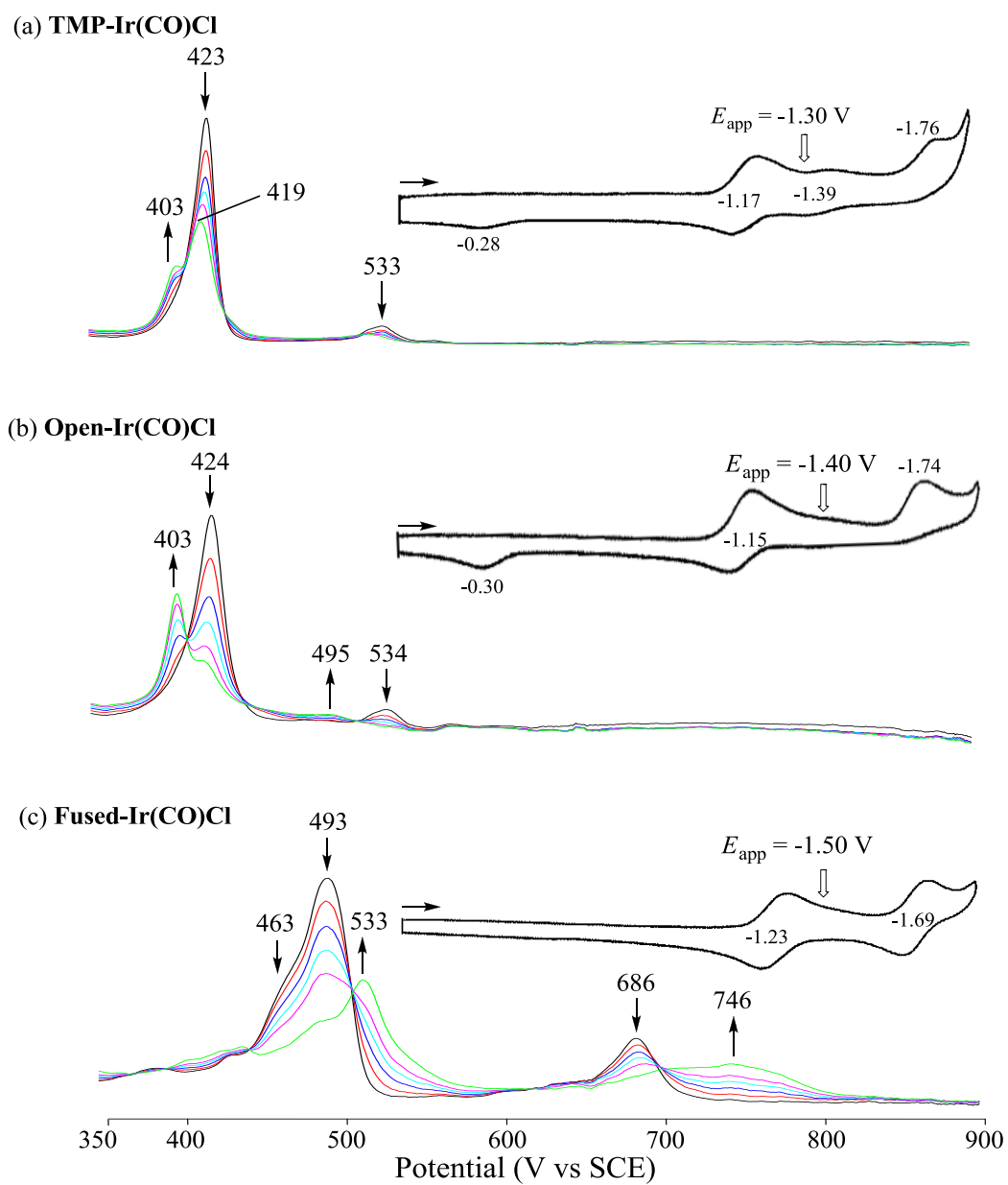


Figure 7-3. UV-visible spectral changes obtained during the first reduction of (a) TMP-Ir(CO)Cl, (b) Open-Ir(CO)Cl, and (c) Fused-Ir(CO)Cl in PhCN, 0.1 M TBAP.

In contrast to TMP-Ir(CO)Cl and Open-Ir(CO)Cl, the electroreduction of Fused-Ir(CO)Cl does not lead to an Ir(I) porphyrin product but rather to an Ir(III) porphyrin π -anion radical whose UV-visible spectrum is characterized by bands at 533 and 746 nm. In addition, the reduction of Fused-Ir(CO)Cl at $E_{1/2} = -1.23$ V is more difficult than the reduction of TMP-Ir(CO)Cl (-1.17 V) or Open-Ir(CO)Cl (-1.15 V), a result which is unexpected when considering that the Fused porphyrins with π -extended systems are all easier to reduce than the TMP or Open porphyrins by 80-130 mV (seen Figure 7-2 and Table 7-2).

The differences in the HOMO-LUMO gaps of the TMP, Open, and Fused Ir(CO)Cl porphyrins should also be noted. This potential separation is equal to 2.44 V for TMP and 2.37 V for Open-Ir(CO)Cl as compared to 2.40 V for (TPP)Ir(CO)Cl in CH₂Cl₂ or PhCN. This contrasts with a HOMO-LUMO gap of 1.76 V for Fused-Ir(CO)Cl (See Figure 7-4), a difference of 610 to 680 mV, all of which is due to the greatly facilitated oxidation of the π -extended porphyrin.

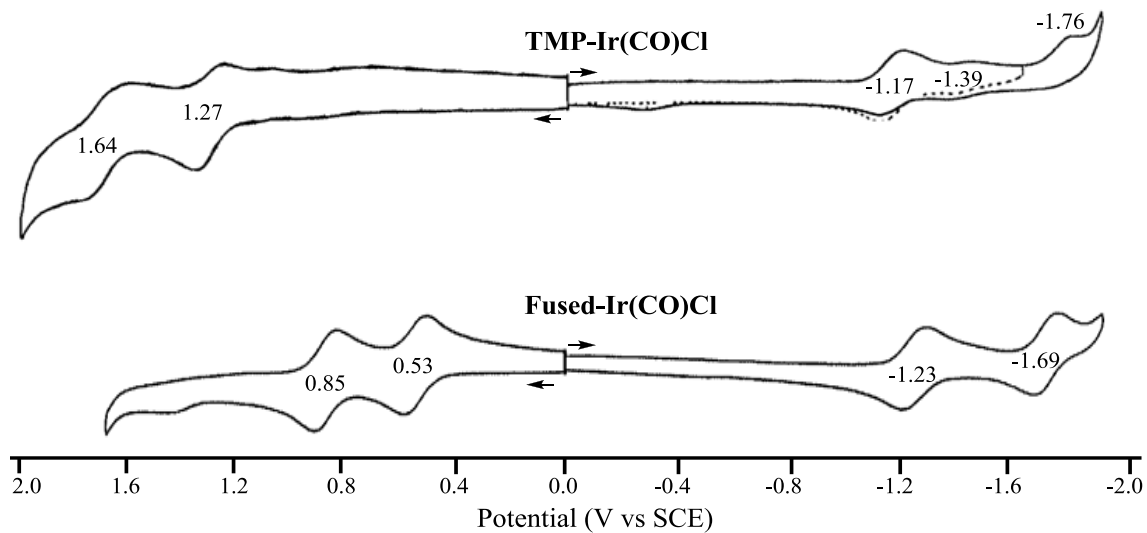


Figure 7-4. Cyclic voltammograms of Ir(CO)Cl centered orphyrins with TMP and Fused macrocycles in PhCN, 0.1 M TBAP.

Finally, it should be noted that the redox potentials for oxidation and reduction of Fused-Ir(CO)Cl are virtually identical to the potentials for oxidation and reduction of Fused-Zn. This type of result is without precedent in the porphyrin literature for Zn(II) and Ir(III) porphyrins with other macrocycles and can only be explained by the fact that Ir(III)COCl processes a great deal of Ir(II) character.

7.2.2.2 Electrosynthesis of metallated π -extended porphyrins. Electrosynthesis of the metallated fused porphyrins in Chart 1 was carried out from the *meso*-substituted naphthalene porphyrins as described in an earlier publication for the case of Ni(II) derivatives having the same structure.⁴⁷ In the present study, we wished to determine if the same fusion mechanism would be followed for porphyrins with different coordination geometries (4, 5 and 6-coordinate), different central metal oxidation states (+2 and +3) and different potentials for electrogeneration of the porphyrin dication, the chemically reactive species which converts to the fused product.

As described above, the chemically synthesized Zn(II) porphyrin with a π -extended system Fused-Zn is reversibly oxidized in two one electron steps located at $E_{1/2} = 0.53$ and 0.85 V in PhCN, 0.1 M TBAP. This compares to the Open Zn(II) porphyrin, which exhibits two reversible one-electron oxidations at $E_{1/2} = 0.81$ and 1.12 V under the same solution condition. The product of the one electron oxidation of the Open-Zn is stable on the cyclic voltammetry time scale and it is also stable after holding the potential for 2 min at 1.05 V and then reversing the potential sweep direction to reduce the Open porphyrin π -cation radical to its neutral form again. This is shown by the top cyclic voltammogram in Figure 7-5a.

The dication of the Zn(II) Open porphyrin generated in PhCN at $E_{1/2} = 1.12$ V is unstable on the cyclic voltammetry timescale of 0.10 V/s, and undergoes a slow chemical conversion to the dication of the Fused porphyrin, as demonstrated by the decreased current for the second oxidation on the return sweep and the appearance of a new cathodic peak at $E_p = 0.48$ V (see Figure 7-5a). The process for this new peak corresponds to that for reduction of the electrogenerated singly oxidized Fused porphyrin to its neutral form.

The magnitude of the current for the peak at 0.48 V depends upon both the scan rate and switching potential and significantly increases in intensity when the potential is held for 2 min at 1.50 V prior to rereduction, a condition where larger amounts of the Fused porphyrin are generated at the electrode surface (see third cyclic voltammogram in Figure 7-5a). Under these experimental condition, the process at $E_{1/2} = 1.12$ V has a much decreased reverse cathodic peak current, while the cathodic peak current at 0.81 V seems to be unchanged but actually corresponds to two overlapping processes, one for reduction of the fused porphyrin dication at 0.85 V and the other for reduction of the starting Open porphyrin cation radical at 0.81 V. This cyclic voltammogram is shown at the bottom of Figure 7-5a, where the two oxidation peaks on the initial positive scan have identical currents and the sum of the first and third rereduction peak currents are about equal to that for the combined overlapping reoxidation processes at 0.81 and 0.85 V.

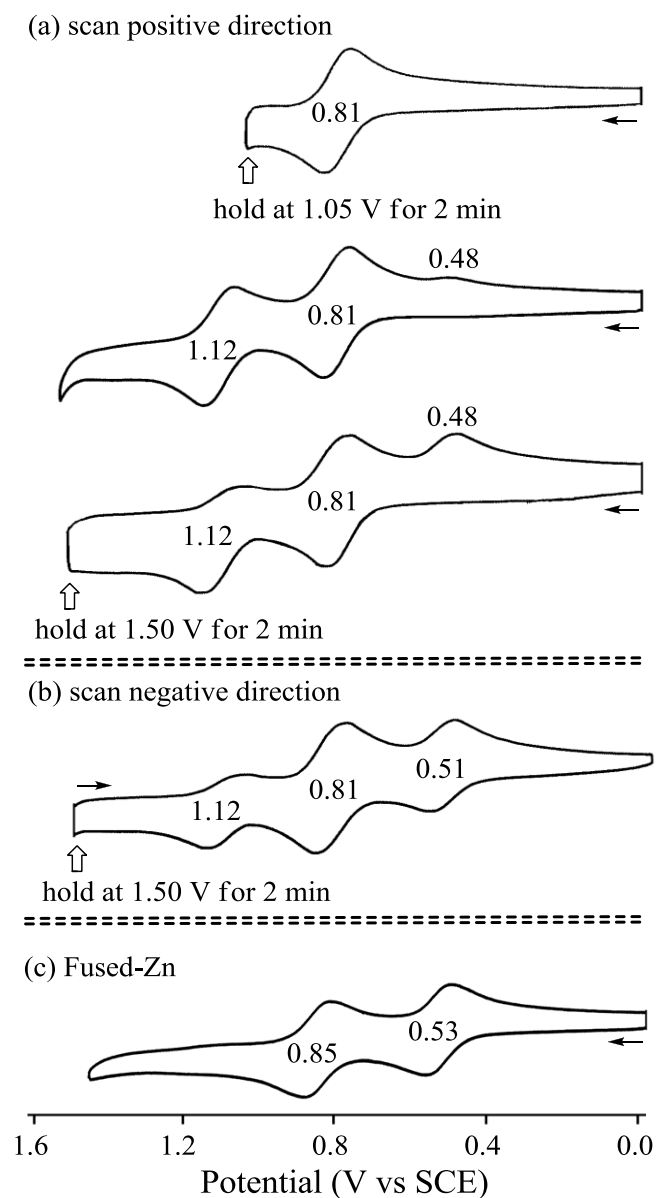


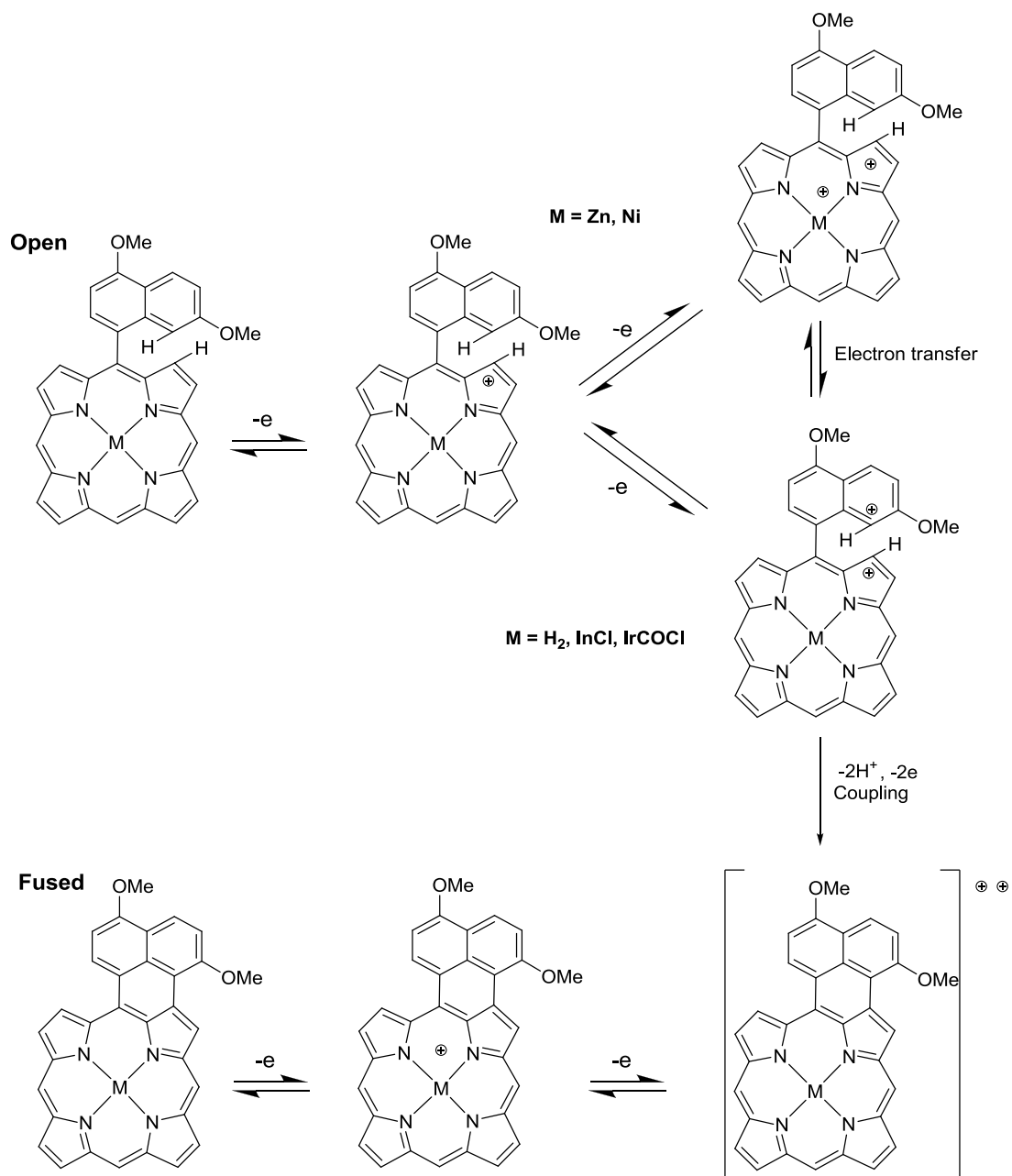
Figure 7-5. Cyclic voltammograms showing electrochemically induced generation of the fused Zn(II) complex from the porphyrin dication of the related open macrocycle (a) after initial positive scans from 0.0 to 1.50 V and (b) after an initial negative scan from 1.50 to 0.0 V in PhCN, 0.1 M TBAP, scan rate = 0.1 V/s. For comparison, a cyclic voltammograms of the chemically generated Zn(II) porphyrin with the fused π -extended system is shown in part c.

Additional evidence for electrosynthesis of the π -extended porphyrin is given by the cyclic voltammogram in Figure 7-5b where the potential was held for 2 min at 1.50 V before initiating the scan in a negative direction. Under these conditions, a larger amount of the Open porphyrin reactant is consumed and the redox process associated with the electrosynthesized Fused Zn(II) porphyrin at $E_{1/2} = 0.51$ V exhibits an increased peak current, consistent with larger amounts of this material being formed at the electrode surface. A comparison of the cyclic voltammogram in Figure 7-5b with that of the chemically synthesized Zn(II) Fused porphyrin in Figure 7-5c, shows clearly that the same chemical species has been formed by electrosynthesis in PhCN as by classical chemical synthetic methods.

As shown in Table 7-2, the second oxidation is reversible for Zn(II) and Ni(II) centered Open-M located at $E_{1/2} = 1.12$ and 1.14 V, respectively. But irreversible second oxidation is observed for In(III), Ir(III), and free-base Open-M. This difference in second oxidation could be accounted as different site of electron abstraction on the second oxidation. The second oxidation on porphyrin macrocycle for Zn and Ni, but on naphthalene group for In, Ir, and 2H centered complex. This electron abstraction site assignment is proved by compare the second oxidation potential of its TMP macrocycled complex to naphthalene oxidation potential. If the second oxidation of TMP-M is easier than the first oxidation of Naphthalene ($E_{pa} = 1.36$ V), porphyrin second oxidation will be processed first, so the second oxidation of its Open macrocycle complex will be reversible as Zn and Ni, otherwise, second oxidation will be on naphthalene group and become irreversible.

In summary, the mechanism for conversion of the Open to the Fused porphyrin involves two one-electron oxidations followed by a radical coupling to give the Fused porphyrin dication as shown in Scheme 7-1. The first oxidation is porphyrin centered for all the Open-M to form porphyrin π -cation radical, while depends on the site of second electron abstraction to form porphyrin dication or porphyrin-naphthalen diradical. Generated porphyrin dication will transfer the positive charge to naphthalene group to form porphyrin-naphthalen diradical before ring fusion. This doubly oxidized porphyrin with an extended π -system is then reduced by two one-electron transfers to give the final Fused neutral porphyrin product.

Scheme 7-1. Electrosynthesis mechanism for conversion of Open porphyrin to the Fused porphyrin.



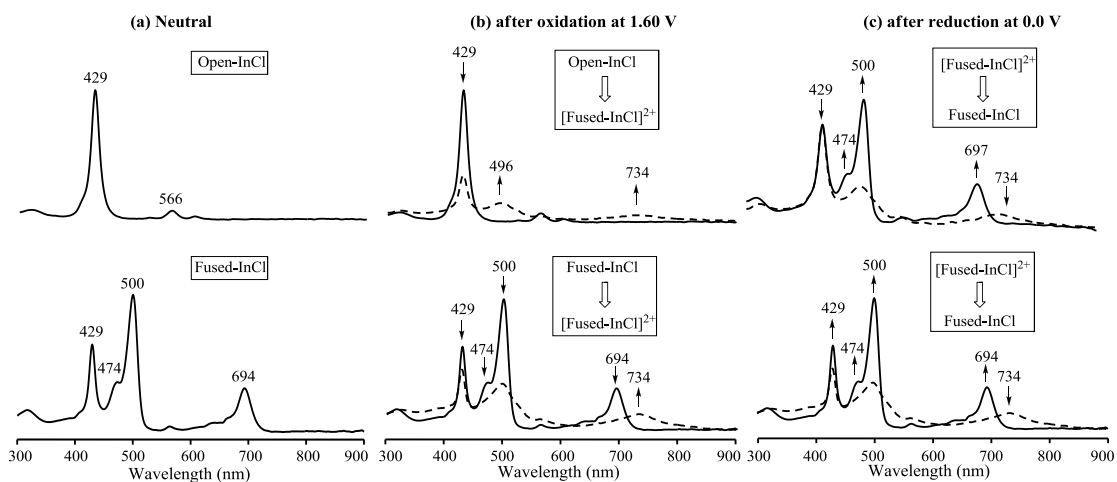


Figure 7-6. UV-visible spectrum of Open-InCl and Fused-InCl in PhCN, 0.1 M TBAP (a) before electrochemistry, (b) after a two-electron oxidation and (c) after a two-electron rereduction of the doubly oxidized species.

Data from electrochemistry and thin-layer UV-visible spectroelectrochemistry (Figure 7-6) gives evidence that the mechanism illustrated in Scheme 7-1 also occurs in the case of the InCl derivatives, where the Open-InCl porphyrin is converted to the doubly oxidized Fused-InCl porphyrin after controlled potential oxidation, followed by controlled potential reduction of the electrogenerated product. Quite different UV-visible spectra are observed for Open-InCl ($\lambda_{\text{max}} = 429$ and 566 nm) and Fused-InCl ($\lambda_{\text{max}} = 429$, 474, 500 and 694 nm) in their neutral form (Figure 7-6a), but after controlled potential oxidation by two electrons at 1.60 V, products with exactly the same UV-visible spectra are observed. These products are assigned as $[\text{Fused-InCl}]^{2+}$ and characterized by bands at 429, 496, and 734 nm (see dashed line in Figure 7-6b).

Rereduction of the electrochemically generated $[\text{Fused-InCl}]^{2+}$ at 0.0 V gives the same neutral Fused-InCl compound, independent of the starting material, either Open-InCl (top of Figure 7-6c) or Fused-InCl (bottom of Figure 7-6c). The resulting neutral π extended porphyrin products in Figure 7-6c have bands at 429, 474, 500, and 697 nm, and the overall shape of the spectrum is identical to that for the chemically generated Fused-InCl porphyrin prior to the electrochemistry (Figure 7-6a). Like the case of the Zn(II) porphyrins, the conversion of Open-InCl to Fused-InCl involves an overall two-electron oxidation followed by a radical coupling reaction to give the Fused porphyrin dication.

A similar mechanism as shown in Scheme 7-1 also occurs for conversion of Open-Ir(CO)Cl to the Fused Ir(III) derivatives, but slight differences are seen in the UV-vis spectra of the chemically and electrochemically generated π -extended porphyrins

(Figure 7-7). The chemically synthesized Fused-Ir(CO)Cl has a split Soret band at 463 and 493 nm and a Q band at 686 nm (See Experimental and Figure 7-7c).

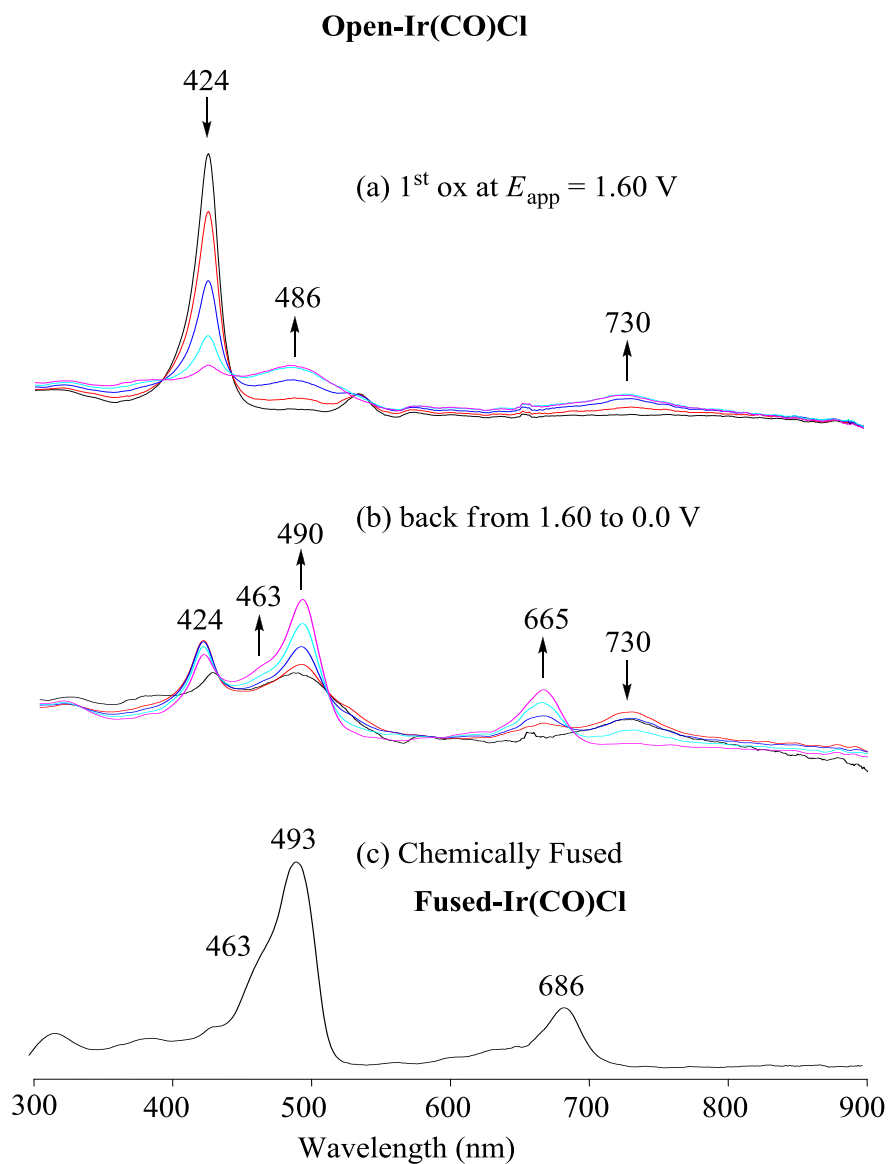


Figure 7-7. UV-visible spectral changes (a) during oxidation of Open-Ir(CO)Cl in a thin-layer cell at an applied potential of 1.60 V, (b) after rereduction of the above compound at $E_{\text{app}} = 0.00$ V to electrogenerate the neutral fused compounds in PhCN, 0.1 M TBAP, and (c) UV-vis spectra of the chemically synthesized Fused-Ir(CO)Cl under the same solution condition.

The electrochemically generated Fused Ir(III) porphyrin also has a split Soret band at 463 and 490nm, but the Q band is located at 665 nm (Figure 7-7b). The electrochemistry of the chemically and electrochemically generated compounds are similar to each other, and the difference in the position of the Q bands is attributed to a different axially bound anion in the two compounds, ClO_4^- from the TBAP supporting electrolyte, in the case of the electrochemically generated compound, and Cl^- in the case of the chemically synthesized Fused-Ir(CO)Cl.

Electrochemistry of free-base π -extended porphyrin was also investigated. The mechanism for conversion of Open- H_2 to Fused- H_2 is similar to that described above for the other Open porphyrins, but it differs from the metallated complexes in that the final electrochemically generated Fused product is produced as a mixture of the free-base porphyrin with an extended π ring system, Fused- H_2 , and the diprotonated Fused free-base porphyrin represented as $[\text{Fused-H}_4]^{2+}$. Evidence for this assignment is given by cyclic voltammetry and thin-layer spectroelectro-chemistry.

The cyclic voltammetric data is illustrated in Figure 7-8 which compares the oxidation of (a) TMPH_2 and naphthalene, (b) Open- H_2 , which contains linked naphthalene, and (c) Fused- H_2 , which contains fused naphthalene. The two oxidations of TMP-H_2 (Figure 7-8a) are both reversible in CH_2Cl_2 and occur at $E_{1/2} = 1.03$ and 1.46 V while the first two oxidations of Open- H_2 occur at $E_{1/2} = 1.02$ V and $E_p = 1.27$ V (Figure 7-8b). The similar half-wave potentials and similar reversibility in the initial one electron oxidation of TMP-H_2 and Open- H_2 is consistent with the same site of electron transfer (the porphyrin conjugated π system) and the same electrogenerated product (a porphyrin

π cation radical). The different potentials and different reversibility in the second electron abstraction from TMP-H₂ and Open-H₂ is consistent with a different site of electron transfer in the second oxidation, in this case, the porphyrin π system in TMP and the naphthalene group in Open-H₂. Naphthalene is oxidized at $E_p = 1.33$ V (Figure 7-8a), but after being linked to the porphyrin, the potential shifts to 1.27 V (Figure 7-8b).

Because the second oxidation of Fused-H₂ ($E_{1/2} = 1.00$ V) occurs at almost the same potential as the first oxidation of Open-H₂ ($E_{1/2} = 1.02$ V), the return sweep in Figure 7-8b for doubly oxidized Open-H₂ shows what appears to be an unchanged process at 1.02 V. There is also a new peak at $E_p = 0.65$ V which is not seen until after the second oxidation. In fact, the peak at 1.02 V in Figure 7-8b is due to overlapping processes for the reversible first oxidation/reduction of Open-H₂ and the reversible second oxidation/reduction of the fused product (See Figure 7-8c), both of which occur at an almost identical half-wave potential. This is similar to what was observed for the Zn porphyrins whose cyclic voltammograms are shown in Figure 7-5.

Although the electrochemical data in Figure 7-8 suggests a clean formation of Fused-H₂ in the absence of any side product, UV-visible spectroelectrochemistry data shows the electrogenerated porphyrin product with an extended π system exists in its diprotonated form.

The spectral data giving evidence for electrogeneration of Fused-H₂ and [Fused-H₄]²⁺ after oxidation and rereduction of Open-H₂ are shown in Figure 7-9, which illustrates the overall conversion of Open-H₂ to [Fused-H₄]²⁺ and compares the UV-visible spectrum of electrochemically generated [Fused-H₄]²⁺ with that of chemically

generated $[\text{Fused-H}_4]^{2+}$ which was formed by addition of trifluoroacetic acid (TFA) to solutions of pure Fused-H₂.

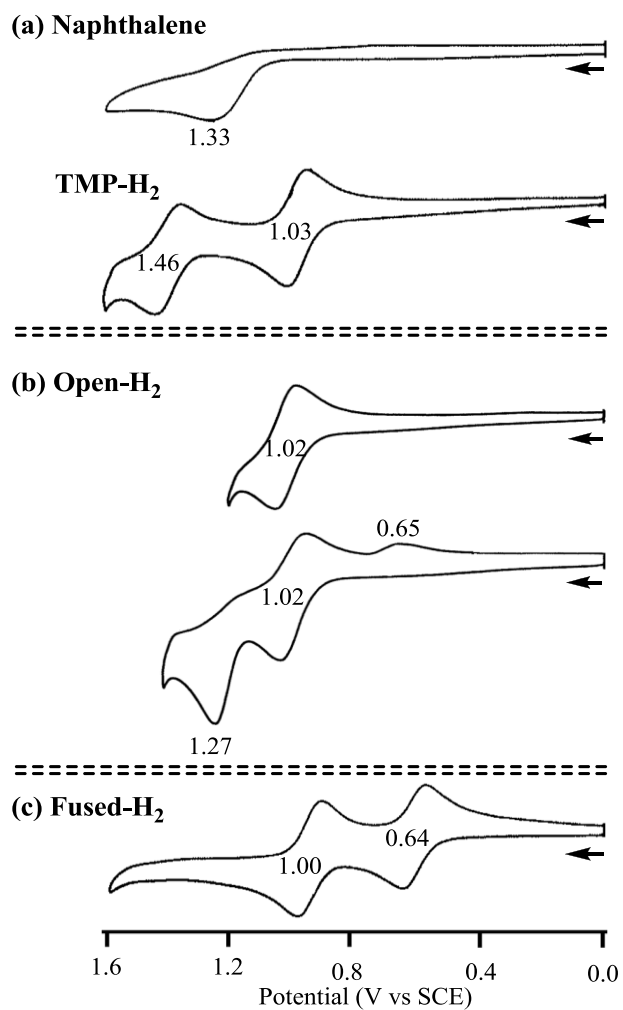


Figure 7-8. Cyclic voltammogram of (a) naphthalene and TMP-H₂, (b) Open-H₂, and (c) Fused-H₂ in CH₂Cl₂, 0.1 M TBAP.

The first set of spectra changes upon oxidation of Open-H₂ in CH₂Cl₂ at 1.40 V leads reversibly to a free-base porphyrin π -cation radical which exhibits a decreased intensity Soret band and a broad Q band centered at 655 nm. Further oxidation of [Open-H₂]⁺ at 1.70 V leads to the dication of the Fused porphyrin, either [Fused-H₂]²⁺ or [Fused-H₄]⁴⁺ as shown in Scheme 7-2. Rereduction of the oxidation product(s) at 0.00 V gives a spectrum with bands at 433, 507, 729, and 771 nm. This spectrum is shown in Figure 7-9a. It is different than that of Fused-H₂ but closely resembles the spectrum of [Fused-H₄]²⁺ which was generated in CH₂Cl₂ by addition of acid in the form of TFA to Open-H₂. The bands for this diprotonated compound are located at 436, 506, 722, and 760 nm (Figure 7-9b). Based on the above electrochemistry and spectroscopic data, the mechanism shown in Scheme 7-2 is proposed for formation of the π -extended free-base porphyrin.

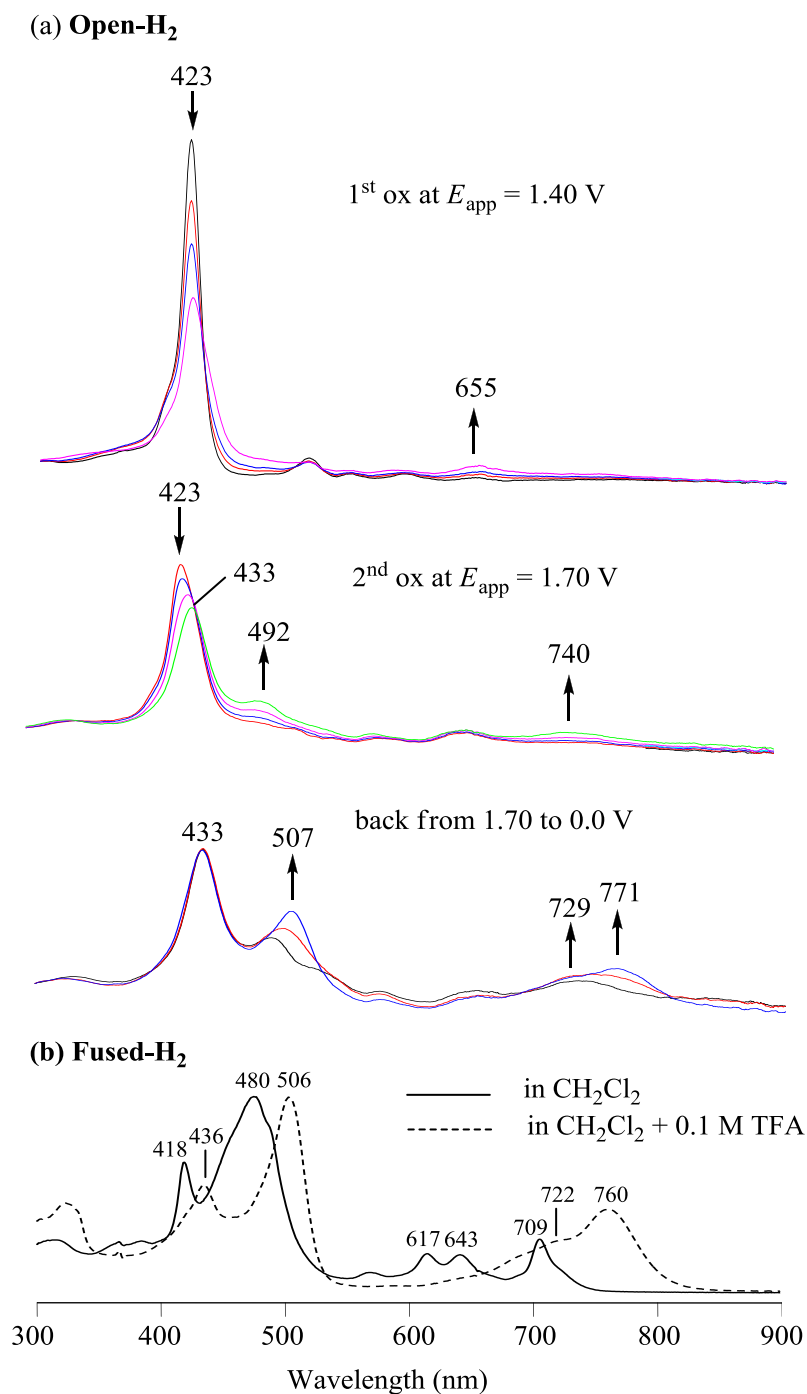
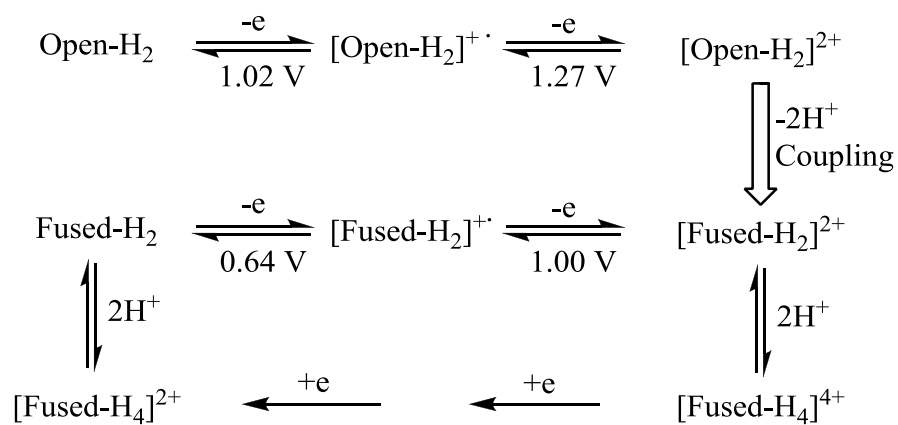


Figure 7-9. UV-visible spectrum of (a) Open-H₂ during oxidation and rereduction in CH₂Cl₂, 0.1 M TBAP and (b) Fused-H₂ before (—) and (-----) after addition of TFA in CH₂Cl₂.

Scheme 7-2. Electrosynthesis mechanism for conversion of Open-H₂ porphyrin to [Fused-H₄]²⁺ porphyrin.



7.2.3 Synthesis of Fused-freebase porphyrins by electrochemistry

Controlled-potential bulk electrolysis was carried out in a 10 ml CH₂Cl₂ solution containing 0.1 M TBAP and **Open-H₂** (5.37 mg, 0.0064 mmol). The controlled oxidizing potential was set at +1.50 V which was sufficient to generate the species [**Open-H₂**]²⁺ which was converted to [**Fused-H₄**]⁴⁺ in solution. The potential was held at +1.50 V for two hours and then switched to +0.0 V, which resulted in a conversion of [**Fused-H₄**]⁴⁺ to [**Fused-H₄**]²⁺. The doubly protonated dication was converted to Fused-H₂ by adding dry Et₃N (0.1 mL) in DCM (5 mL). After 15 min, solvent was removed in vacuum and the residue was dissolved in CH₂Cl₂. The crude product was first purified by silica gel column chromatography, with a solvent mixture of hexanes and CH₂Cl₂ (3:2) as eluent. Additional DCVC (CH₂Cl₂:hexanes) gave pure green solid product with 53% yield.

7.3 Conclusions

The use of electrochemical oxidation allows for one to overcome problems with oxidative aromatic coupling of free-base porphyrins using chemical one-electron oxidants, which protonate (or form complexes) with these porphyrins, effectively stopping further transformations. In contrast, oxidative aromatic coupling can be driven by electrochemistry giving rise directly to a fused porphyrin as a dication. The use of electrochemically mediated oxidation also makes it possible to perform intramolecular oxidative coupling on a suitably substituted Zn-porphyrin without extrusion of the zinc cation. Finally even indium(III) and iridium(III) porphyrins, possessing relatively high oxidation potentials, were successfully coupled to the π -extended porphyrins for the first time.

The electrochemical and spectroelectrochemical data demonstrate that oxidative aromatic coupling does not occur after formation of a radical-cation, but only after formation of a dication where the first electron is abstracted from the porphyrin π ring system and the second from the electroactive naphthalene group. The results in our current study should open new avenues towards π -extended porphyrins with strongly bathochromically shifted absorptions, which were previously impossible to obtain or problematic using chemical oxidants.

7.4 References

- (1) Sessler, J. L.; Seidel, D. *Angew. Chem. Int. Ed.* **2003**, *42*, 5134.
- (2) Lewtak, J. P.; Gryko, D. T. *Chem. Commun.* **2012**, *48*, 10069.
- (3) Kim D.; Osuka, A. *Acc. Chem. Res.* **2004**, *37*, 735.
- (4) Ono, N.; Yamada, H.; Okujima, T. in *the Handbook of Porphyrin Science*, Kadish, K. M.; Smith, K. M.; Guillard, R., eds; World Scientific, Singapore, **2009**, *vol. 2*, pp. 1.
- (5) Tsuda A.; Osuka, A. *Science* **2001**, *293*, 79.
- (6) Osuka, A. *Adv. Mater.* **2002**, *14*, 75.
- (7) Pereira, A. M. V. M.; Richeter, S.; Jeandon, C.; Gisselbrecht, J.-P.; Wytko, J.; Ruppert, R. *J. Porphyrins Phthalocyanines* **2012**, *16*, 464.
- (8) Osuka, A.: Single-molecule photophysical properties of various directly linked porphyrin arrays, in *Multiporphyrin arrays*, Kim, D., Ed.; Pan Stanford Publishing, Singapore, **2012**, pp. 1.
- (9) Gill, H. S.; Harmjanz, M.; Santamaria, J.; Finger, I.; Scott, M. J. *Angew. Chem., Int. Ed.* **2004**, *43*, 485.
- (10) Diev, V. V.; Hanson, K.; Zimmerman, J. D.; Forrest, S. R.; Thompson, M. E. *Angew. Chem., Int. Ed.* **2010**, *49*, 5523.
- (11) López-Duarte, I.; Reeve, J. E.; Pérez-Moreno, J.; Boczarow, I.; Depotter, G.; Fleischhauer, J.; Clays, K.; Anderson, H. L. *Chem. Sci.* **2013**, *4*, 2024.
- (12) Davis, N. K. S.; Pawlicki, M.; Anderson, H. L. *Org. Lett.* **2008**, *10*, 3945.
- (13) Davis, N. K. S.; Thompson, A. L.; Anderson, H. L. *Org. Lett.* **2010**, *12*, 2124.
- (14) Davis, N. K. S.; Thompson, A. L.; Anderson, H. L. *J. Am. Chem. Soc.* **2011**, *133*, 30.
- (15) Ishizuka, T.; Saegusa, Y.; Shiota, Y.; Ohtake, K.; Yoshizawa, K.; Kojima, T. *Chem. Commun.* **2013**, *49*, 5939.
- (16) Lewtak, J. P.; Gryko, D.; Bao, D.; Sebai, E.; Vakuliuk, O.; Scigaj, M.; Gryko, D. *T. Org. Biomol. Chem.* **2011**, *9*, 8178.
- (17) Boerner, L. J. K.; Mazumder, S.; Pink, M.; Baik, M.-H.; Zaleski, J. M. *Chem. - Eur. J.* **2011**, *17*, 14539.

- (18) Nakamura, Y.; Aratani, N.; Shinokubo, H.; Takagi, A.; Kawai, T.; Matsumoto, T.; Yoon, Z. S.; Kim, D. Y.; Ahn, T. K.; Kim, D.; Muranaka, A.; Kobayashi, N.; Osuka, A. *J. Am. Chem. Soc.* **2006**, *128*, 4119.
- (19) Fox, S.; Boyle, R. W. *Chem. Commun.* **2004**, 1322.
- (20) Shen, D.-M.; Liu, C.; Chen, Q.-Y. *Chem. Commun.* **2005**, 4982.
- (21) Shen, D.-M.; Liu, C.; Chen, Q.-Y. *J. Org. Chem.* **2006**, *71*, 6508.
- (22) Hayashi, S.; Matsubara, Y.; Eu, S.; Hayashi, H.; Umeyama, T.; Matano, Y.; Imahori, H. *Chem. Lett.* **2008**, *37*, 846.
- (23) Lash, T. D.; Smith, B. E.; Melquist, M. J.; Godfrey, B. A. *J. Org. Chem.* **2011**, *76*, 5335.
- (24) Chou, J.-H.; Kosal, M. E.; Nalwa, S. H.; Rakow, N. A.; Suslick, K. S. in *The Porphyrin Handbook*; Kadish, K. M.; Smith, K. M.; Guilard, R., eds; Academic Press: San Diego, CA, **2000**; Vol. 6. pp. 43.
- (25) Jiang, L.; Engle, J. T.; Sirk, L.; Hartley, C. S.; Ziegler, C. J.; Wang, H. *Org. Lett.* **2011**, *13*, 3020.
- (26) Sessler, J. L.; Gebauer, A.; Vogel, E. in *the Handbook of Porphyrin Science*, Kadish, K. M.; Smith, K. M.; Guilard, R., Eds.; World Scientific, Singapore, **2012**, Vol. 2, pp. 1;
- (27) Sanienda, A. Zeitschrift fuer Naturforschung, Teil B: Anorganische Chemie, Organische Chemie, Biochemie, Biophysik, Biologie **1967**, *22*, 1107-1111.
- (28) Bucher, C.; Buda, M. in the Handbook of Porphyrin Science, Kadish, K. M.; Smith, K. M.; Guilard, R., Eds.; World Scientific, Singapore, **2012**, Vol. 17, pp. 240.
- (29) McKeown, N. B.; Makhseed, S.; Msayib, K. J.; Ooi, L. L.; Helliwell M.; Warren, J. E. *Angew. Chem. Int. Ed.* **2005**, *44*, 7546.
- (30) Sahoo, K.; Nakamura, Y.; Aratani, N.; Kim, K. S.; Noh, S. B.; Shinokubo, H.; (31) Kim D.; Osuka, A. *Org. Lett.* **2006**, *8*, 4144.
- (31) Ahn, T. K.; Kim, K. S.; Kim, D. Y.; Noh, S. B.; Aratani, N.; Ikeda, C.; Osuka, A.; Kim, D. *J. Am. Chem. Soc.* **2006**, *128*, 1700.
- (32) Tsuda, A.; Furuta, H.; Osuka, A. *Angew. Chem. Int. Ed.* **2000**, *39*, 2549.

- (33) Sugiura, K.; Matsumoto, T.; Ohkouchi, S.; Naitoh, Y.; Kawai, T.; Takai, Y.; Ushiroda, K.; Sakata, Y. *Chem. Commun.* **1999**, 1957.
- (34) Yamane, O.; Sugiura, K.; Miyasaka, H.; Nakamura, K.; Fujimoto, T.; Kaneda, T.; Sakata, Y.; Yamashita, M. *Chem. Lett.* **2004**, 33, 40.
- (35) Whiting, D. A. In *Comprehensive Organic Synthesis*, 1991, vol. 3, pp. 659.
- (36) Grzybowski, M.; Skonieczny, K.; Butenschön, H.; Gryko, D. T. *Angew. Chem. Int. Ed.* **2013**, 52, 9900.
- (37) Mori, H.; Tanaka, T.; Osuka, A. *J. Mater. Chem. C*, **2013**, 1, 2500-2519.
- (38) Cammidge, A. N.; Scaife, P. J.; Berber, G.; Hughes, D. L. *Org. Lett.* **2005**, 7, 3413-3416.
- (39) Hammerich, O.; Parker, V. D. *Acta Chem. Scand.* **1982**, B36, 519.
- (40) Schäfer, H. J. *Electrolytic oxidative coupling, in Organic Electrochemistry*, 4th ed. (eds. H. Lund, O. Hammerich), Marcel Dekker, New York, **2001**, pp. 883.
- (41) Kirste, A.; Elser, B.; Schnakenburg, G.; Stecker, F.; Waldvogel, S. R. *J. Am. Chem. Soc.* **2012**, 134, 3571.
- (42) Nepomnyashchii, A. B.; Bröring, M.; Ahrens, J. Bard, A. J. *J. Am. Chem. Soc.*, **2011**, 133, 19498–19504.
- (43) Kirste, A.; Schnakenburg, G.; Stecker, F.; Fischer, A.; Waldvogel, S. R. *Angew. Chem. Int. Ed.* **2010**, 49, 971-975.
- (44) Kirste, A.; Schnakenburg, G.; Stecker, F.; Waldvogel, S. R. *Org. Lett.* **2011**, 13, 3126-3129.
- (45) Morofuji, T.; Shimizu, A.; Yoshida, J. *Angew. Chem. Int. Ed.* **2012**, 51, 7259-7262;
- (46) Nyberg, K. *Acta Chem. Scand.* **1973**, 27, 503-509.
- (47) Buda, M.; Iordache, A.; Bucher, C.; Moutet, J.-C.; Royal, G.; Saint-Aman, E.; Sessler, J. L. *Chem. Eur. J.* **2010**, 16, 6810.
- (48) Bui, T.-T.; Iordache, A.; Chen, Z.; Roznyatovskiy, V.V.; Saint-Aman, E.; Lim, J. M.; Lee, B. S.; Ghosh, S.; Moutet, J.-C.; Sessler, J. L.; Kim, D.; Bucher, C. *Chem. Eur. J.* **2012**, 18, 5853.

- (49) Chen, P.; Fang, Y.; Kadish, K. M.; Lewtak, J. P.; Koszelewski, D.; Janiga, A.; Gryko, D. T. *Inorg. Chem.* **2013**, *52*, 9532.
- (50) Imahori, H., Matano, Y., Tanaka, M., *Chem Comm.*, **2007**, *20*, 2069-2071.
- (51) Mack, J.; Stillman, M. J. in *The Porphyrin Handbook*; Kadish, K. M.; Smith, K. M.; Guilard, R., eds; Academic Press: San Diego, 2000; Vol. 16. pp. 43.
- (52) Hansch, C.; Leo, A.; Taft, R. W. *Chem. Rev.* **1991**, *91*, 165-195.
- (53) Chen, P.; Finikova, O. S.; Ou, Z.; Vinogradov, S. A.; Kadish, K. M. *Inorg. Chem.* **2012**, *51*, 6200.
- (54) Swistak, C.; Cornillon, J.-L.; Anerson, J. E.; Kadish, K. M. *Orgnometallics*, **1987**, *6*, 2149.